Theses and Dissertations

2017

Low-Cost Fishing Net-Reinforced Cement Matrix Overlay for Substandard Concrete Masonry in Coastal Areas

Mohammed A. Mousa
University of South Carolina

www.manaraa.com

LOW-COST FISHING NET-REINFORCED CEMENT MATRIX OVERLAY FOR SUBSTANDARD CONCRETE MASONRY IN COASTAL AREAS

by

Mohammed A. Mousa

Bachelor of Science
University of Al-Qadisiyah, 2011

_____

Submitted in Partial Fulfillment of the Requirements

For the Degree of Master of Science in

Civil Engineering

College of Engineering and Computing

University of South Carolina

2017

Accepted by:

Fabio Matta, Director of Thesis

Juan Caicedo, Reader

Paul Ziehl, Reader

Cheryl L. Addy, Vice Provost and Dean of the Graduate School

DEDICATION

To my wife, Hind Shabbani, mother, and family members for their continued
support and encouragement.

ACKNOWLEDGEMENTS

ABSTRACT

The aim of this project is to investigate a novel and affordable option to externally strengthen substandard concrete masonry (CM) walls for out-of-plane loads (e.g., high winds and flying debris). Two types of strengthening materials for fiber-reinforced cement mortar (FRCM) overlays are investigated; namely, fishing net (FN) and welded wire steel mesh (WWSM) reinforcements.

Salient mechanical properties of representative materials including substandard concrete masonry unit (CMU) blocks, mortar, nylon FN and WWSM reinforcements, and FRCM composite, were experimentally characterized. A simple bilinear model is proposed to describe the tensile behavior of the FRCM composite. An analytical model was then used to estimate the flexural capacity and failure mode of strengthened CM walls as a function of the amount of FN reinforcement. The wind velocity that a strengthened CM wall can withstand was evaluated based on a standard velocity pressure equation, and a parametric study was performed to determine the influence of the CM compressive strength (as a measure of substandard properties) on the out-of-plane flexural capacity.

Finally, an experimental program was implemented to provide a proof of concept. A four-point bending test was implemented on four concrete masonry specimens, including: one plain masonry (control) specimen; two specimens strengthened with one and two layers of FN-reinforced mortar overlay, respectively; and, one specimen

strengthened with a WWSM-reinforced mortar overlay, which served as benchmark specimen for the newly-conceived FN system.

It is shown that the out-of-plane flexural capacity of substandard CM walls can be made suitable to resist high wind pressures by means of FN- as well as WWSM-FRCM overlays. In fact, the out-of-plane capacity contributed by the FN-FRCM system is comparable to that contributed by the WWSM-FRCM counterpart. However, the FN-FRCM overlay outperforms the WWSM system in term of deformability and thus energy-absorption capacity. The evidence produced through this research attests to the potential of the novel FN-FRCM system presented herein to retrofit substandard CM walls against high-wind pressures, and possibly the impact of flying debris during hurricanes and tornadoes.

TABLE OF CONTENTS

LIST OF TABLES

LIST OF FIGURES

xiii

xv

LIST OF SYMBOLS

A_b Cross-sectional area of concrete masonry unit (mm^2).

A_f Nominal area of fishing net per unit width (mm^2/mm).

b_w Width of concrete masonry prism (mm).

C_c Compression force (kN).

E_1 First elastic modulus of composite (GPa).

E_2 Second elastic modulus of composite (GPa).

f_a Tensile strength of composite at transition point (MPa).

f_e Effective tensile strength of composite (MPa).

f'_m Masonry compressive strength (MPa).

f_r Modulus of rupture of masonry (MPa).

f_u Ultimate strength of composite (MPa).

H Height of concrete masonry prism (mm).

kd Depth of neutral axis (mm).

L Length of clear span of masonry prism specimens (mm).

M_{1fu} Ultimate flexural strength of masonry prism reinforced with FN-FRCM overlay (one layer) (kN-m).

M_{2fu} Ultimate flexural strength of masonry prism reinforced with FN-FRCM overlay (two layers) (kN-m).

M_{cr} Cracking moment (kN-m).

M_{uu} Flexural strength of unreinforced masonry prism (kN-m).

n_f Number of reinforcement layers.

q Wind pressure (Pa).

S_b Static moment of area of concrete masonry unit (mm^3).

s_f On-center spacing between FN threads (mm).

S_w Static moment of area of masonry prism specimen (mm^3).

T_t Tensile force of textile (kN).

t_w Thickness of masonry prism specimen (mm).

v Wind velocity (m/s).

w_f Width of FRCM overlay (mm).

γ and

β_1 Concrete stress block factors.

φ Modification factor for the analytical masonry flexural strength.

ρ Reinforcement ratio.

ρ_a Air density (kg/m^3).

ρ_b Balanced reinforcement ratio.

ε_a Strain at transition point in FRCM overlay composite.

ε_e Effective strain in FRCM overlay composite.

ε_{mu} Ultimate compressive strain of concrete masonry.

ε_u Ultimate strain of FN-FRCM composite.

LIST OF ABBREVIATIONS

BMC .... Brittle Matrix Composite

CM .... Concrete Masonry

CMC .... Ceramic Matrix Composite

CMU .... Concrete Masonry Unit

Den. .... Denier

FN .... Fishing Nets

FRCM .... Fiber Reinforced Cementitious Matrix

PP .... Polypropylene

RM .... Reinforced Masonry

SEM .... Scanning Electron Microscope

T .... Thread

Tex. .... Textile

TRC .... Textile Reinforced Concrete

UM .... Unreinforced Masonry

WWSM .... Welded Wire Steel Mesh

CHAPTER 1

INTRODUCTION

1.1 Background

About 40% of the world's population lives and works within 60 miles of a coastline (UN 2008). These areas comprise only 10% of the earth's land surface (Hinrichsen 1998). The overwhelming bulk of this population and their infrastructures are vulnerable to the natural hazards caused by extreme weather events such as hurricanes. In fact, these natural phenomena have an enormous impact on developing countries and low-income communities also because of common substandard dwelling construction. For example, in 2016 Hurricane Matthew (Category 5) hit the Caribbean and the US. In Haiti alone, 210,000 houses were destroyed (Stewart 2017). This country also suffered 85% of the total casualties caused by the tragic event. Therefore, it is important in these coastal regions to meet the demand for sustainable, affordable and resilient building techniques for residential structures.

From the 1950s, the common wooden constructions found in Caribbean countries were gradually replaced with concrete masonry structures (Prevatt et al. 2010). The ease and simplicity of construction contributed to their spread. Also, in general, the affordability of building with masonry makes it predominant in the low-income communities (Fothergill et al. 1999). However, most of the existing buildings in developing countries are facing challenges due to substandard construction (Ghorbani

1

et al. 2013; Kijewski-Correa and Taflanidis 2012; Audefroy 2011; Meli and Alcocer 2004; Suaris and Khan 1995). The term "substandard" is defined in this context as (1) low-quality construction materials, (2) poor construction practices (e.g., detailing), and (3) insufficient maintenance.

As a result, an important reason for the devastating consequences of weather events compared to similar events in developed regions is the use of shoddy construction materials (McWilliams and Griffin 2013; Marshall et al. 2011). For example, Marshall et al. (2011) reported a low compressive strength of concrete (about 2.8 MPa) for one of the impacted structures in Haiti. The low compressive strength stems from a lack of cement in the mix as it is the most expensive ingredient. Also, the low compressive strength results from using low-quality aggregates in the mix such as beach sand and smooth river rocks. Furthermore, the workers have poor construction skills and techniques due to their limited formal training and technical resources (Audefroy 2011; Krimgold 2011; Ramamurthy and Nambiar 2004). For example, one of the common practices in these regions is, increasing the water to cement ratio to have a good workability of the mix (Ghorbani 2014; Kijewski-Correa and Taflanidis 2012; Marshall et al. 2011; Cuny 1982). Here, the need for affordable and resilient structural retrofitting materials and techniques is pressing.

However, using typical commercially available materials may result in an excessive financial burden to local homeowners. In addition, structural retrofitting with effective but relatively expensive strengthening materials and techniques (e.g., externally-bonded fiber-reinforced polymer laminates) may entail prohibitive cost. Therefore, utilizing locally available and affordable materials to strengthen or repair dwelling

2

structures constitutes a more realistic strategy for local builders. For example, masonry structures can be retrofitted using bonded overlays made of mortar, which is a familiar material for local builders. Mortar overlaying is an attractive solution for common concrete masonry (CM) structures in these regions. Also, mortar can effectively embed various reinforcing materials, including those locally available, in the form of fiber reinforced cement mortar (FRCM) (Nanni 2012; Smith and Redman 2009). FRCM composite overlays are composed of a cementitious matrix that sandwiches a reinforcing mesh or fabric used for the purpose of strengthening weak structures or repairing damaged structures.

The characteristics of the FRCM composite depend on the properties of the constituent materials and their volume percentage (Arboleda 2014; Daniel and Ishai 1994). The International Code Council Evaluation Service (ICC-ES) has developed acceptance criteria, AC434-13 (ICC-ES 2013) to evaluate and characterize the performance of FRCM composites as retrofitting systems for masonry and concrete structures (ICC-ES 2013). The performance of FRCM under axial, flexural, and shear loads has been evaluated under these criteria (Arboleda 2014). Ordinary Portland cement mortar is an example of viable cementitious matrix, while the reinforcement can be either natural such as sisal, hemp, and flax (Olivito et al. 2014; Olivito et al. 2012), or synthetic such as carbon (De Santis et al. 2016; Donnini et al. 2016; Ebead et al. 2015; Koutas et al. 2015; Maso et al. 2014; de Felice et al. 2014; D'Ambrisi et al. 2013b; Papanicolaou et al. 2011; Badanoiu and Holmgren 2003; Kolsch 1998), steel (Kadam et al. 2014, 2015; Maso et al. 2014; de Felice et al. 2014; Shrestha et al. 2012; Rupika 2010; El Debs and Naaman 1995), glass (Koutas et al. 2015; Maso et al. 2014; Mu et al.

3

2002b), polymeric (Sathiparan and Meguro 2013; Shrestha et al. 2012; Mayorca and Meguro 2004; Mu et al. 2002b; Marshall et al. 2000; El Debs and Naaman 1995), and others such as PBO and basalt (Arboleda et al. 2016; Ebead et al. 2015; Koutas et al. 2015; Babaeidarabad et al. 2014; Maso et al. 2014; de Felice et al. 2014; Larrinaga et al. 2013). FRCM has drawn the attention of researchers recently due to its attractive physical and mechanical properties. FRCM composites are mainly used for flexural and shear reinforcement where they are utilized to strengthen and repair concrete and masonry structures. Figure 1.1 shows some of the FRCM strengthening applications to concrete and masonry structures (Nanni 2012). The advantages gained by using an FRCM are fire resistance, nontoxicity, and water and vapor permeability (Donnini et al. 2017; Vasconcelos et al. 2012; Bisby et al. 2011). For example, Triantafillou et al. (2017) devised a method that combines the use of FRCM as thermal insulation and structural reinforcement. These benefits contribute to reducing the installation cost and time.

In this research, fishing nets (FNs) were combined with Type N masonry mortar to create an FRCM overlay system to strengthen substandard concrete masonry. These mortar and the reinforcement materials are locally available in coastal communities in Mexico and the Caribbean. A welded wire steel mesh (WWSM) was used as FRCM reinforcement for the purpose of comparison with the proposed FN-FRCM overlay. WWSMs also represents an accessible reinforcement material (Kadam et al. 2014, 2015; Maso et al. 2014; de Felice et al. 2014; Shrestha et al. 2012; Rupika 2010; El Debs and Naaman 1995). Both FN and WWSM reinforcements were tested as materials and in FRCM composites under uniaxial tensile load to characterize their stress-strain response and progressive failure mechanisms. The FN (nylon) material and FRCM composite has

4

shown comparable load carrying capacity to their WWSM counterparts. In addition, the FN material and FRCM composite have a remarkably higher deformability that attests to the energy-absorption capacity.

1.2 Objectives

The first objective of this research is to conceive an affordable and locally available material to strengthen or repair CM houses in coastal regions in developing areas. The reinforcing materials such as fishing nets are abundantly available in the coastal regions of developing countries. In fact, the FAO estimates that 90% of those working in the fishing industry are concentrated in small-scale groups in developing countries ("Oceans, Fisheries and Coastal Economies," 2017).

The second objective is to verify that the proposed FN-FRCM overlay material can strengthen substandard CM structures. A part of that goal is to theoretically assess to what extent the reinforcing material can resist out-of-plane wind pressures as they may be imparted during hurricanes and tornadoes.

The third objective is to verify whether FN as a reinforcement material offers a comparable performance to that of a representative welded wire steel mesh.

The fourth objective is to verify the ease and the practicality of installation for the proposed FN-FRCM overlays, by implementing the reinforcing material on masonry prisms as a proof of concept.

5

1.3 State of the art

Unreinforced concrete masonry has an inherently poor performance against out-of-plane loads due to its low flexural strength and brittle failure mode (Carney and Myers 2005). Concrete masonry is among the types of masonry that are used in low-income communities in the US, Mexico, and a number of developing areas (Kijewski-Correa and Taflanidis 2012; Fothergill et al. 1999). Its utilization in these regions stems from its cost efficiency and ease of application (Ramamurthy and Nambiar 2004). In fact, CMs occupy large volumes and require less mortar bedding because of their hollow cores, which also contribute to their sound- and temperature-proofing properties (Ramamurthy and Nambiar 2004). However, many issues are facing the development of the building techniques practiced by the communities in these regions, among these vital issues are:

1. Using non-engineered construction materials and techniques such as poor quality aggregates, lack of cement, and excessive water addition to the mix which results in a low (substandard) material strength. The substandard construction material dedicated to this research is concrete masonry units (CMU), which are often manufactured locally in the regions of the developing countries where they are used (Marshall et al. 2011; Tena-Colunga et al. 2009; Meli and Alcocer 2004; Moroni et al. 2004; Lafuente and Castill 1998; Cuny 1982). For example, the reported compressive strength of CMU ranges between 3 and 10 MPa in Chile (Ghorbani 2014; Moroni et al. 2004) while in Venezuela the CMU strength ranges between 1.4 and 8 MPa (Ghorbani 2014; Lafuente and Castill 1998).

2. Most concrete and masonry structures have not followed standard building code practices to an extent that they performed poorly during natural disasters such as

6

hurricanes and earthquakes (McWilliams and Griffin 2013; Kijewski-Correa and Taflanidis 2012; Audefroy 2011; Marshall et al. 2011). The reason is that either the buildings were built before these guidelines were established, or they were constructed in the absence of administrative and technical supervision, which is a common problem in poor and developing regions (McWilliams and Griffin 2013; Kijewski-Correa and Taflanidis 2012; Audefroy 2011; Marshall et al. 2011; Meli and Alcocer 2004). For example, around 45% of the houses built in Mexico are not following code regulations related to natural disasters such as earthquakes (Meli and Alcocer 2004).

3. Due to the geographic location of these regions, they are prone to hurricanes and other natural disasters that can cause widespread structural failures and collapses (Audefroy 2011).

4. There is limited accessibility to technical and engineering resources for builders in these communities (Kijewski-Correa and Taflanidis 2012; Ramamurthy and Nambiar 2004; "BBC News - Haiti devastation exposes shoddy construction," 2010). In addition, most of the homeowners and builders in these developing countries lack knowledge and experience in regard to hazard mitigation and structural resilience (McWilliams and Griffin 2013; Krimgold 2011; Meli and Alcocer 2004).

1.4 Methodology

The research plan has been designed based on multiple stages, starting from selecting the constituent materials that form the FRCM composite and ending with their performance evaluation on scaled CM specimens. The following steps provide an explanation for each stage of the research.

7

1.   Selecting the constituent materials: this includes the reinforcing materials, the cement mortar, and the CMU blocks. The nylon fishing nets, steel mesh, mortar, and CMU blocks were purchased from local retailers. In particular, the CMU block were manufactured using a customized mix design to obtain a substandard compressive strength. This was done by reducing the cement content, making it comparable to those used in developing regions.

2.   Material characterization: all materials were experimentally characterized to determine salient mechanical properties. Compression tests were used to characterize mortar, CMU blocks, and masonry prisms. Tensile tests were performed to characterize the reinforcing materials and the FRCM overlay composites.

3.   FRCM composite characterization: the composites were cast in the form of dogbone coupons to verify their properties in terms tensile strength, deformation, and failure mode. The dogbone specimens were tested under uniaxial tensile loads.

4.   Assessing structural performance: the masonry out-of-plane flexural capacity was estimated using applicable bending theory (ACI 2013). Furthermore, masonry prisms were constructed and strengthened with FN-FRCM overlays to evaluate constructability as well as structural performance, including out-of-plane flexural strength, deflection, and progressive failure mechanisms.

8

Figures:

Figure 1.1 (1) Tunnel lining with PBO-FRCM in Greece, (2) chimney strengthening with carbon FRCM in France, (3) railway bridge strengthening with PBO-FRCM in Italy, and (4) Concrete railway bridge pedestal strengthening with PBO-FRCM in northern New York (Nanni 2012).

9

CHAPTER 2

NYLON FISHING NETS AS INTERNAL REINFORCEMENT

The use of fishing nets as internal reinforcement for FRCM overlays in the field of civil engineering represents a novel approach to structural strengthening and repair. This chapter explains the salient characteristics of the fishing nets (FN). Also, relevant mechanical properties of the FNs are compared to welded wire steel mesh (WWSM) counterparts.

2.1 Fishing nets

2.1.1 Scope

The definition of netting, according to the International Organization for Standardization (ISO), is "a mesh structure of indefinite shape and size, composed of one yarn or more systems of yarns interlaced or joined…" (ISO 1806 2002; Klust 1982, p. 1). The nets are made of either natural fibers such as cotton, hemp, and sisal, or synthetic fibers like nylon and polypropylene. However, the use of synthetic fibers is preferable due to their durability and alkali resistance (Balaguru and Slattum 1995; Khajuria et al. 1991). Fishing nets are either made of mono or multifilament threads. The construction of the netting yarn is composed of three principle types which are twisted, braided, and knotless threads and are shown in Figure 2.1; further details are provided by Klust (1982).

10

Table 2.1 lists the mechanical properties of representative synthetic and natural fibers used for manufacturing FN yarns such as nylon, polypropylene, and hemp fibers. Twisted multifilament fishing nets made of nylon were employed in this research. The multifilament thread is made of a bundle of fine filaments sometimes thinner than 0.05 mm diameter (Klust 1982). It is difficult to measure the dimensions of the filaments and threads due to their small size and the presence of spaces between the filaments. Therefore, the size of the filaments is typically measured by using different systems (e.g., Tex, Denier), which consider the linear density of the filaments as recommended by ISO 1806 (ISO 2002; Klust 1982).

The term linear density represents the mass of the filament or the thread per unit length. In the Tex system, the filament size is measured by considering its mass in grams per 1000 meters, while the Denier system considers the mass in grams per 9000 meters. The Denier (den) system uses yarn (210 den) which is commercially well known among fishermen and FN makers as a measuring unit for nylon yarn fishing nets (Klust 1982). However, there is also a common designation for the thread size in the Denier system where, for example, the current thread sizes are designated by 210/3, 210/4, 210/15, 210/21, 210/60 which in fact mean multiplication, 210 x 3 den, 210 x 4 den…etc. In order to convert between the Tex and Denier systems, one should either divide or multiply (by 9000 or 0.111, respectively). For example, a thread size of 210/21 den equals (210 x 21) den x 0.111 = 485 tex, which means a single thread of the (210/21 fishing net) weighs 485 g per 1000 m.

Two types of FN threads were utilized in this research, namely, 210/15 and 210/21, which are henceforth designated as #15 and #21, respectively. Fishing nets are

11

also characterized based on their mesh size, which refers to the spacing or the thread length bounded between the knots. The mesh size is measured by taking the distance between either the sequential or the opposite knots as illustrated in Figure 2.2 (Fonteyne and Galbraith 2004). In this document, the spacing, which is 15.6 mm, is given by the distance between sequential knots as the net layout is square.

2.1.2 Test procedure

The mechanical properties of the fishing nets, specifically the mesh breaking strength, is determined by following the ISO 1806 (ISO 2002) testing procedure, which determines the mesh breaking strength in the wet and dry state. The tensile testing procedure is implemented by using a machine that imparts a constant rate of either elongation or force. Another method based on ASTM C1557 (Bertelsen 2016; ASTM 2003) was utilized in the literature to characterize the strength and the Young's modulus of the fibers. However, these testing procedures are intended only for determining the fiber or mesh breaking force and do not provide a comprehensive characterization of the force-elongation behavior. Therefore, a modified tensile test method was devised to characterize the selected FN materials, as explained in detail in Section 2.4.

2.1.3 Durability of nylon and polypropylene fibers in cementitious matrices

Evaluation of the durability of nylon and polypropylene is necessary when they are intended to be used in an alkaline environment such as ordinary Portland cement mortar.

The long term durability of nylon 6, polypropylene, and polyester have been tested by using accelerated aging methods (Khajuria et al. 1991). The parameters used to

12

determine durability were flexural strength, flexural toughness, and the toughness indices I5, I10, and I30 of the 10 x 10 x 35 cm concrete prism specimens. The prisms were tested in four-point bending loads. The results showed that both nylon and polypropylene are durable in alkaline environments whereas polyester is less effective. Conversely, it was found that the flexural strength of nylon and polypropylene had increased slightly. The accelerated aging process simulated the aging of concrete at times of 0, 4, 8, 16, 32 and 52 weeks. The samples were placed in a lime saturated water bath maintained at 50°C temperature. This process was adapted from glass fiber reinforced concrete durability test practices (Balaguru 1992; Khajuria et al. 1991).

Another research study dealt with cement sheets strengthened with fibrillated polypropylene fibers (Balaguru 1992; Hannant 1989). The specimens were tested for a field exposure duration of 10 years by following an accelerated aging method. The exposure conditions simulated outdoor weathering and indoor storage. Both cracked and uncracked samples were tested in three-point bending to evaluate the durability effectiveness of the fibers in the mortar. The weathering conditions had little influence on the initial and ultimate flexural strength of the samples.

Balaguru and Slattum (1995) tested the susceptibility of nylon and polypropylene fibers to damage by ultraviolet radiation and moisture, which can effectively deteriorate the performance of these fibers. The experiments were conducted by exposing the fibers to ultraviolet radiation for up to 500 hours at a temperature of 65 C°. The test results showed that nylon fibers retained 95% of their initial strength while the polypropylene fibers only retained 63% of their original strength (Johnston 2010; Balaguru and Slattum 1995).

13

In summary, the performance of the fibers in an alkaline environment over time showed that nylon fibers tend to retain their stiffness and strength. Instead, the polypropylene fibers had a lower durability compared to nylon in terms of fiber strength, and in terms of resistance to ultraviolet radiations.

2.2 Welded wire steel mesh

The welded wire steel mesh consists of a prefabricated grid of stainless steel wires that are connected by means of electric fusion weldments. The welded mesh is manufactured by machines that produce a mesh of precise spacing. The wire cloth is often made of galvanized steel to provide better corrosion performance. The shapes of the mesh are square, rectangular, and diamond. WWSMs are often used for barrier fencing and window screening.

The steel wire size is measured by using the gauge system, which is defined as a series of standard sizes which describe the wire diameter. The gauge number refers to the number of draws that the wires passed through a chain of increasingly smaller dies. The higher the gauge number, the smaller the wire size it indicates. Different methods of wire gauge measurement were used such as Birmingham wire gauge (stubs iron wire gauge), and the American wire gauge. These methods are providing tables for unit conversions between the gauge and the metric system. For example, according to the American wire gauge method, the 9 gauge equals 3.75 mm. The wire size employed in this research has 19 gauge (1.0 mm) nominal wire size and a 12.5 mm square mesh opening. Welded wire mesh mechanical properties that are used in the previous studies are summarized and listed in Table 2.2.

14

2.3 Selecting fishing nets with benchmark

The rationale for selecting the fishing net is summarized by the following points.

1. Affordability and ease of use: the price of the FN is 2.5 times cheaper than a similar WWSM and is 5.5 times lighter. For instance, the cost of 1 m^2 of the fishing nets used in this research is $2.85 and steel wire mesh is $6.45. The fishing net flexibility made it easier to be embedded into cementitious mortar to be applied onto CM surfaces.

2. Availability: fishing nets are intended to be used in the coastal communities of developing areas. In fact, FAO estimates that 90% of those working in the fishing industry are concentrated in small-scale groups in developing countries ("Oceans, Fisheries and Coastal Economies," 2017).

3. Material and configuration: the fishing nets used in this research are made of nylon material which is common worldwide. The use of nylon has a high potential for material recycling as it helps to reduce non-biodegradable waste. New and used fishing nets can be used in FRCM overlays. Here, the fishing nets were used as continuous fibers in the form of mesh to reinforce masonry mortar. The FRCM composite was utilized as an overlay masonry reinforcement. In addition, reinforced overlay can be used as thermal and sound insulation for masonry structures (Triantafillou et al. 2017).

The fishing nets can be used as a reinforcement in different configurations such as continuous and discrete fibers. Spadea et al. (2015) used recycled fishing net as discrete fibers by dispersing them in cementitious mortar to enhance its compression and bending behavior. The research findings showed an increase in the flexural strength (around 35%). Also, the toughness and the residual strength was enhanced due to the addition of

15

the fibers to the cementitious matrix. Bertelsen and Schmidt (2016) used fishing net as continuous fibers reinforcement by combining them with epoxy coating as near-surface mounted fiber reinforced polymer (FRP) to reinforce concrete beams. A four-point bending test was implemented to evaluate the FRP effect on the flexural strength. The test results showed a slight increase in the flexural strength around 5-12%.

4. Energy absorption capacity: experimental evidence showed that polymeric nets have a high capacity to absorb energy (toughness). Figure 2.3 a, b, and c show the stress-strain behavior of steel, polypropylene PP band, and nylon, respectively (Rupika 2010; Shackelford 2005). It is observed from the figure that the energy absorbed by PP bands is 1636×10^4 J/m^3, nylon 66 is 600×10^4 J/m^3 (dry as molded type), and steel is 355×10^4 J/m^3. The figure also shows that the deformability of the PP band is 25 times that of the steel and nylon is 10 times that of the steel.

5. Durability: the durability of the nylon material was reviewed in section 2.1.3. The long term durability of nylon 6, polypropylene, and polyester have been tested by using accelerated aging methods (Khajuria et al. 1991). Test results showed that both nylon and polypropylene have better durability in alkaline environments than polyester.

6. Bonding: in this research, the preliminary laboratory observations for the net-mortar composite bonding has shown that the net has an excellent bond to the cementitious matrix. Figure 2.4 shows that mortar fragments were kept in position by the net after the net-mortar composite was crushed with a hammer. The reason is due to the textile nature of the thread surface. Also, mesh openings are providing an efficient mechanical interlocking between the mortar and the reinforcement.

2.4 Reinforcement characterization

The fishing nets are made of twisted multifilament nylon yarns. Salient physical and mechanical properties were characterized based on several parameters. These paramter are; thread size, threads with and without the knot, and thread as a mesh. Table 2.3 lists the test matrix of the tested specimens, specimen shape, number of specimens for each combination, and the average tensile strength and deformation with standard deviation. The selected thread sizes were #15, and #21 both tested under uniaxial tensile load to determine their knotted and knotless tensile strength. Figure 2.6. shows some of the specimens before and after test for #15 and #21 thread types.

The fishing nets used in this research have 15 mm mesh openings as shown in Figure 2.5. The thread size (diameter), which is considered nominal, was measured by using an electronic caliper. The thread diameter was measured multiple times in different directions and at several locations. The flexible threads were kept straight for measurement purpose.

The FN and WWSM materials were tested under uniaxial tensile loads to characterize the tensile stress-strain response following the test setup for the boundary conditions used by De Santis and De Felice (2015), which includes embedding the ends of the sample in epoxy resin as illustrated in Figure 2.6 and 2.7.

The steel wire mesh is made of galvanized stainless steel wires for enhanced corrosion resistance. The steel wire size used in the research is 19 gauge (1.0 mm nominal diameter), and the mesh opening is 12.5 mm for the square layout as shown in Figure 2.5. The mesh spacing was selected to be comparable to the FN. The testing

17

procedure is similar to the FN tensile test method, but only one combination was tested, i.e., in mesh form, and illustrated in Figure 2.8.

2.4.3 Tensile testing of FN and WWSM

1. Preparation: the specimens were prepared by casting the ends of the FN in resin using plastic molds that have dimensions of 50 mm L x 28 mm W x 11 mm T. The gripping region is the area of the two faces of 50 mm length by 28 mm width on each side of the specimen. The ends of the sample are compressed between two hydraulic grips which have slightly bigger dimensions than the specimens. The gage length was kept consistent for all samples (100 mm). For each type (i.e., combination), 5 specimens were tested.

2. Instrumentation: the uniaxial tensile test was performed by using a test frame equipped with 9 kN load cell and a 125 mm displacement sensor. The machine was connected to a data acquisition system that collected data at a frequency of 100 Hz.

3. Testing procedure: The following points summarize the testing procedure and are illustrated in Figure 2.7 and Figure 2.8.

- The specimen is mounted to the grips of the machine, and its initial length is measured.

- The test starts with an initial small pretension value (around 2% of the thread strength).

- The specimen is loaded under displacement control at a rate of 0.2 mm/sec.

- The test is stopped until all threads fail, or the maximum displacement of the test machine (127 mm) is reached (typically with failure of one or more threads).

18

2.5 Uniaxial tensile test results

2.5.1 Test results

The test results are reported for the types, number of specimens, maximum load, and deformation of the FN and WWSM specimens, in Table 2.3. The FN and WWSM materials strength per unit length is presented in Table 2.4. Figure 2.9 provides the load-displacement response of representative specimens of FN and WWSM materials. Figure 2.10 shows the manufacturer and the average experimental strength of knotted and knotless threads, which illustrates the effect of knots on the tensile strength. The full dataset is available in Figure 2.11 and Figure 2.12 show the average strength and strain values of the FN specimens respectively. Also, the lower and upper bounds in the Figures 2.11 and 2.12 represent the range of the values of the individual tested specimens.

2.5.2 Discussion of the results

Figure 2.9 shows that the FN threads have a significantly higher deformability (by about 15 times) compared to than the WWSM. The high deformation capacity of the fishing nets results from the low stiffness of the nylon material and the behavior of the knot. The knot contributes to the thread deformation due to tightening, thread slippage. The energy absorbed (i.e., area under the load-displacement curve) by the FN and WWSM specimens is calculated from the representative load-displacement curves shown in Figure 2.9. The percentage increase of the energy absorbed of the FN over the steel mesh is (+622%, +1347%, +1011%, and +2098% for the #15(1L), #15(2L), #21(1L), and #21(2L), respectively).

The presence of the knot decreases the thread strength because the failure is initiated by the knot unraveling or thread slippage through the knot as reflected in Figure 2.10. The fishing net and the threads are failing in a progressive manner where the failure initiated in one of the threads then extend to the neighboring threads. Moreover, the thread itself is also failing progressively as a result of being composed of multiple twisted subthreads (filaments).

The nominal stress values are calculated by dividing the maximum load that the specimens carry by the nominal area of the threads. It is noticed that the maximum stress carried by the specimens decreases as the number of threads in the specimen increases as shown in Figure 2.11. Stress reduction is resulting from the uneven stress distribution among the threads leading to premature failure of the most loaded thread.

The nominal (average) strain values at failure are calculated by dividing the deformation at the peak load by the original length of the specimen. It is shown that the strain at failure increases as the number of threads increases as illustrated in Figure 2.12. Strain increase at failure results from the fact that the maximum elongation increases when the width of the specimen increases (has more threads) due to the structure of the FN mesh where each longitudinal or transverse thread changes its direction at every knot, as illustrated in Figure 2.13. Finally, the presence of the knot increases the ultimate strain value of the thread as a result of the thread slippage through the knot as shown in Figure 2.12 where the ultimate strain ratio of the knotted to the knotless thread is approximately 4:1 for a #21 thread size.

20
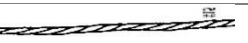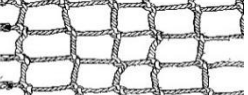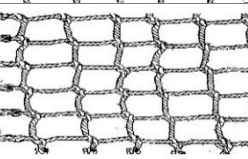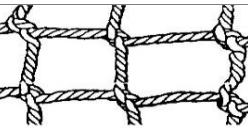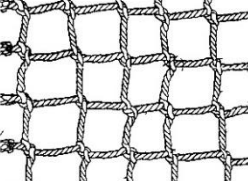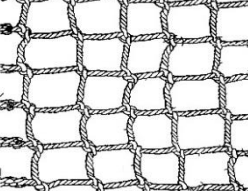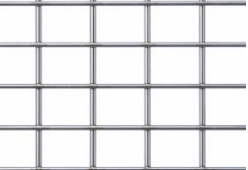
Tables:

Table 2.1 Properties of polymeric and hemp fibers.

Reference	Tensile strength, MPa			Modulus of rupture, GPa			Melting point, °C	
	Polypropylene	Nylon	Hemp	Polypropylene	Nylon	Hemp	Polypropylene	Nylon
Alhozaimy et al. (1996)	628-760	-	-	3.50	-	-	160-170	-
Khajuria et al. (1991)	553-759	897	-	-	5.18	-	160-170	242
Mu et al. (2002a)	620	-	-	3.50	-	-	-	-
Zhang and Li (2013)	450	-	-	4.10	-	-	160-170	-
Banthia and Nandakumar (2003)	375	-	-	3.50	-	-	-	-
Tang et al. (2007)	350	-	-	3.50	-	-	160	-
Cai et al. (2006)	350	-	-	3.50	-	-	160	-
Yetimoglu and Salbas (2003), Yetimoglu et al. (2005)	320-400	-	-	3.50-3.90	-	-	-	-
Tang et al. (2010)	350	-	-	3.50	-	-	165	-
Song et al. (2005)	413	896		4.11	5.17	-	160	225
Mamlouk and Zaniewski (2011)	-	1000	-	-	4.8	-	-	-
Spadea et al. (2015)	-	289-348	-	-	0.723 (wet), 1-3 (dry)	-	-	-
Sawpan (2010)	-	-	442-577	-	-	23-26.5	-	-
Efendy and Pickering (2014)	-	-	1077-866	-	-	20.9-28.9	-	-
Olivito et al. (2012)	-	-	240	-	-	-	-	-

Table 2.2 Properties of steel welded wire mesh.

Reference	Steel type	Mesh type	Wire size, diameter, mm	Tensile strength, (ultimate), MPa	Modulus of rupture, GPa
Paramasivam and Ravindrarajah (1988)	Welded wire steel mesh	Square, 8.5 mm	0.87	245	140
El Debs and Naaman (1995)	Welded wire steel mesh	Square, 25.4, and 50.8 mm	2.03 2.67	364 556	
Arif et al. (1999)	Machine woven galvanized mesh	Rectangle, 7.5 x 6.0 mm	0.72	295	89
Arif et al. (1999)	Welded galvanized mesh	Square, 15 mm	1.44	307	111
Ghorbani (2014)	Welded wire steel mesh	Rectangle, 50 x 100 mm	2.0	525	
Kadam et al. (2014, 2015)	Welded wire steel mesh	Square, 5.91 mm	2.42	850	127
Chithambaram and Kumar (2017)	Chicken wire	Hexagonal, 12.5 mm per side	0.9	400	100

Table 2.3 Characteristics of tested FN threads and WWSM samples.

Specimen type (thread diameter, mm)	Number of threads	Specimens shape (loading direction) ⟺	Number of specimens	Average tensile strength per thread, N (SD)	Average deformation, mm (SD)
#15 T knotted (1.20)	1		5	154 (±8)	100.9 (±3.5)
#15 T knotless (1.20)	1		5	193 (±17)	23.0 (±1.5)
#15 FN knotted (1.20)	2		5	175 (±27.7)	76.0 (±19.7)
#15 FN knotted (1.20)	4		5	124 (±7.1)	94.1 (±9.9)
#15 FN knotted (1.20)	6		5	131 (±15)	99.9 (±9.4)
#21 T knotted (1.75)	1		5	291 (±26)	95.2 (±9.5)
#21 T knotless (1.75)	1		5	424 (±24.3)	48.9 (±9.3)
#21 FN knotted (1.75)	2		5	304 (±40.9)	82.5 (±9.9)
#21 FN knotted (1.75)	4		5	186 (±18)	121.8 (±3.2)
#21 FN knotted (1.75)	6		5	240 (±5.9)	118.9 (±8.1)
WWSM (0.90)	5		3	274 (±72)	6.1 (±1.9)

1. T = thread.
2. FN = fishing net.
3. WWSM = welded wire steel mesh.
4. SD = standard deviation.

23

Table 2.4 Strength of representative samples of FN and WWSM material.

Reinforcement material	Number of layers	Thread size (diameter, mm)	FN threads area per unit length, mm^2/m	Material tensile strength, kN/m
FN	2	#15 (1.20±0.02)	150	20.6 (±0.75)
FN	1	#21 (1.75±0.03)	160	17.5 (±1.68)
FN	2	#21 (1.75±0.03)	320	35.1 (±3.36)
WWSM	1	Gage-19 (0.89±0.02)	50	21.9 (±5.70)

Figures:
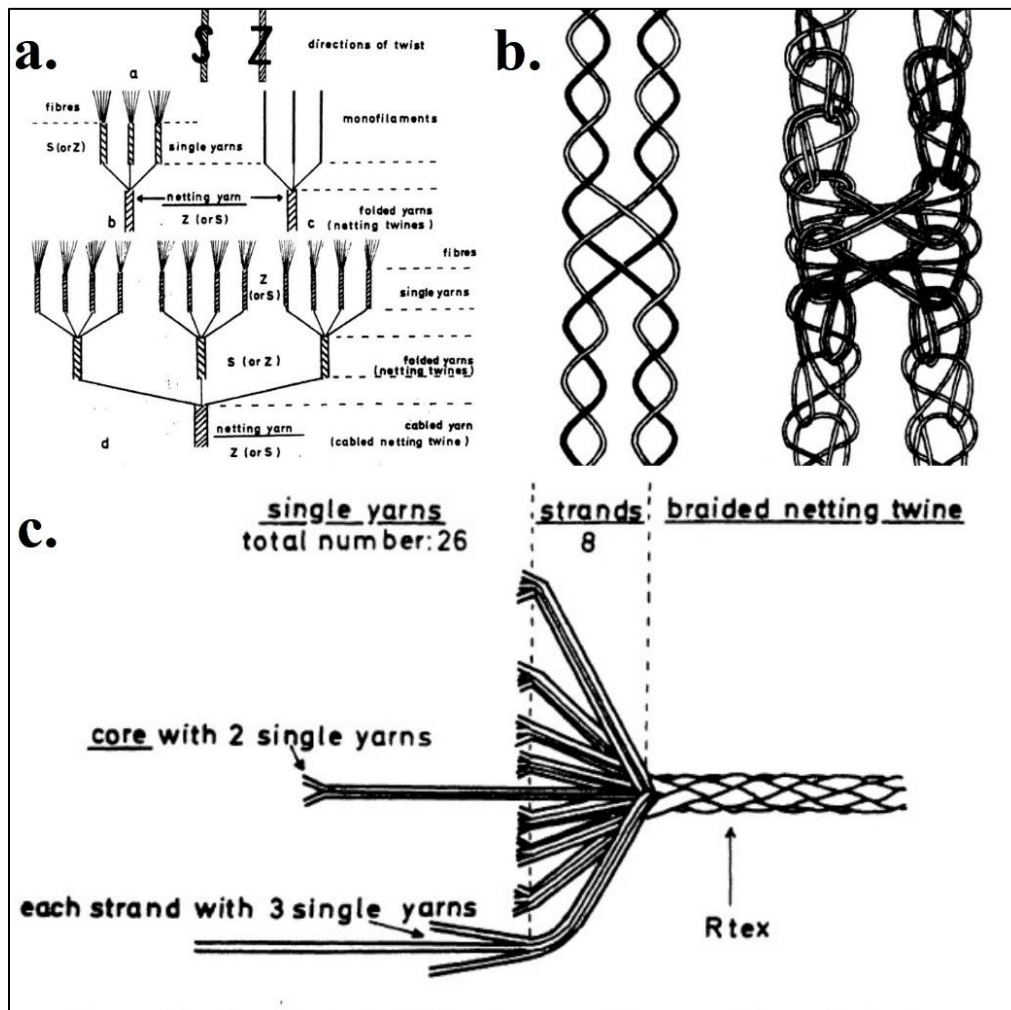
Figure 2.1 Fishing net thread types: (a) twisted, (b) knotless, and (c) braided (Klust 1982).
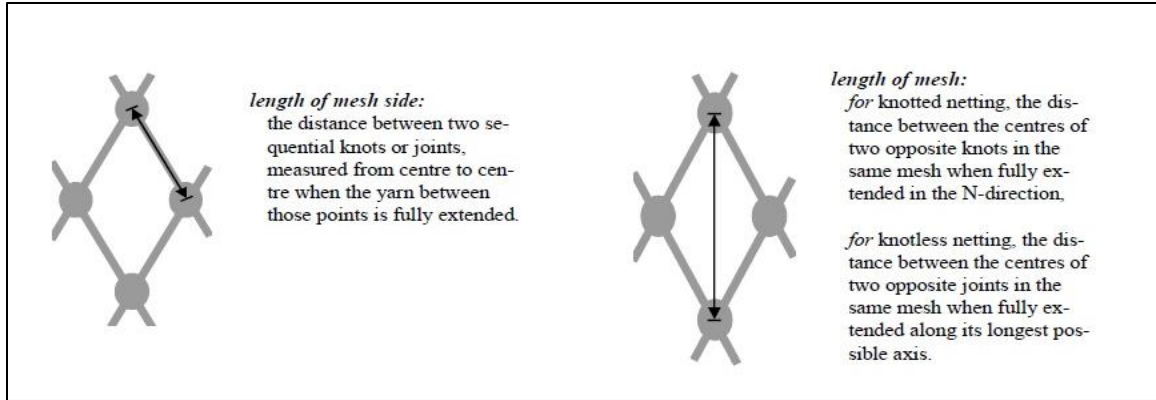
Figure 2.2 Mesh size measuring methods (Fonteyne and Galbraith 2004).
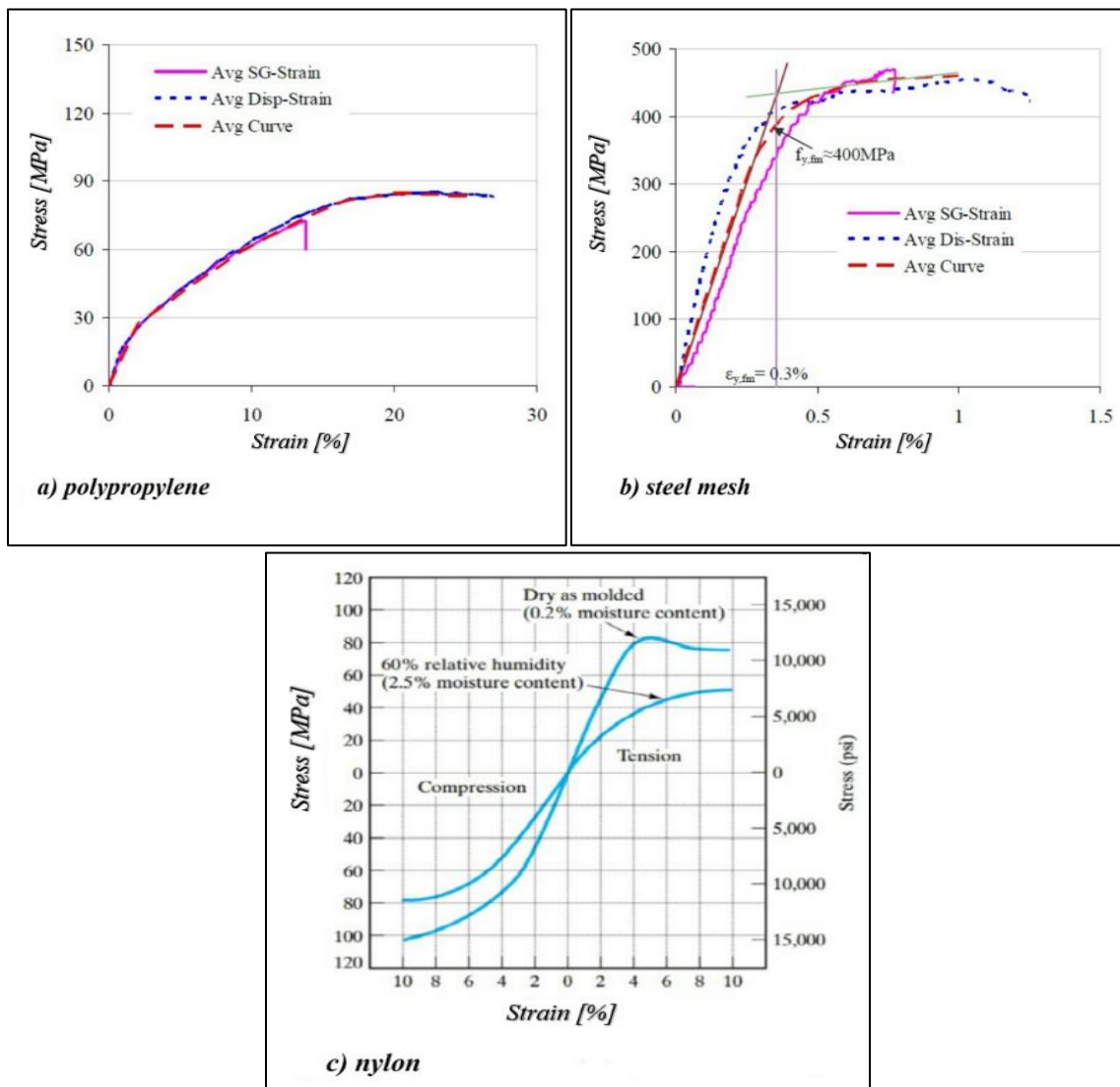
Figure 2.3 Representative stress-strain response of (a) polypropylene band (b) steel mesh (Rupika 2010), and (c) nylon (Shackelford 2005).

Figure 2.4 Crushed mortar with embedded FN reinforcement.
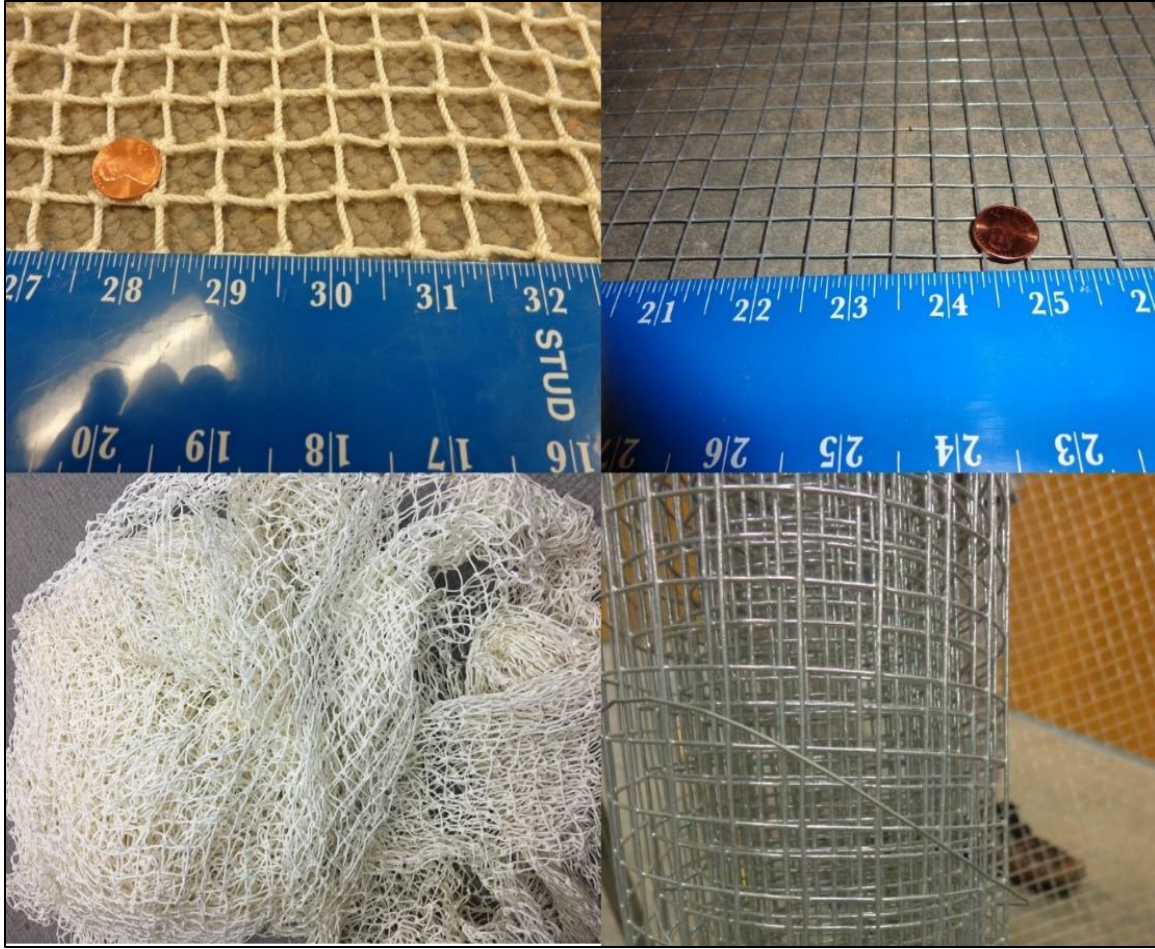
Figure 2.5 FN and WWSM materials used in research.
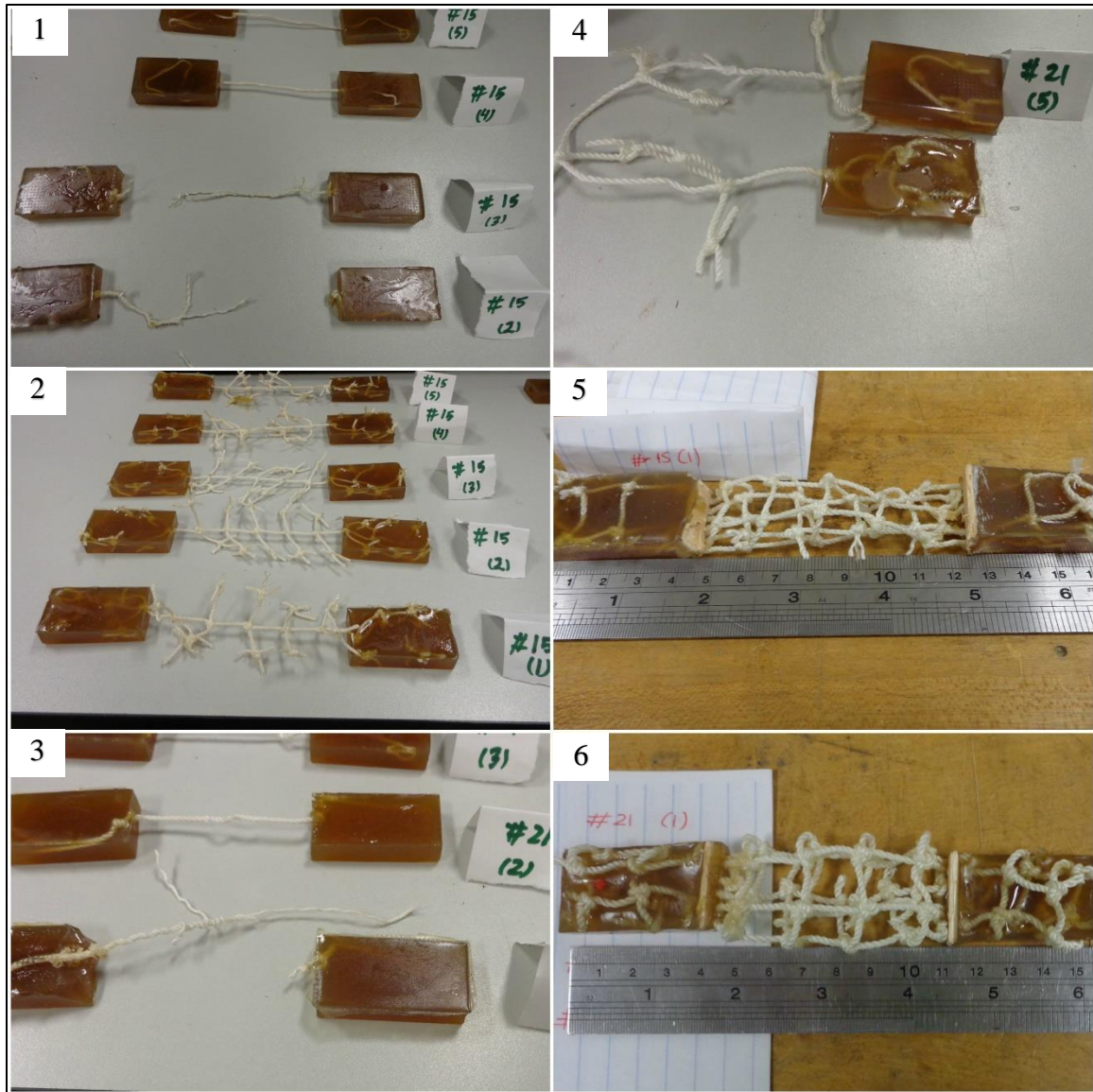
Figure 2.6 FN material specimens including (1) #15 knotless thread, (2) #15 knotted thread, (3) #21 knotless thread, (4) #21 knotted thread, (5) #15, 6 threads, (6) #21, 6 threads.
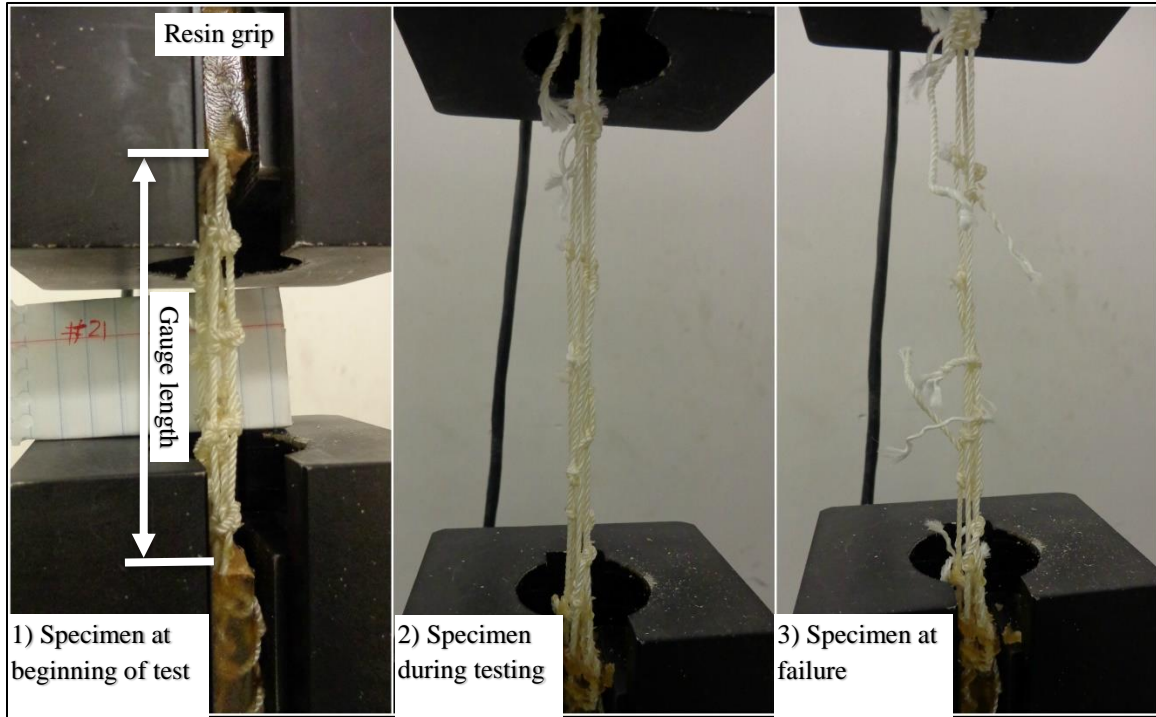
Figure 2.7 FN uniaxial tensile test procedure.
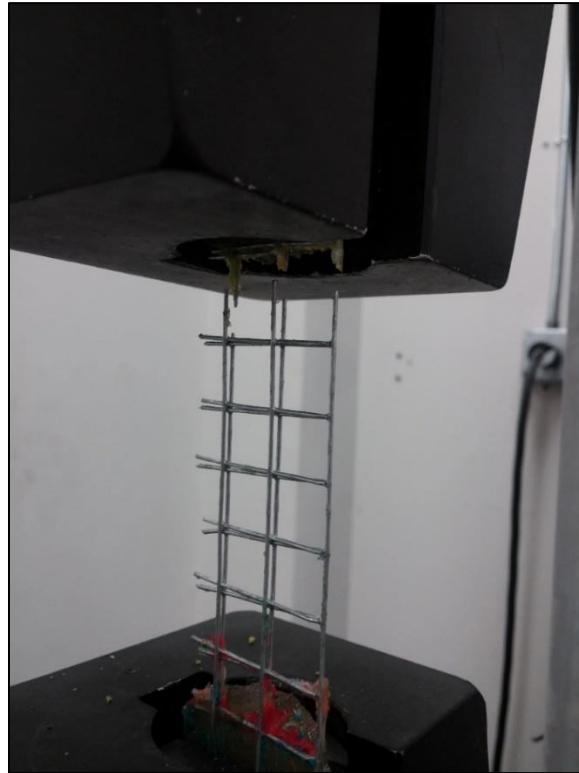
Figure 2.8 WWSM uniaxial tensile test setup and failed specimen.
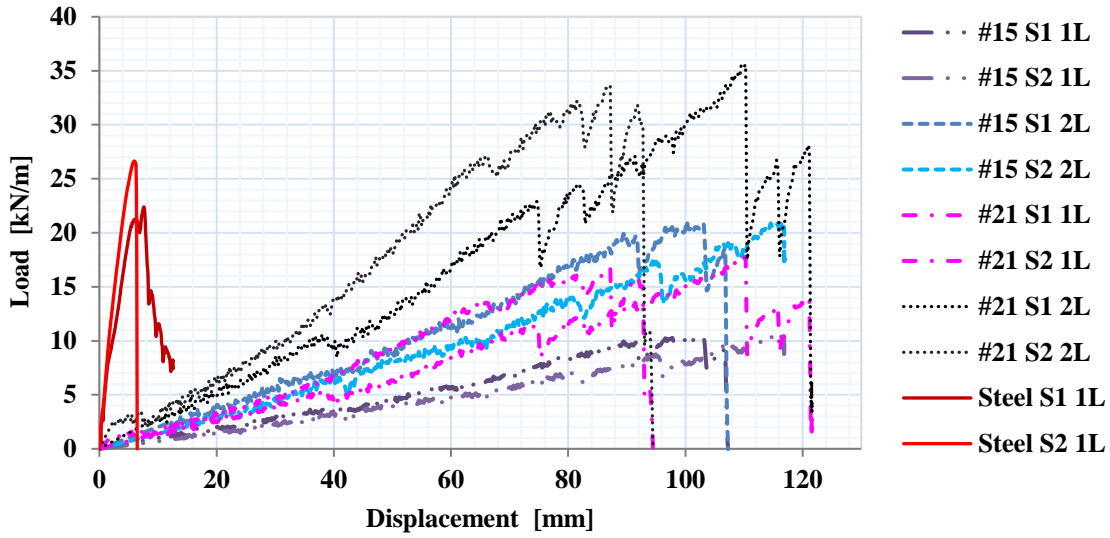
Figure 2.9 Representative tensile load-displacement response of FN and WWSM
materials.
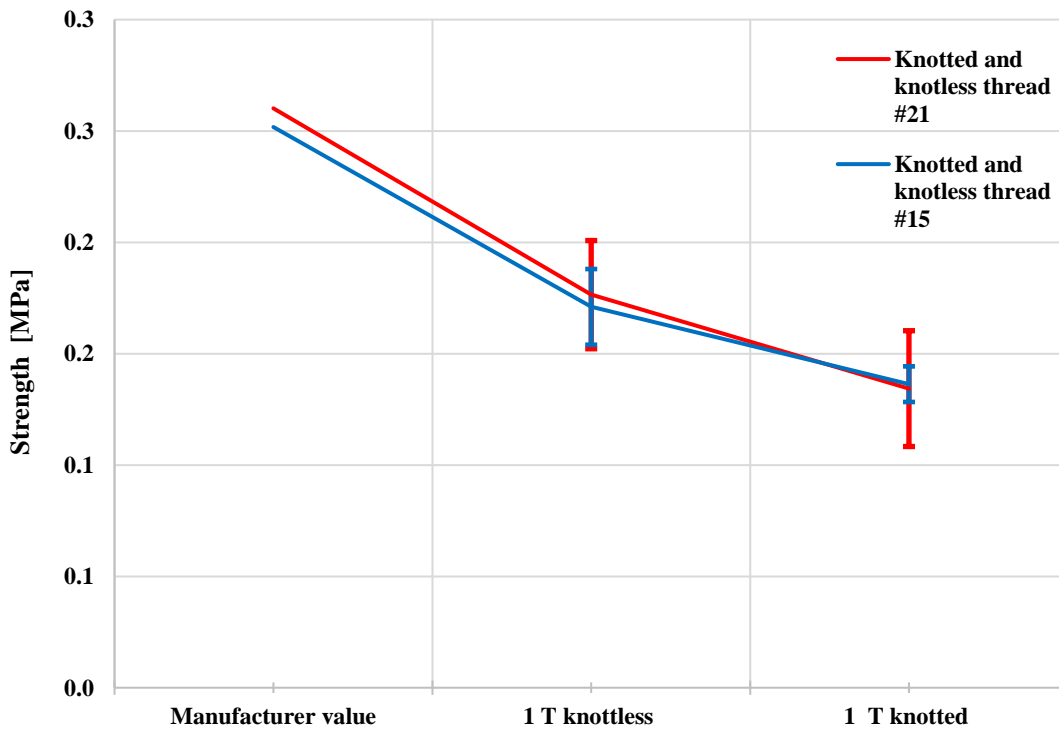
Figure 2.10 Manufacturer and average experimental strength of single knotted and
knotless FN threads and their standard deviations.

www.manaraa.com
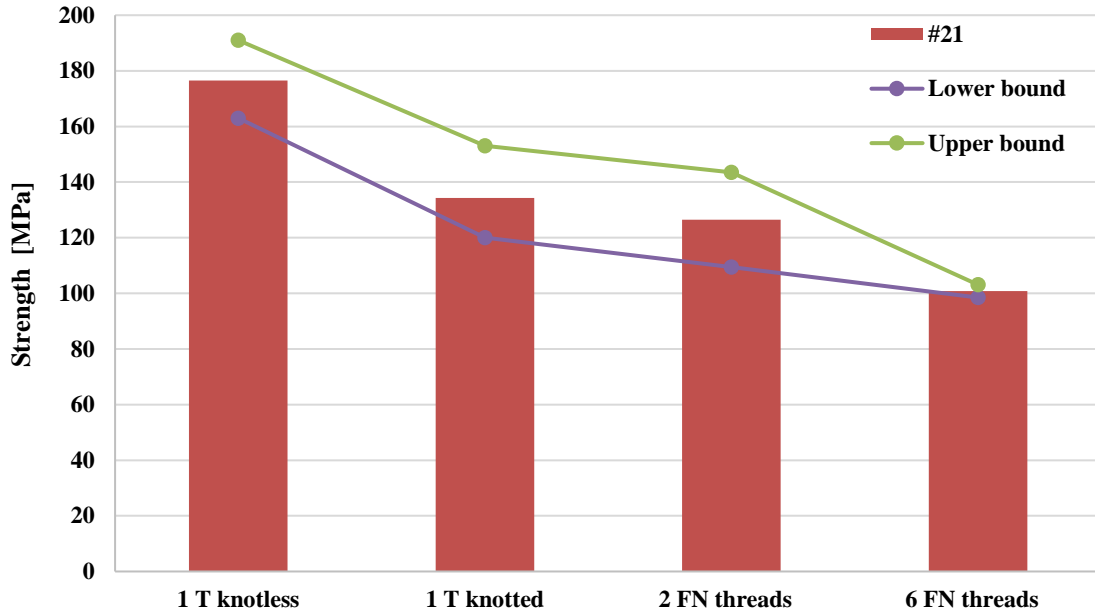
Figure 2.11 Nominal strength values of different fishing nets specimens (lower and upper bounds represent minimum and maximum stress values of individual specimens).
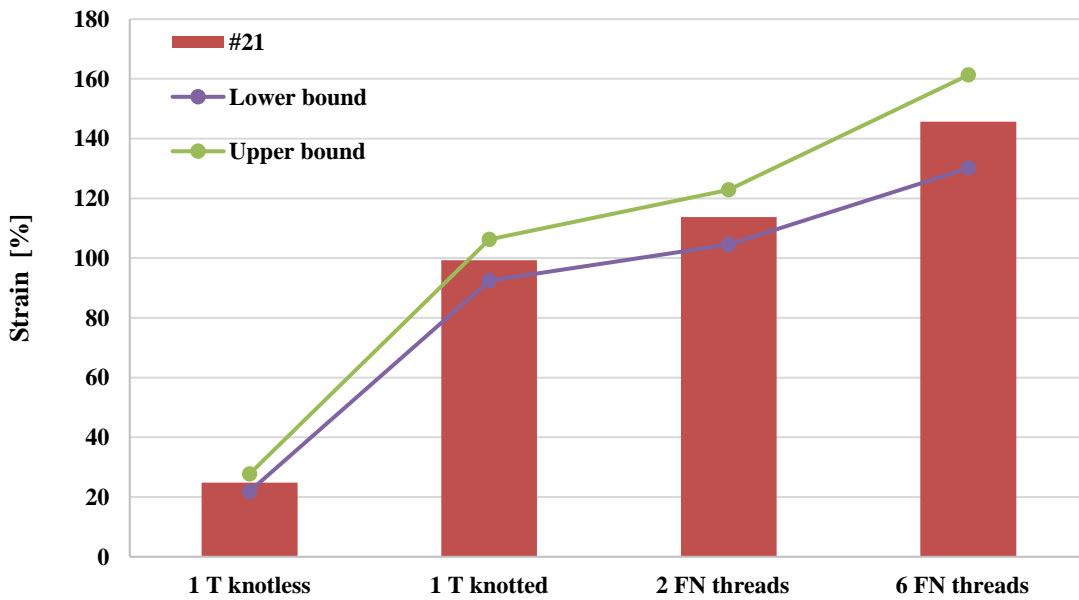
Figure 2.12 Nominal average strain values of different fishing nets specimens (lower and upper bounds represent minimum and maximum strain values of individual specimens).
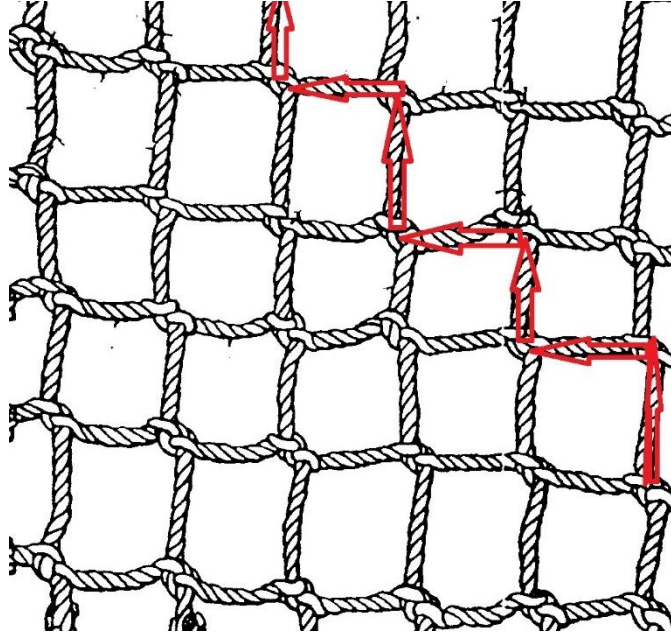
Figure 2.13 Structure of knotted fishing net.

CHAPTER 3

MORTAR AND CONCRETE MASONRY MATERIALS

This chapter focuses on the prototyping, selection, and characterization of the mortar used for masonry overlaying, concrete masonry units (CMU), the mortar used for masonry building, and concrete masonry. Cement mortars were used in this research because they are familiar materials to local builders.

3.1 Mortar

3.1.1 Mortar prototyping

Initially, different mortar mixtures were considered based on properties that are favorable for masonry overlaying, such as ability to encapsulate the reinforcing material and bond onto the concrete masonry substrate. The selected mortars were Portland cement mortar with 1:4 ratio cement:sand in volume, Portland cement mortar with 1:5 ratio cement:sand, and Type N masonry mortar. The Type N masonry mortar is a ready-mix mortar that has cement:sand ratio ranging between 2.25 - 3.5 times the total volume of cement.

The prototyping process included mortar mixing, handling, and masonry overlaying to assess workability and applicability as an overlay. The selected water to cement ratio is 0.55 which provided a suitable mortar workability without any additives or admixtures. Mortar overlaying is illustrated in Figure 3.1. The overlaying process

33

starts by cleaning the masonry surface from any dust, then the masonry is sprayed with water upon overlaying. After that, the first (base) mortar layer with 8 mm thickness is plastered which is immediately followed by mesh layout and fixed to the mortar by gentle pressing. Then, the second (cover) mortar layer is plastered to encapsulate the mesh. The applicability was checked by controlling the overlay thickness and capability to adhere to the masonry surface. The total mortar thickness is 18 mm for one layer of FN reinforcement, and 25 mm for two layers. Overlay mortar curing is done by wrapping it with moist burlaps. The mortar texture and bonding to the masonry was check after curing, Figure 3.2 shows mortar samples of the targeted mixtures after curing where the ready-mix mortar shows no shrinkage cracks and a good consistency of the texture.

3.1.2 Mortar selection

The overlay mortar selection depends on several factors such as availability, affordability, workability, as well as the ability to bond to the reinforcement and substrate surface. Therefore, the prototyping process included multiple mortar types which have been mentioned earlier and used as trials to determine the suitable mortar. The mortar bonding to the reinforcement and the substrate was checked manually by hand by pulling the reinforcement out of the mortar as illustrated in Figure 3.3. The selected mortar for masonry overlaying was the Type N masonry mortar as it showed a good workability and bonding to the masonry. Also, the cost is comparable to the Portland cement mortars.

The selected mortar for building the masonry prisms was also the ready-mix Type N mortar. However, the water cement ratio was increased to decrease the compressive strength of the mortar and make it comparable to substandard mortars.

34

3.1.3 Mortar characterization

The overly mortar was characterized by determining its compressive and flexural strength. Other properties such as water retention and air content were provided by the manufacturer, as listed in Table 3.1. Mortar samples were cast by using six 50 mm cubes, then cured in lime water for 28 days. The compression test was done according to ASTM C109 and illustrated in Figure 3.4 (ASTM 2005a). The average compressive strength of the overlaying mortar is 18.4 (±1.15) MPa.

The flexural strength of the mortar was characterized by testing five prisms having dimensions of 40 x 40 x 160 mm. The test was implemented by per ASTM C348 (ASTM 2014). The test setup is shown in Figure 3.5. The average flexural strength is 3.4 (±0.30) MPa.

The mortar used for the concrete masonry was characterized by testing three mortar cubes under uniaxial compression per ASTM C109 (ASTM 2005a). The average compression strength is 6.8 (±0.50) MPa.

All tests were implemented by using a servo-hydraulic machine using a 45 kN loading module under displacement control mode at a rate of 0.2 mm/sec. The test results and the manufacturer-suggested mortar properties are summarized in Table 3.1.

3.2 CMU blocks

The CMU blocks were manufactured to obtain a representative substandard compressive strength. This objective was accomplished by reducing the cement content to half of the standard block mix. The test procedure was done according to ASTM C140 (ASTM 2005b). Six blocks with nominal dimensions 20 x 20 x 40 mm were measured as

35

shown in Table 3.2. The measured blocks were tested with a compression machine at a load rate of 6.67 kN/s. The test setup is illustrated in Figure 3.6. The results of the blocks net, gross, and nominal compressive strengths are given in Table 3.3. The net, gross and nominal strengths are resulting from dividing the applied load by the corresponding areas. The net area is the solid part of the block, omitting the block openings. The gross area represents the whole measured area of the block, including the openings. The nominal area is the area given by the manufacturer without considering the openings 20 x 40 mm^2.

3.3 CMU masonry prisms

Three CM masonry prisms were tested under uniaxial compression load according to ASTM C1314 (ASTM 2003a). The dimensions of the specimen are 410 mm x 400 mm x 200 mm, i.e., two blocks stacked with a 10 mm thick mortar bed joint. The average compressive strength of the blocks (based on net area) is 6.2 ($\pm$0.30) MPa, and the average compressive strength of the mortar is 6.8 ($\pm$0.50) MPa.

Three specimens were tested by using a hydraulic compression jack with a capacity of 660 kN. The load was measured using a load cell having capacity of 450 kN. The load cell was seated on 25 mm thick plates at the top and the bottom of the specimen. Four LVDT displacement measuring devices were used to calculate the axial deformation over a 175 mm gauge length. Figure 3.7 shows the test setup and the instrumentation. The failure mode is compared with the failure types shown in the ASTM (2003a) standard as illustrated in Figure 3.8. The load and the displacement were recorded using the data

36

acquisition system. The stress-strain curves were calculated from the load-displacement data, where the stress is calculated by dividing the load by the net area of the block.

Figure 3.9 shows the stress-strain behavior. The average compressive strength and the standard deviation are 5.5 MPa and ($\pm$0.30) MPa, respectively. The average strain at peak load is 0.003 mm/mm. The modulus of elasticity is calculated as the slope of the chord connecting the points between 5% and 33% of the maximum compressive stress (MSJC, 2011). The modulus of elasticity is 6.55 ($\pm$0.12) GPa. The failure mode was observed as a combination of conical, semi-conical shear and split, i.e., Type 2, 3, and 5 as shown in Figure 3.8. The test results for each specimen are shown in Table 3.4.

Tables:

Table 3.1 Properties of the masonry cement mortar (Type N).

Type N masonry mortar	Properties by manufacturer	Experimental tests	
Minimum compressive strength, MPa	5.2	Compressive strength of mortar for overlay, MPa	18.4 ($\pm$1.15)
Water retention minimum %	75	Compressive strength of mortar for masonry, MPa	6.8 ($\pm$0.50)
Air content maximum %	20	Flexural strength, MPa	3.4 ($\pm$0.30)

Table 3.2 Dimensions of CMU blocks.

Specimen #	Length, mm	Width, mm	Height, mm	Web thickness, mm	Face-shell thickness, mm
1	396.8	196.9	193.6	33.2	35.1
2	396.8	196.8	194.7	33.4	34.9
3	396.7	193.8	194.9	34.1	34.8
4	397.7	193.8	193.8	33.8	35.2
5	397.8	196.8	194.2	33.2	37.3
6	396.8	193.7	193.4	34.0	35.1

Table 3.3 CMU block compression test results.

Specimen #	Loads, kN	Net area, mm^2	Gross area, mm^2	Nominal area, mm^2	Net strength, MPa	Gross strength, MPa	Nominal strength, MPa
1	224.1	40697	78116	47097	5.5	2.9	4.8
2	254.9	40697	78116	47097	6.3	3.3	5.4
3	256.2	40387	76826	47097	6.3	3.3	5.4
4	255.6	40129	76258	47097	6.4	3.3	5.4
5	274.3	41935	77471	47097	6.5	3.5	5.8
6	243.0	40387	76826	47097	6.0	3.2	5.2
Avg.	251.3	40710	77290	47097	6.2	3.3	5.3
(SD)	($\pm$3.4)	($\pm$580)	($\pm$709)	-	($\pm$0.30)	($\pm$0.21)	($\pm$0.31)

38

Table 3.4 CM prisms compression test result

Spec imen #	Maxim um load, kN	Maximum displacement, mm	Compre ssive strength, MPa	Compressive strain at peak stress, mm/mm	Ultimate compressive strain, ε_{mu} mm/mm	Modulus of elasticity, GPa
1	201.7	0.44	4.96	0.0025	0.0034	7.78
2	232.6	0.53	5.71	0.0030	0.0052	6.90
3	232.5	0.61	5.71	0.0034	0.0063	5.00
Avg.	222.3	0.53	5.46	0.003	0.005	6.56
(SD)	(±14.5)	(±0.07)	(±0.36)	(±0.0004)	(±0.0012)	(±1.16)

Figures:
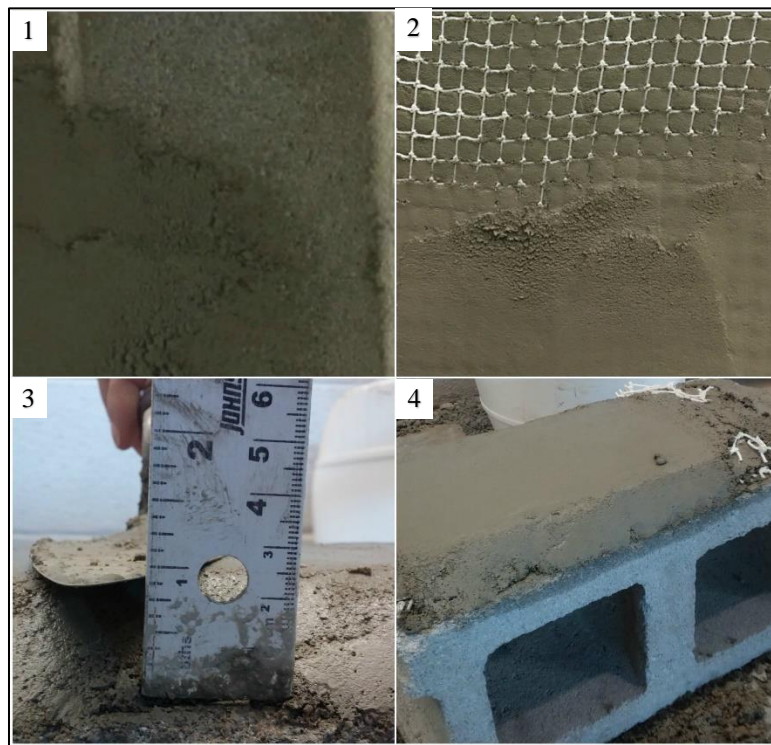
Figure 3.1 Mortar prototyping, (1) plastering first layer, (2) mesh layout, fixing, and plastering of second layer, (3) mortar thickness check (25 mm for 2 layers), and (4) plastered mortar.
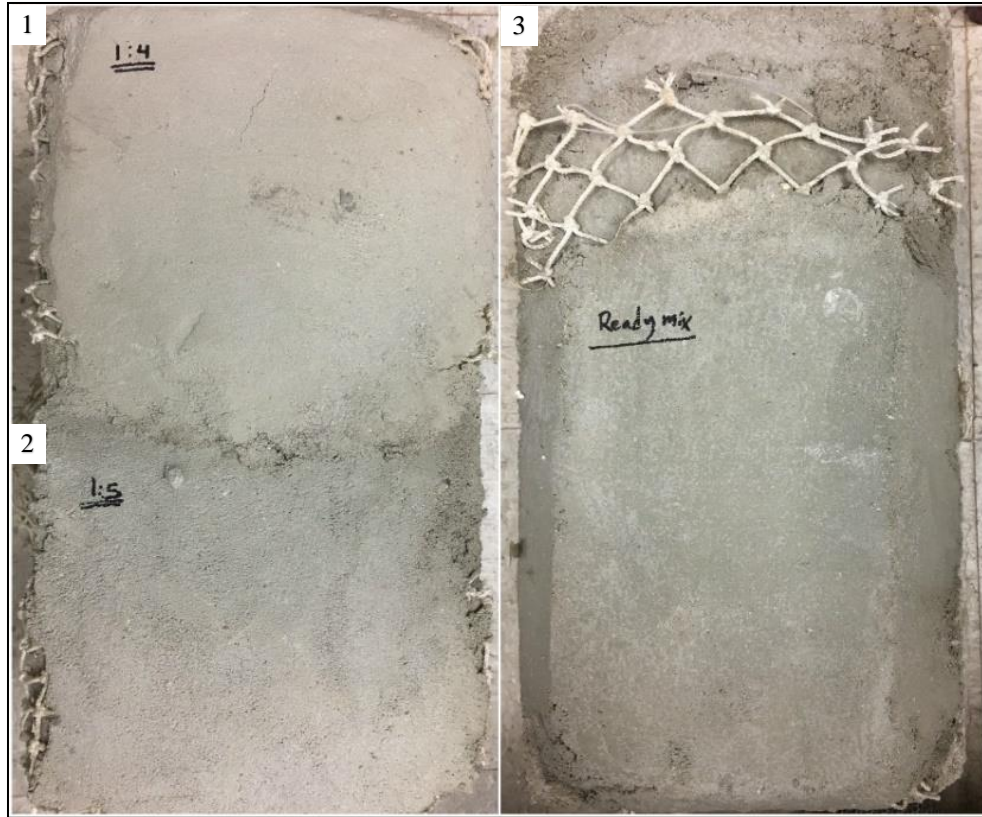
Figure 3.2 Overlay mortar samples after curing, (1) 1:4 Portland cement:sand, (2) 1:5 Portland cement:sand, and (3) ready-mix masonry mortar.
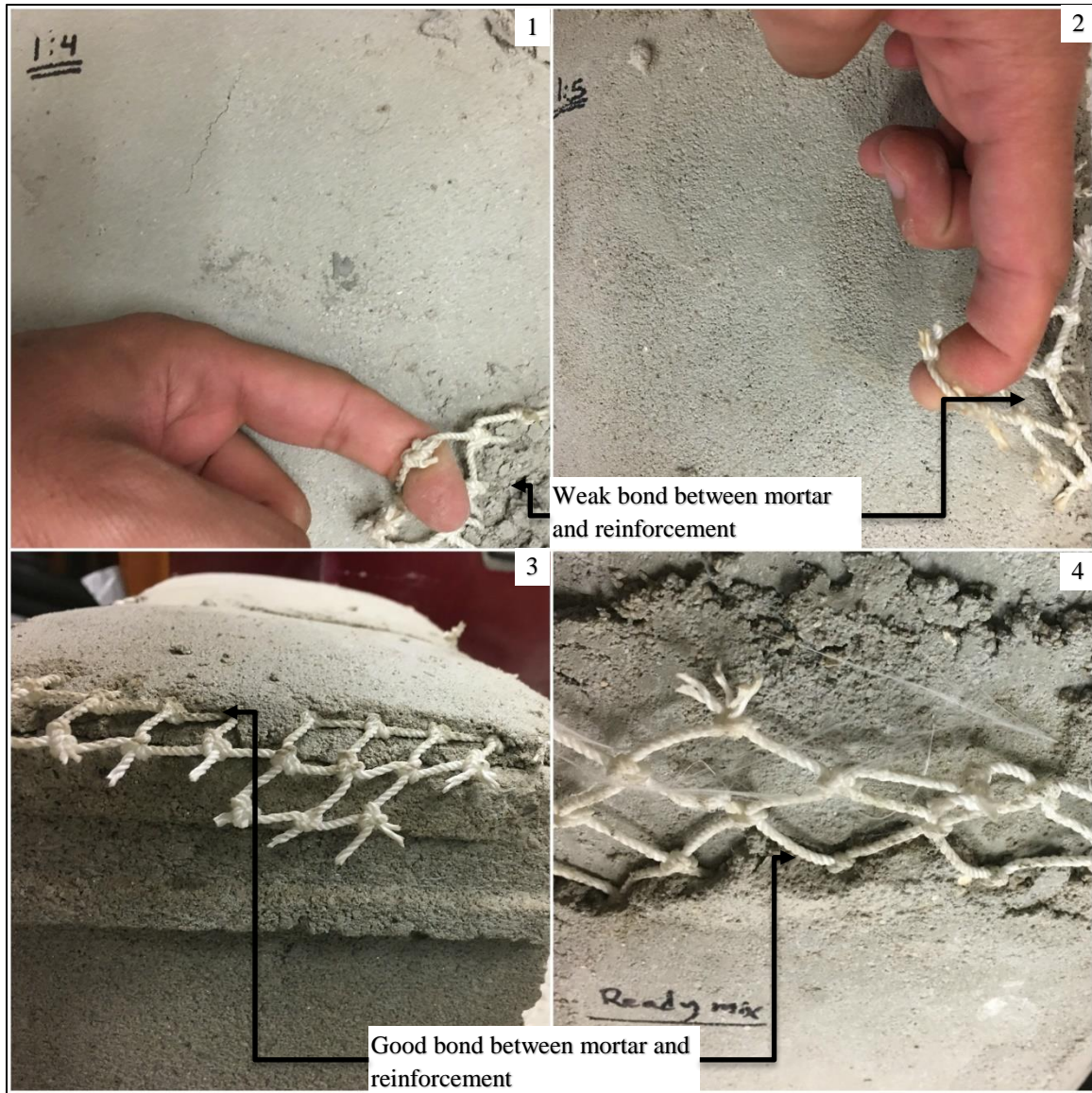
Figure 3.3 Overlay mortar assessment, (1) 1:4 Portland cement:sand, (2) 1:5 Portland cement:sand, and (3, 4) ready-mix masonry mortar are well bonded onto masonry block surface.

www.manaraa.com
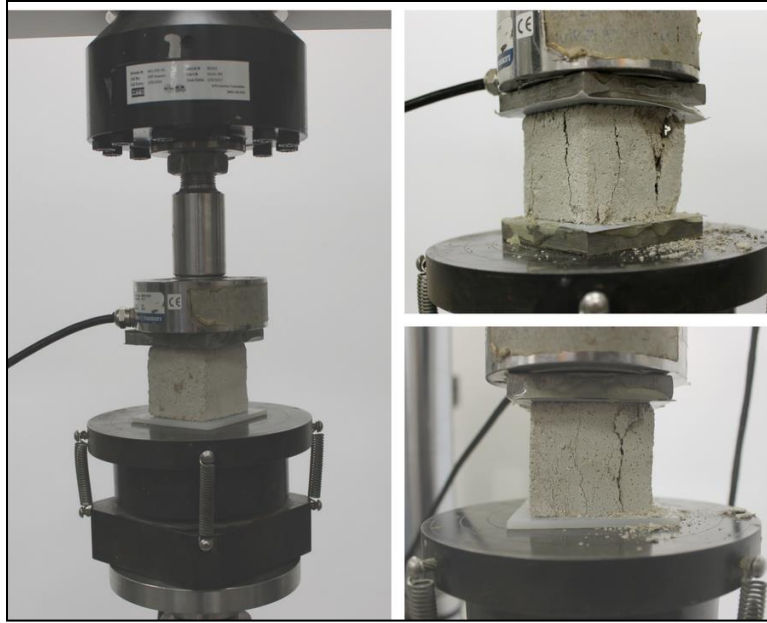
Figure 3.4 Mortar compression test setup (left), mortar cubes during testing (right).
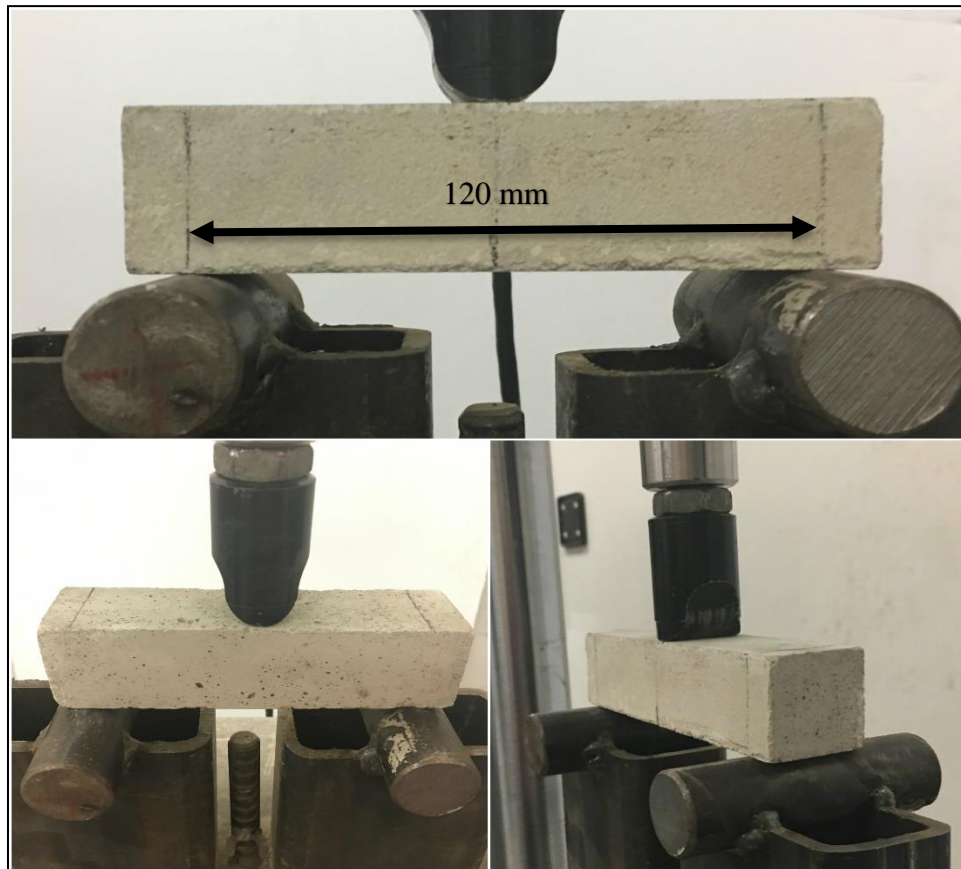
Figure 3.5 Mortar flexural test setup per ASTM C348 (ASTM 2014).

Figure 3.6 Concrete block (left) and block during compression test (right).

Figure 3.7 CM prism compression test setup per ASTM C1314 (ASTM 2003a).
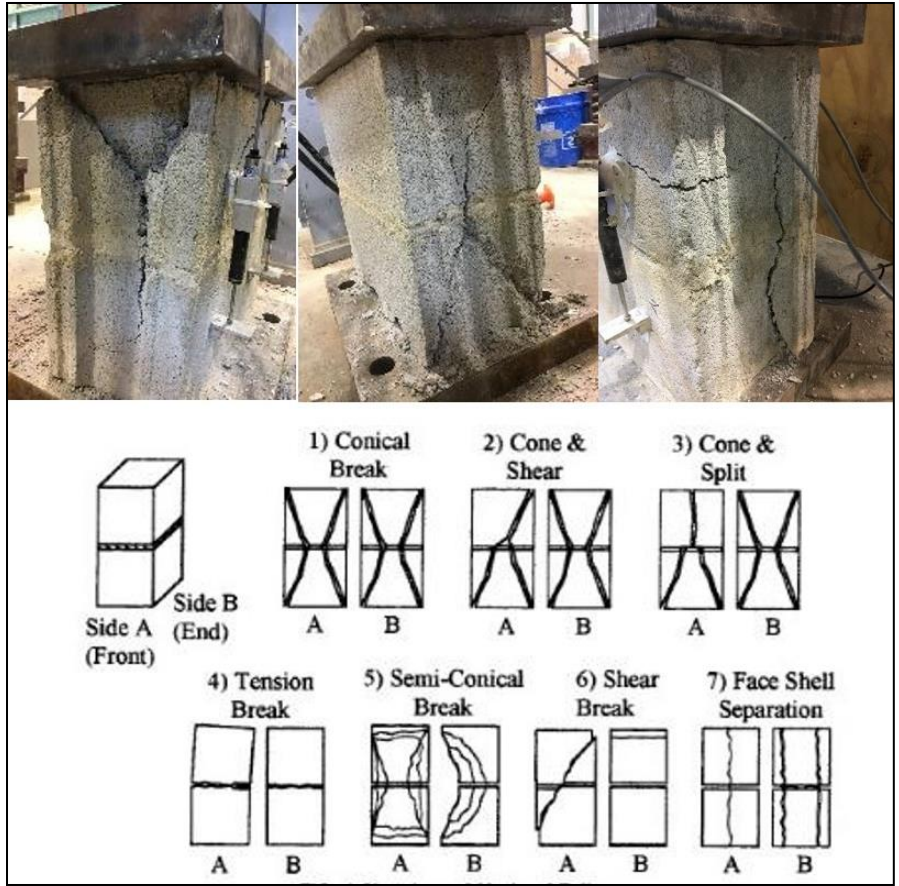
Figure 3.8 Common failure modes compared to ASTM C1314 standard (ASTM 2003a).
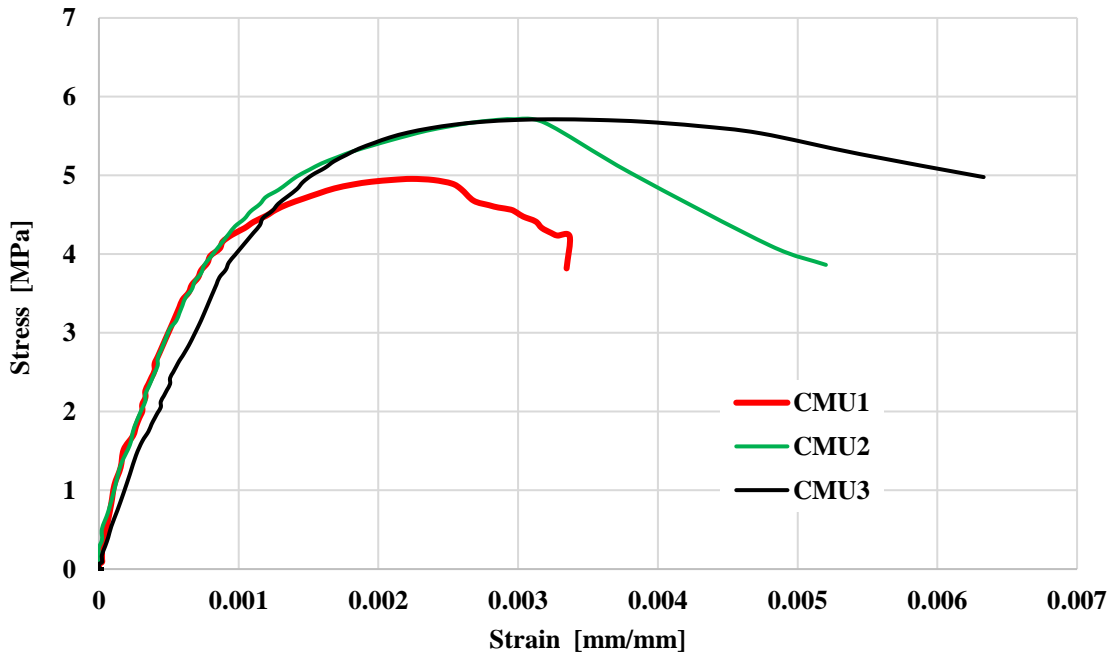
Figure 3.9 Uniaxial compressive stress-strain response of masonry prisms.

CHAPTER 4
COMPOSITE OVERLAY CHARACTERIZATION

Mortar reinforced with fishing nets (FN) as FRCM overlay was characterized by uniaxial tensile testing to determine tensile strength, deformation, and failure mechanisms. To this end, the interfacial bonding between the FN reinforcement and the mortar was investigated using a Scanning Electron Microscope (SEM).

4.1 Fiber Reinforced Cementitious Mortar (FRCM)

Composite materials are classified either by their matrix or reinforcement materials. FRCM composites fall in the category of brittle-matrix composites, similar to fiber-reinforced polymer (FRP) materials. The characteristic tensile behavior of polymer-matrix (FRP) and cement-matrix (FRCM) composites is illustrated in Figure 4.1.

Polymeric matrices, in general, have a high interfacial bond with the reinforcement which has a deformation capacity less than the matrix. Therefore, it is assumed that both the matrix and the reinforcement deform at the same rate.

Cement-based matrices have a relatively low tensile strength and cracking strain, with the reinforcement reaching higher strains (until failure) after the matrix cracks. Cement-matrix composites with continuous reinforcement have an essentially bilinear tensile stress-strain behavior. The first phase of the composite behavior mainly depends

45

on the matrix properties. The second phase mainly depends on the reinforcement properties and the quality of the bond between the reinforcement and the matrix.

4.2 Previous studies on FRCM

The mechanical properties of FRCM composites were studied by several researchers. For example, FRCM bonding to the concrete substrate or between the reinforcement and the matrix have been investigated (Ascione et al. 2015; Awani et al. 2015; Ombres 2015a; Sneed et al. 2014, 2015; D'Antino et al. 2014, 2015; D'Ambrisi et al. 2013b; D'Ambrisi et al. 2012, 2013a; Hashemi and Al-Mahaidi 2011). The uniaxial tensile behavior of FRCM composites was also studied (Arboleda et al. 2016; De Santis and De Felice 2015; Ascione et al. 2015; Bertolesi et al. 2014; de Felice et al. 2014; Mesaglio 2014; Olivito et al. 2014; Larrinaga et al. 2013; Contamine et al. 2011; Colombo et al. 2011). Structural strengthening with FRCM composites was studied for the flexural strengthening of concrete elements (Escrig et al. 2017; Ebead et al. 2015; El-Maaddawy and El Refai 2015; Jung et al. 2015; Babaeidarabad et al. 2014; Elsanadedy et al. 2013; Schladitz et al. 2012; Hashemi and Al-Mahaidi 2011; Ombres 2011; D'Ambrisi and Focacci 2011), flexural strengthening of masonry elements (Alecci et al. 2016; Kadam et al. 2014, 2015; Babaeidarabad et al. 2014; Shrestha et al. 2012; Vasconcelos et al. 2012; ; Rupika 2010; Briccoli et al. 2007; Foraboschi 2004), shear strengthening of concrete and masonry elements (Awani 2015; Ombres 2015b; Tetta et al. 2015; Babaeidarabad et al. 2014; Corradi et al. 2008), confinement (Colajanni et al. 2014; Trapko 2013; Triantafillou et al. 2006), seismic retrofitting (Kadam et al. 2015; Koutas et al. 2015; Ghorbani 2014; Sathiparan and Meguro 2013; Vasconcelos et al. 2012; Kolsch

46

1998), and more recently torsional strengthening of concrete members (Alabdulhady et al. 2017).

Other FRCM applications were also investigated including fire resistance (Donnini et al. 2017; Al-Salloum et al. 2016; Bisby et al. 2011), and thermal isolation of masonry walls (Triantafillou et al. 2017). The strengthening and isulation technique followed by Triantafillou et al. 2017 is illustrated in Figure 4.2.

4.3 Tensile behavior of FRCM

4.3.1 Gripping mechanisms

The properties of FRCM under tensile loads have been the focus of recent research studies. De Santis and de Felice (2015) studied the effects of different gripping mechanisms on the tensile behavior of FRCM composites. The gripping methods were classified into two groups.

The first group includes three test setups where the load is directly applied to the fabrics or the reinforcement. The first setup was realized by direct clamping of the ends of the textile to the gripping wedges and is shown in Figure 4.3a. The setup produced a premature failure in the textile fiber near the grip edges which lead to underestimating the ultimate tensile strength of the composite. The second setup provides an aluminum tab glued to the fabric to help to distribute the pressure and better stress transfer conditions. However, this method also suffers from fabric rupture near the mortar edge as shown in Figure 4.3b. The third setup was developed by protecting the reinforcement from initial failure by using an FRP reinforced epoxy resin applied to the textile. Then, an aluminum plate glued to the specimen's ends as shown in Figure 4.3c. This gripping method has not

produced any premature failure in the textile, and a full crack development was distinguished.

The second group is comprised of two gripping setups where the load is directly applied to the mortar instead of the textile. This method represents more realistic boundary conditions than the first method because the load transfers from the substrate to the mortar, not the reinforcement. The first setup includes clevis grips that produce a load transfer mechanism of adhesive tension and shear. Composite failure was observed by fiber slippage within the mortar because of the deterioration of the interfacial bond between mortar and fibers. The second setup consists of clamping grips where the mortar is clamped to the grips. Arboleda et al. (2016) studied the effect of boundary conditions on the tensile characteristics of the FRCM by implementing these two types of gripping methods, clevis and clamping grips as shown in Figure 4.4 (Arboleda et al. 2016).

4.3.2 Tensile behavior of FRCM composites

The tensile behavior of FRCM composites is typically idealized through a bilinear or trilinear stress-strain curve. The first part of the curve results from the initial elastic behavior of the uncracked section. The second phase arises from the mortar cracking and fiber slippage throughout the mortar which leads to a lower composite stiffness at the second phase. The clamping boundary conditions generate a further material phase beyond the multiple cracking stage. This behavior is illustrated in Figure 4.5a.

A similar composite behavior was observed by Larrinaga et al. (2013) where the tensile response was experimentally and numerically modeled (Larrinaga et al. 2013). The study included testing thirty-one composite coupons built of cement mortar and

48

reinforced with different layers (1, 2, 3, and 4) of basalt textile reinforcement. The specimens were tested under uniaxial tensile load using the clamping boundary conditions. The results of the experiment showed that FRCM composite exhibits a trilinear stress-strain behavior as shown in Figure 4.5b.

Arboleda et al. (2016) tested FRCM tensile coupons using two boundary conditions, clevis, and clamping. The clamped composites generated trilinear stress-strain behavior as shown in Figure 4.5a (Arboleda et al. 2016). The first phase represents the uncracked mortar behavior where the behavior is controlled by the mortar properties. The second phase starts with mortar cracking (multiple cracking stage), and the behavior is governed by the bonding characteristics between the reinforcement and the mortar. The last phase starts when all cracks are formed, leading the composite behavior to be controlled by the reinforcement properties. The layer effect was distinguished by increasing the composite stiffness, tensile strength, and the number of cracks.

Contamine et al. (2011) used a hinged clamping testing procedure to minimize the load eccentricity developed in the specimens which can result from reinforcement asymmetry or warping of the samples (Contamine et al. 2011). Multiple reinforcing materials have been employed which include E-glass, AR-glass, basalt, and Para-aramid. The composite specimens were manufactured using a thixotropic mortar which has an idle fresh viscosity. The composite behavior exhibited a similar behavior, a trilinear stress-strain, to those observed by Arboleda et al. (2016) and Larrinaga et al. (2013) as shown in Figure 4.5c.

Ascione et al. (2015) proposed a qualification procedure for the FRCM composite which combined the uniaxial tensile and shear bonding (Ascione et al. 2015). The method was implemented to five composites having four different materials (carbon, glass, basalt, and steel) and two types of mortars (lime and cement mortar) to account for various reinforcement and mortar types. The direct tensile test was performed by clamping the specimens between the wedges of the testing machine to allow full stress transfer of the specimen and prevent any slipping at the gripping area. This allows a complete response of the composite until reinforcement rupture. The composite tensile behavior was characterized by three stages, (I) uncracked, (II) crack development, and (III) cracked behavior and is shown in Figure 4.5d.

4.4 Experimental program

4.4.1 Tensile characterization of FRCM composite overlay

1. Test matrix: The composite behavior was characterized by using dog-bone shaped specimens tested under uniaxial tensile loads. The test matrix includes 15 specimens, with five groups of three specimens each. The parameters considered are the reinforcing material, the thread thickness, and the number of reinforcing layers. The mesh spacing was kept nominally similar for all specimens. The FN and WWSM specimens are designated by Ts-y-x and Ws-y-x respectively. The letters s, y, and x refer to the thread/wire size, number of layers, and specimens number, respectively. The control specimens are denoted as C-x.

2. Preparation: the composite specimens were prepared by casting in a dog-bone shape having dimensions illustrated in Figure 4.6. The dog-bone shape was used to prevent

50

mortar cracking outside the gauge length. The specimens were cast in acrylic molds and were demolded after 24 hours. The specimens were cast in layers that sandwiched the FN and WWSM reinforcement. The FNs were slightly pre-tensioned to reduce the stress differences among the threads. Figure 4.7 illustrates the casting process for a two-layer specimens. The specimens were cured using wet burlap for 28 days.

3. <u>Instrumentation</u>: The specimens were secured to the loading frame using pinned (clevis) grips (Arboleda et al. 2016). Four 3.0-mm thickness steel plates having a similar width to that of the specimen were inserted between the specimen and the steel grip surface, and epoxy bonded to the specimen surface. The adjacent plates on either side of the specimen were connected to each other by using bolts and clamps to prevent plates from bending or slipping as well as to prevent plate pulling out near the edges while loading as shown in Figure 4.8. Further, an intermediate steel plate with a 12.5 mm thickness was used to connect the plates to the grips as illustrated in Figure 4.9, using a 22-mm bolt. Two linear variable differential transformer sensors (LVDTs) with a 50 mm stroke were used to determine the specimen elongation. The LVDTs were placed on each face of the specimen as a means to monitor eccentricities. The nominal gauge length for all specimens was 93.75 mm. The specimen instrumentation is shown Figure 4.10.

4. <u>Testing procedure</u>: The composite specimens were mounted to the same test frame used for tensile testing of the FN and WWSM materials. After the sample was mounted to the machine, the test was performed under displacement control mode at a rate of 0.2 mm/sec. The data was recorded by using a data acquisition system with a frequency of 100 Hz. Figure 4.11 shows the sequence of the testing procedure.

4.4.2 Test results

Table 4.1 provides the types, number of specimens, maximum tensile load, and deformation of the composite specimens. The tensile stress, strain, and the elastic modulus are provided in   Table 4.2. The tensile tests were performed on unreinforced and reinforced dog-bone specimens. The reinforced specimens had 1 layer of #15 FN, 1 layer of #21, 2 layers of #21 FN, and 1 layer of 19-gage WWSM reinforcement. Figure 4.12 through Figure 4.16 show the load-displacement response of the dog-bone specimens. The strength per unit length of representative specimens is presented in Figure 4.17. Table 4.3 and Figure 4.18 present the load carrying capacity and the strength of the composites vis-à-vis that of the stand-alone reinforcement. Material strength per unit length was provided by Table 2.4 (Chapter 2). Figure 4.19 shows the cracking behavior of the tested specimens. Also, Figure 4.20 through Figure 4.25 show the thread-mortar interfacial bonding observation by SEM imaging. Finally, Figure 4.26 through Figure 4.30 show the stress-strain response of the dog-bone specimens.

4.4.3 Discussion of results

1. <u>Load</u>: Figure 4.17 shows the load-deformation response of the FN and WWSM composites where the initial load peak represents the mortar load carrying capacity. The second part represents the cracked response. It is noted that the FN carrying capacity is comparable to that of the WWSM, because of the larger area of the FN threads compared to the steel wires as shown in Table 4.3. Also, both the FN and WWSM reinforcements produce higher FRCM composite capacity than the stand-alone reinforcing material. The load enhancement is attributed to (1) the mortar contribution to more uniformly

52

distributing the load to the FN threads and the steel wires, (2) the mesh confinement, and (3) the prevention of the unraveling of the knots in the case of the FN reinforcement.

2. <u>Deformation and cracking</u>: Figure 4.17 shows that the FN-FRCM composite has a much higher deformation capacity than WWSM. The FN reinforcement can stretch almost (30-50) times longer than the WWSM. The reason for the high deformation capability of FN lies in the mesh structure and flexibility. Also, each FN thread is composed of multiple twisted sub-threads which allow them to slip among each other under tension forces. Moreover, the presence of the knots, which are an extra length lumped in a small volume, are contributing to mesh deformation. The FN and WWSM materials tested alone have even higher displacement, almost four and nine times of their corresponding composites, respectively. The mortar embedment of the reinforcement mesh contributes to reducing the deformation of the reinforcement in the case of the composite. The cracking behavior of all specimens consists of only one crack that formed in the middle region of the specimen as shown in Figure 4.19.

4.4.4 Interfacial bonding

The observation of the interfacial bonding between the reinforcement and the mortar at the cracked section (Section A in Figure 4.6) is based on SEM imaging. The FN thread has shown a good mechanical interlocking to the mortar because of the porous surface and surface irregularity of the twisted multifilament thread as shown in Figure 4.20. However, the FN thread does have slippage that results from the knot tightening as shown in Figure 4.21. Figure 4.22 shows the SEM image of the steel wire embedded in the mortar at the cracked section (section A in Figure 4.6). The steel wire seems

disengaged from the mortar upon failure. Wire disengagement is attributed to yielding of the steel wire, As highlighted by the reduced area of the wire at the cracked section as shown in Figure 4.23. Further observation of mortar bonding to FN threads and WWSM wires was done by taking another section (section B in Figure 4.6) at a distance of 12.5 mm from the cracked section. The process is done by cutting the specimen to examine if there is any indication of slippage. Figure 4.24 shows the FN thread-mortar interface both longitudinally and at cross section B, where there is a good embedment in mortar. The steel wire at section B appears well embedded in the mortar and the wire-mortar interface indicates no disengagement as shown in Figure 4.25.

4.4.5 Stress-strain behavior

The tensile stress-strain behavior of the dog-bone composite specimens reinforced with FNs and WWSM are shown in Figure 4.26 through Figure 4.30. Also, Table 4.2 provides the stress at failure, nominal strain, and elastic modulus of the #15 FN, #21 FN, and 19 gauge WWSM dog-bone specimens.

1. Stress: The stress-strain response of the FN-FRCM composites is initially assumed as bilinear which can be distinguished by (blue-green), and (grey-white) regions for the first and second part, respectively, as shown in Figure 4.27 through Figure 4.29. The first part of the curve has two phases that are distinguished by blue for the first phase and green for the second phase. The blue region represents the uncracked mortar response. The mortar tensile strength is small compared to the reinforcement tensile strength and cannot be distinguished from the second part of the curve. The second phase (green region) represents the reinforcement response at low tensile loads. The second phase of the first

part of the curve has higher stiffness than the second part of the curve due to the negligible thread slippage from the knot. The second part of the curve (grey-white region) also has two phases that cannot be distinguished by a specific point. Therefore, the transition region has been marked by two gradient colors. The initial phase of the third part has a lower stiffness than the first part of the curve due to the (1) progressive slippage of the threads through the knots as the load increases, (2) stress redistribution, and (3) knot tightening. The second phase has even lower stiffness than the initial phase because of the combined effect of slippage and the partial thread failure. After the partial thread failure is initiated, it is followed by a progressive thread failure. The composite behavior during testing is illustrated in Figure 4.11.

2. Strain: The composite strain is considered as a nominal value because the reinforcement deformation of the FN results from multiple factors such as the knot slippage, twisted thread filaments, and mesh flexibility. It is noticed that the strain value of the reinforcement as a composite is less than the strain of the reinforcing material when tested alone. The strain reduction is due to the mortar contribution which is obtained by confining the reinforcement. Moreover, the thread size influences the deformation capacity of the composite, where the bigger the size, the higher the deformation value. The thread size effect results from two components. The first factor results from the twisted thread structure, where the bigger the thread size, the longer length of its filaments. The second factor results from a larger area of the core not contacting the mortar in the case of the bigger thread size.

55

Tables:

Table 4.1 Maximum tensile strength and deformation of composite reinforcement.

Specimen type	Ultimate tensile strength, kN	Average, kN (SD)	Maximum deformation, mm	Average, mm (SD)
C-1	1.87		0.29	
C-2	2.95	2.89 (±0.81)	0.50	0.36 (±0.09)
C-3	3.87		0.30	
T15-2-1	2.00		16.4	
T15-2-2	1.63	1.76 (±0.17)	17.3	15.6 (±1.74)
T15-2-3	1.64		13.2	
T21-1-1	1.80		31.4	
T21-1-2	1.73	1.81 (±0.07)	22.6	27.5 (±3.68)
T21-1-3	1.90		28.6	
T21-2-1	2.81		29.4	
T21-2-2	2.84	2.93 (±0.15)	28.9	28.3 (±1.22)
T21-2-3	3.14		26.6	
W19-1-1	2.51		0.68	
W19-1-2	2.52	2.45 (±0.09)	0.50	0.60 (±0.08)
W19-1-3	2.32		0.61	

Table 4.2 Tensile characteristics of dog-bone specimens.

Specimen type	Tensile stress at transition point[1] f_a, MPa	Ultimate tensile stress f_u, MPa	Tensile strain at transition point[2], ε_a %	Ultimate tensile strain, ε_u, %	Modulus of elasticity E, MPa, E_1[3], E_2[4]	
C-1				0.18		
C-2	-	1.5 (±0.42)	-	(±0.05)	737.3 (±233)	
C-3						
T15-2-1				16.67		
T15-2-2	19.5	153.9 (±14.6)	1.05	(±1.85)	1852 (±620)	858 (±118)
T15-2-3						
T21-1-1				23.4		
T21-1-2	9.5	155 (±5.0)	0.50	(±3.8)	1900 (±218)	660 (±57)
T21-1-3						
T21-2-1				16.7		
T21-2-2	37	120.0 (±5.97)	1.10	(±1.3)	3177 (±80)	600 (±15)
T21-2-3						
W19-1-1				0.64		
W19-1-2	-	631.2 (±40.4)	-	(±0.1)	4464 (±265)	
W19-1-3						

1. The stress values (f_t) at the point where the slope changes are ranging between (9.5-37) MPa.
2. The strain values (ε_t) at the point where the slope changes are ranging between (0.5-1.1)%.
3. Initial slope of the stress-strain curve.
4. The slope of the cracked specimens.

56

Table 4.3 Tensile strength per unit length of FN and WWSM materials and their corresponding dog-bone specimens.

Reinforcement material	Number of layers	Thread size (diameter, mm)	Area of reinforcement per unit length, mm²/m	Material tensile strength, kN/m	Composite tensile strength, kN/m
FN	2	#15 (1.20±0.02)	150	20.6 (±0.61)	23.5 (±2.29)
FN	1	#21 (1.75±0.03)	160	17.5 (±1.77)	24.1 (±0.93)
FN	2	#21 (1.75±0.03)	320	35.1 (±3.55)	39.1 (±1.99)
WWSM	1	#19 (0.89±0.02)	50	21.9 (±5.70)	32.7 (±1.23)

Figures:
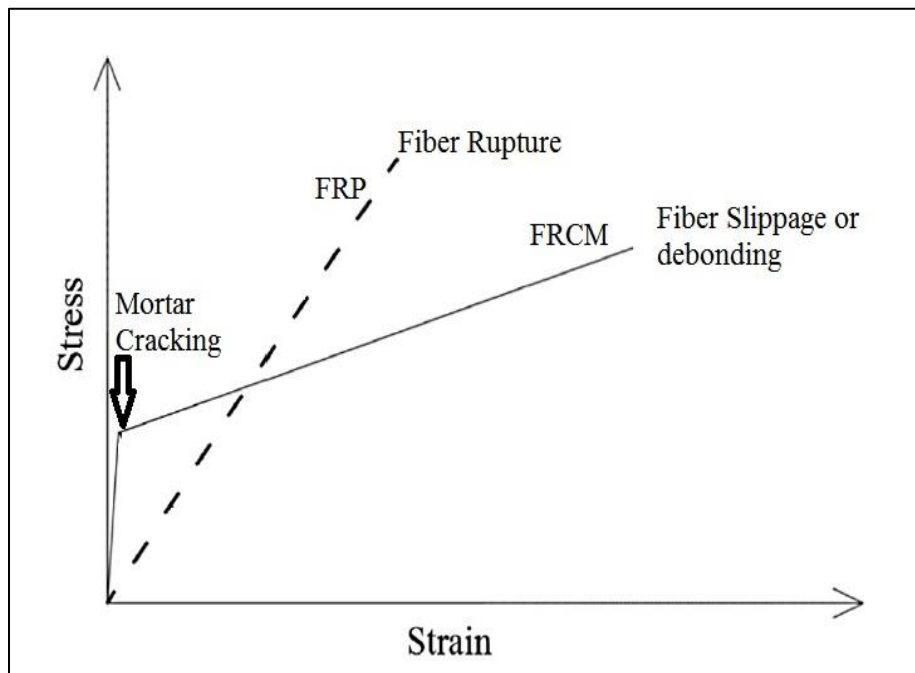
Figure 4.1 Characteristics behavior of FRCM and FRP composites (Awani et al. 2017).
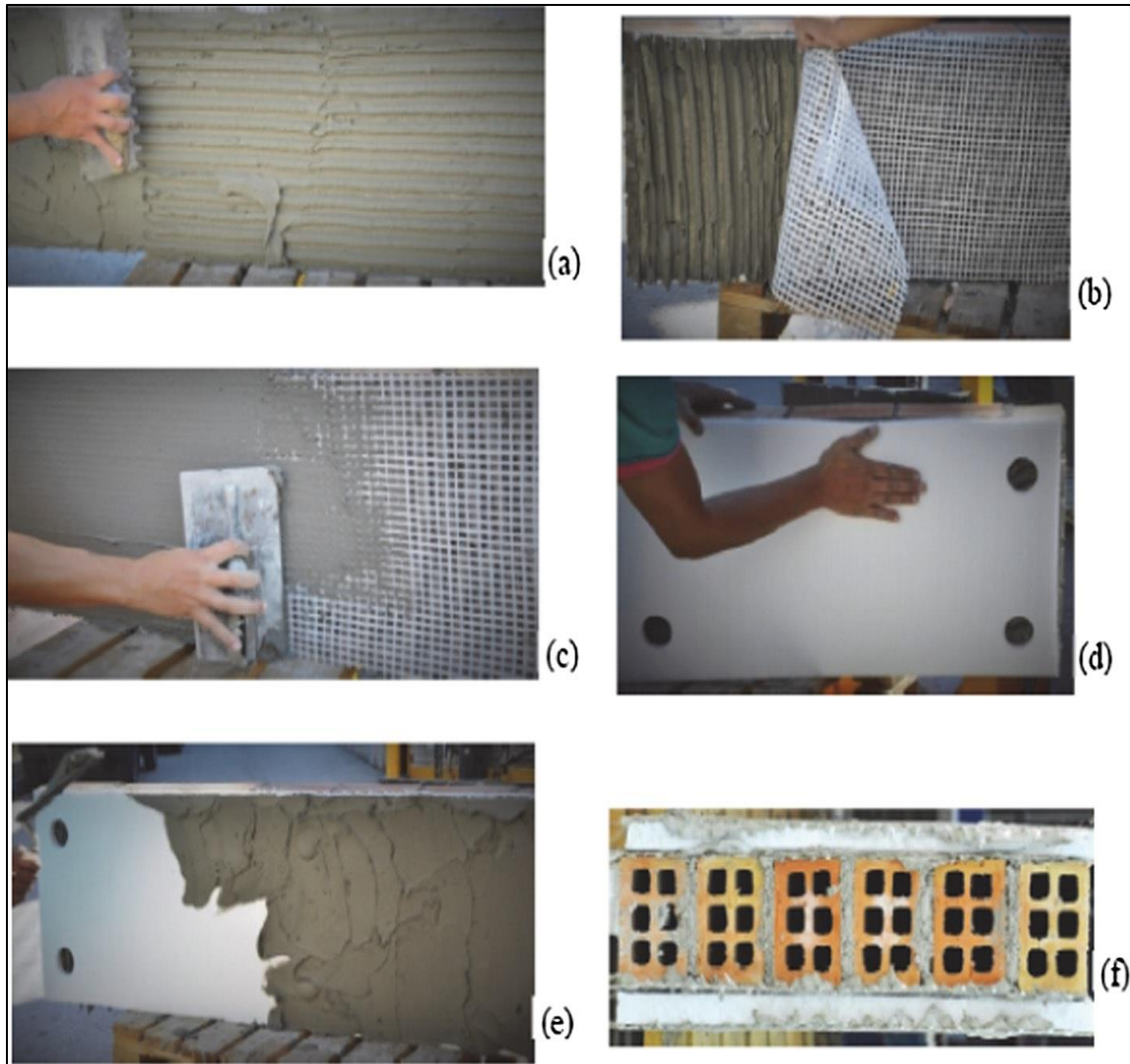
Figure 4.2 Application method of FRCM made of glass fiber textile together with insulation material on masonry surface, (a) application of the base layer, (b) textile application, (c) textile impregnation, (d) application of the insulation material, (e) application of the top mortar layer, and (f) masonry cross section after overlaying (Triantafillou et al. 2017).
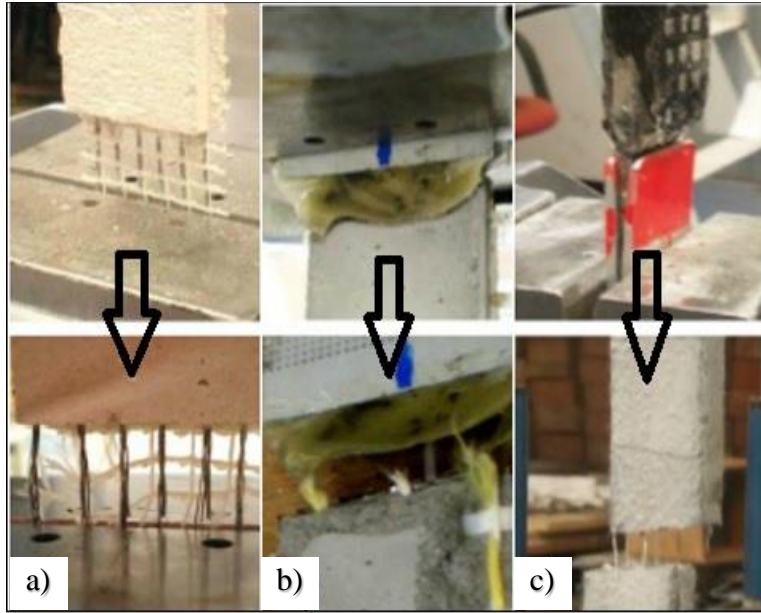
Figure 4.3 (a) Direct clamping of textile (textile rupture), (b) aluminum tabs glued to textile ends (textile rupture), and (c) aluminum tabs glued to FRP reinforced ends (mortar cracking, satisfactory failure pattern) (De Santis and de Felice 2015).
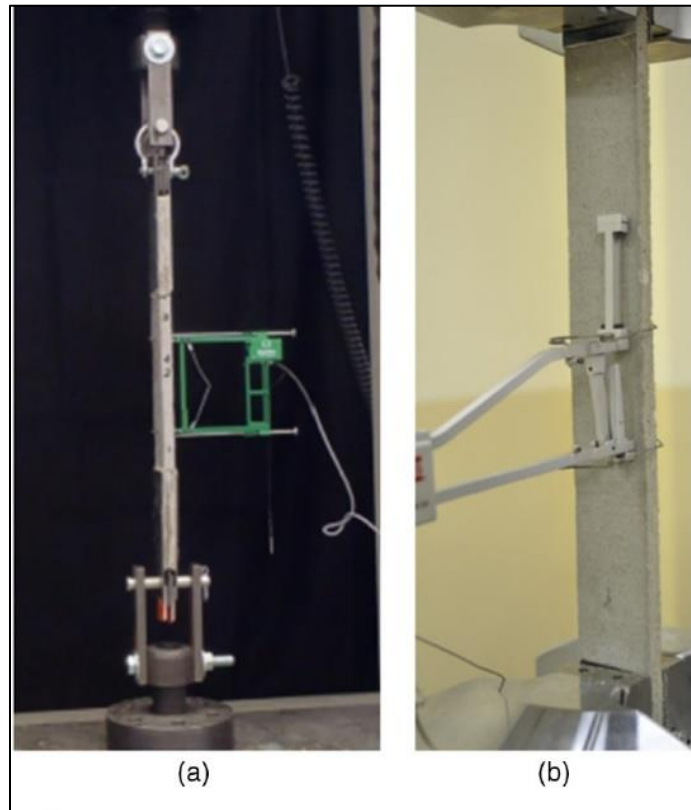
Figure 4.4 Gripping mechanisms of FRCM composite (a) clevis grip, (b) clamping grip (Arboleda et al. 2016).
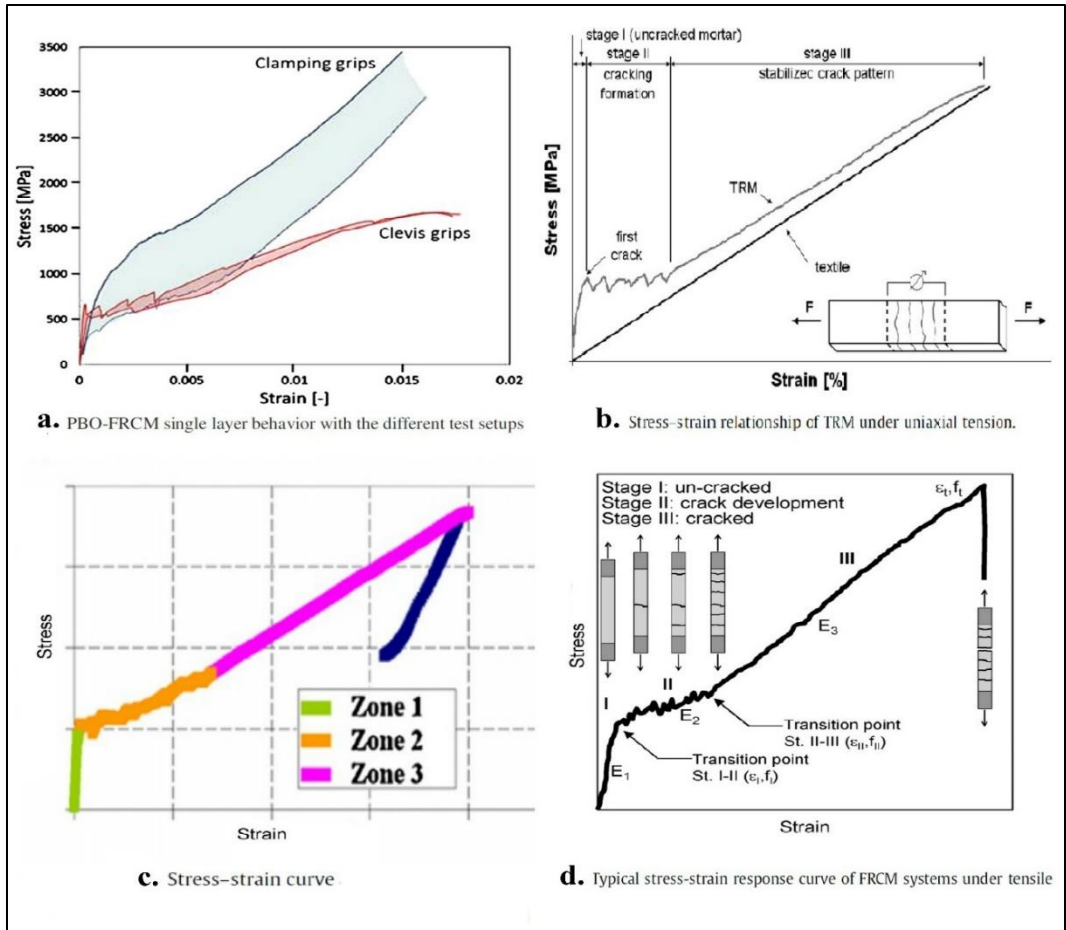
Figure 4.5 Tensile behavior of FRCM composite, (a) Arboleda et al. (2016), (b) Larrinaga et al. (2013), (c) Contamine et al. (2011), (d) Ascione et al. (2015).
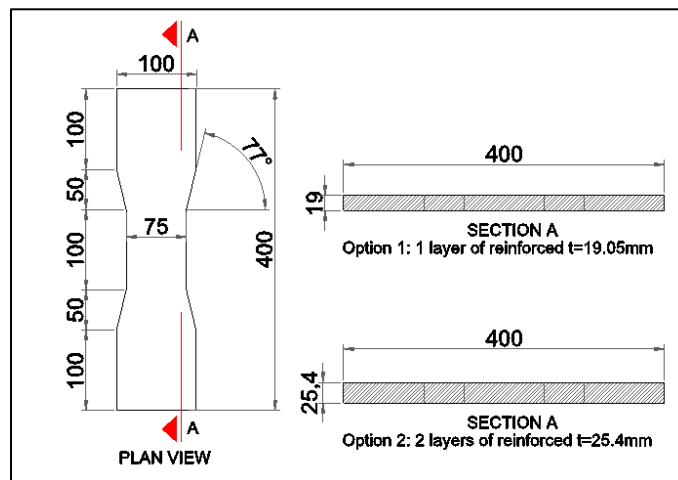
Figure 4.6 Dog-bone specimen dimensions (mm).
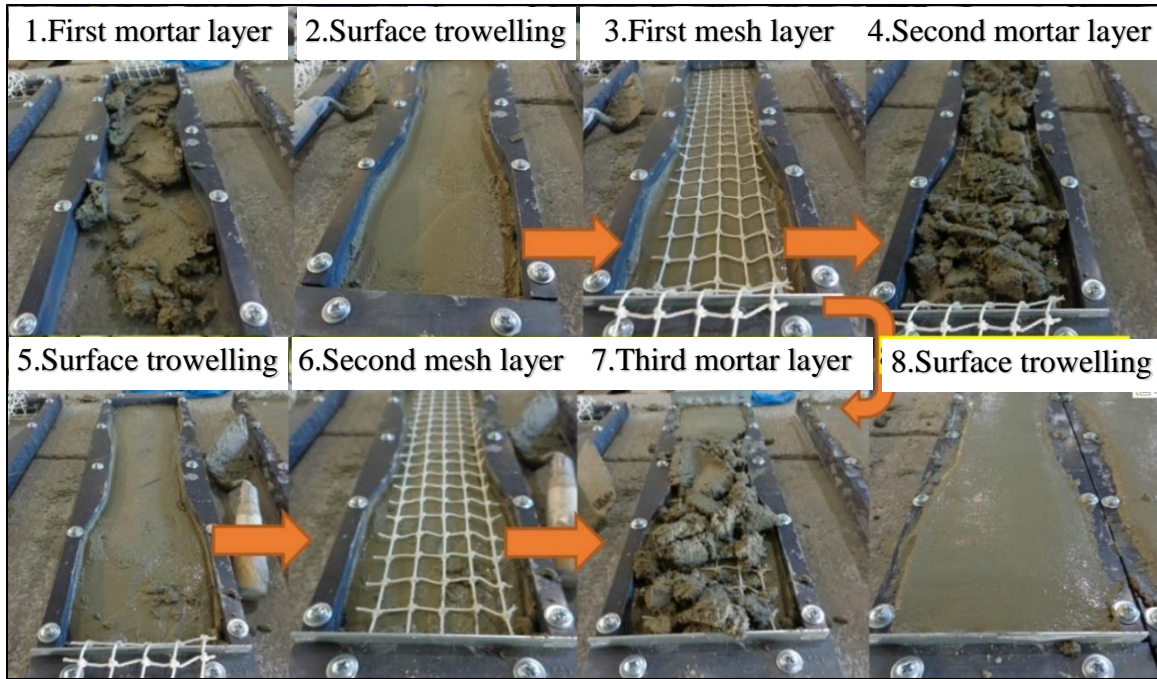
Figure 4.7 Casting procedure for dog-bone specimens.
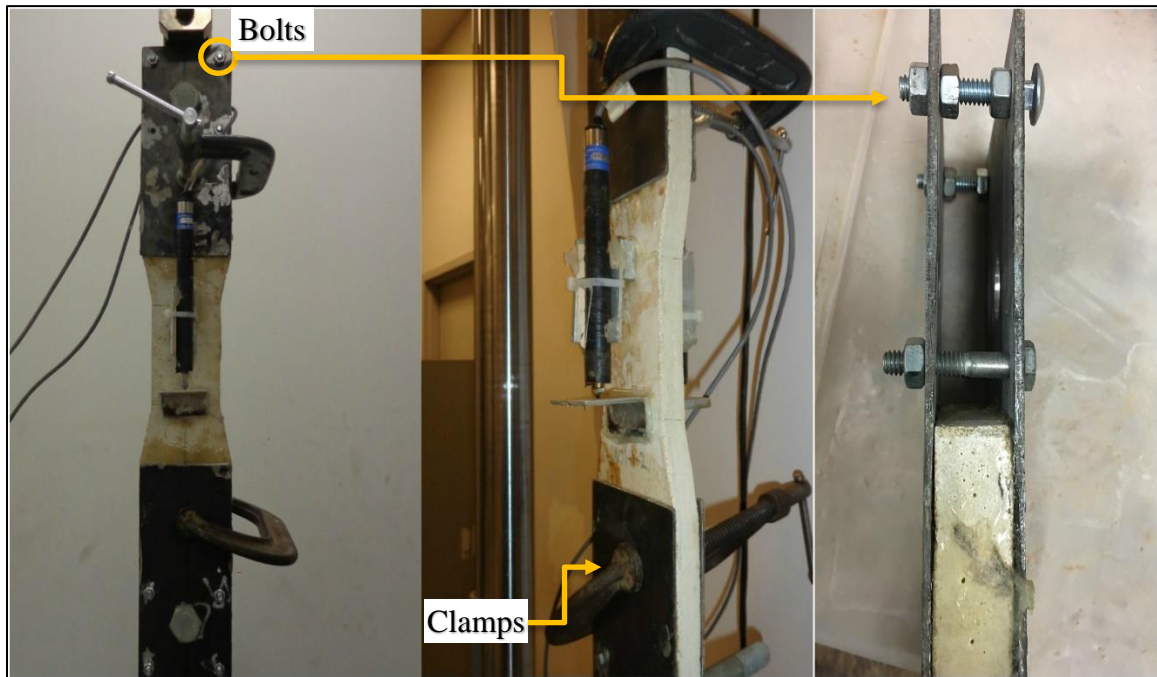
Figure 4.8 Plate connections to prevent slipping and bending.
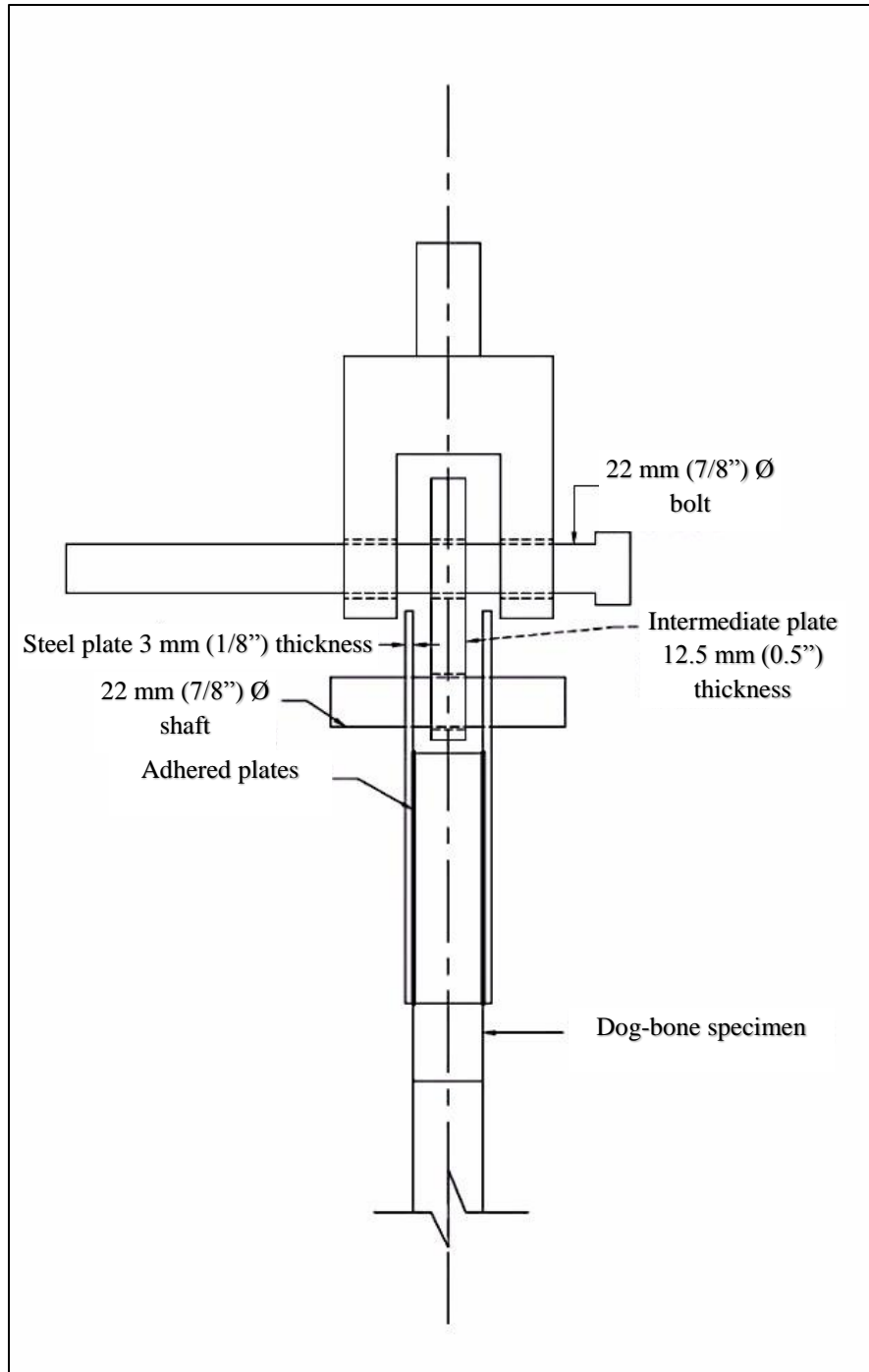
Figure 4.9 Gripping mechanism for dog-bone specimens.
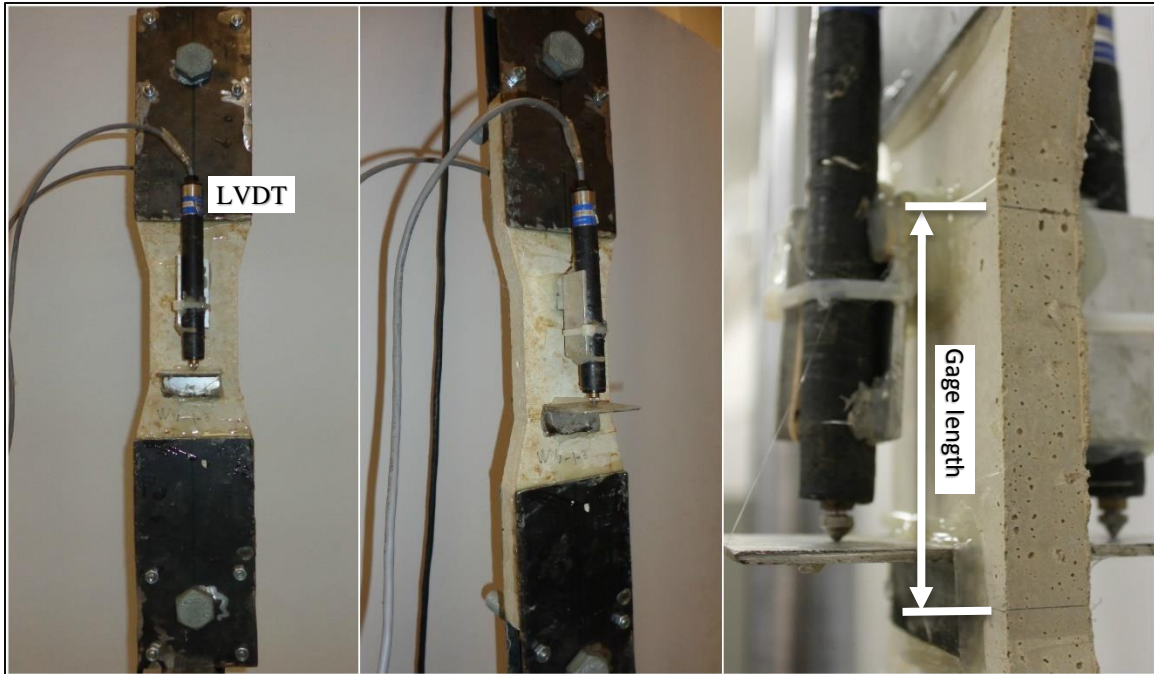
Figure 4.10 Tensile test instrumentation.
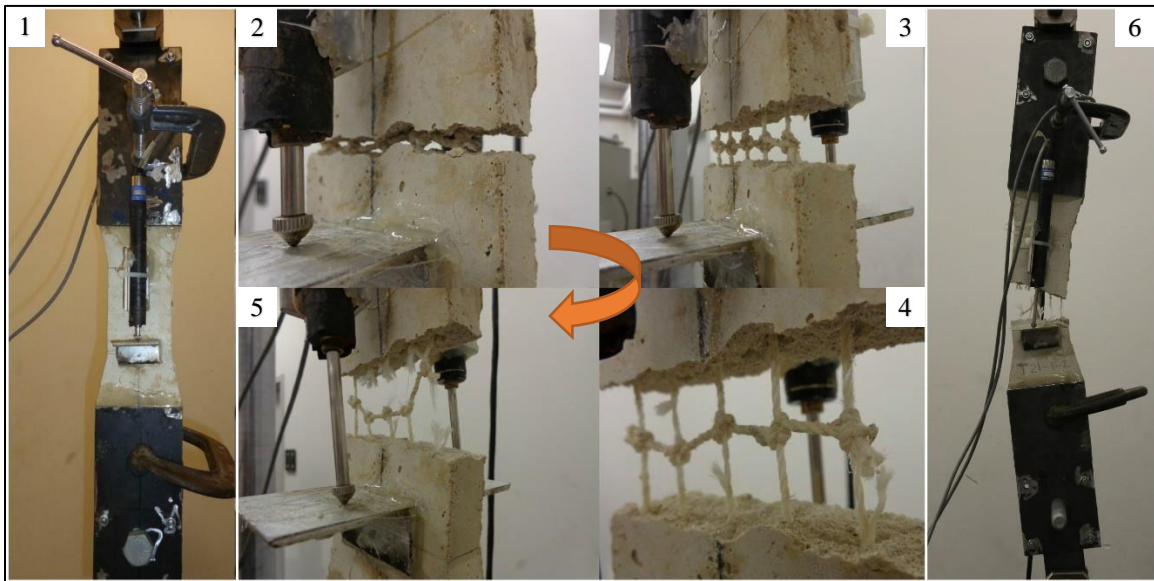
Figure 4.11 Dog-bone composite specimen during testing (#21 FN, 1 layer), (1)
uncracked specimen, (2) mortar cracking, (3) crack expansion, (4) partial thread failure,
(5) complete thread failure, and (6) failed specimen.
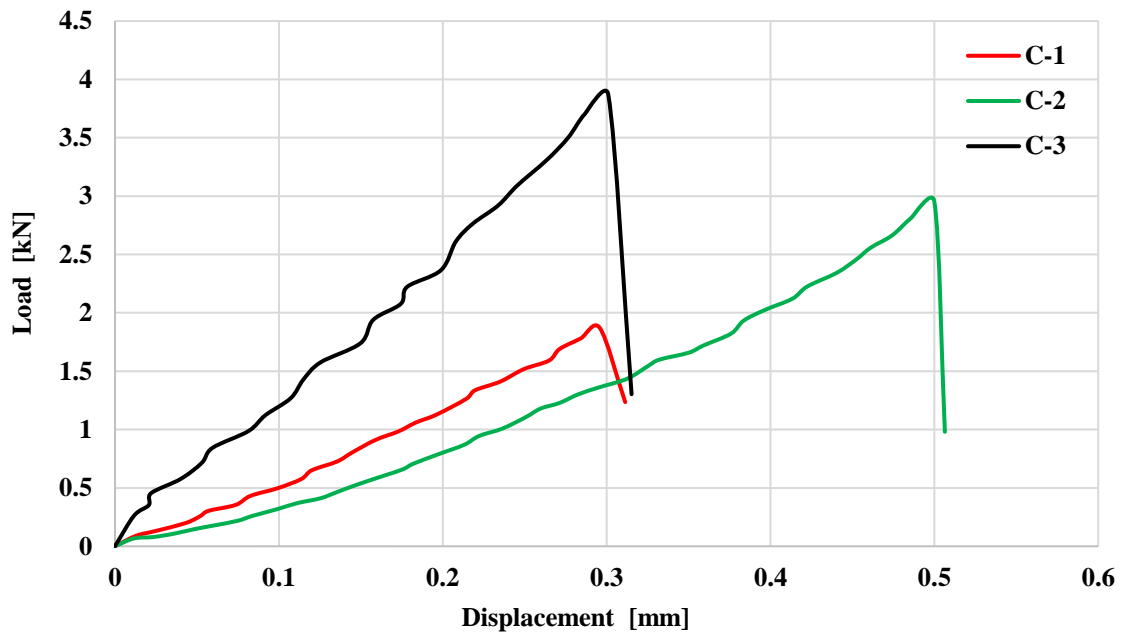
Figure 4.12 Load-displacement tensile response of control (unreinforced) mortar dog-bone specimens.
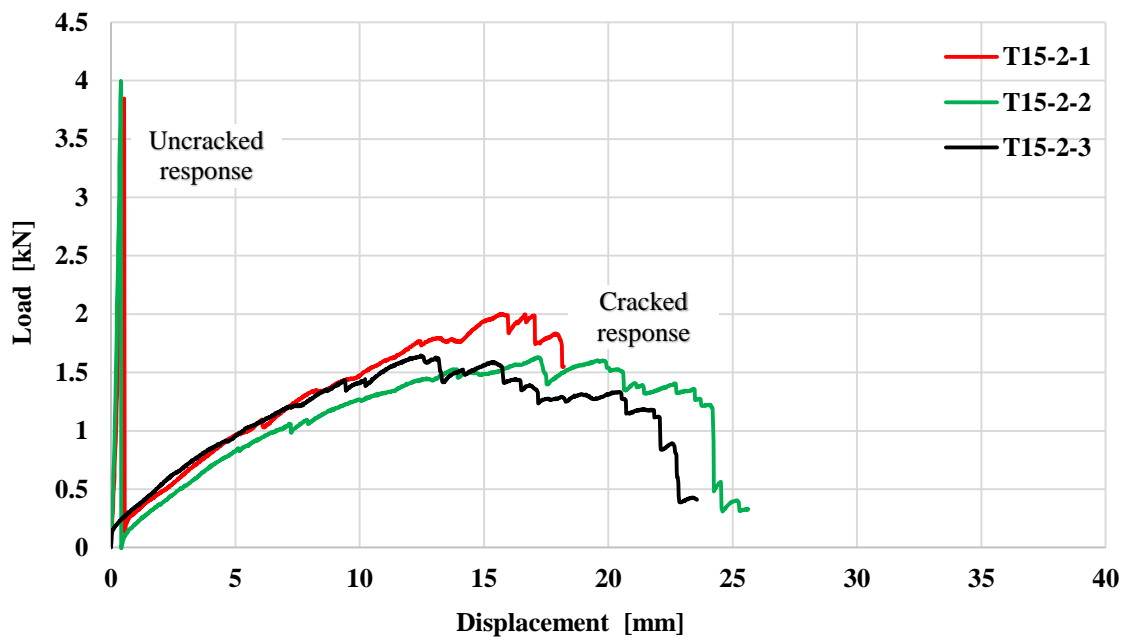
Figure 4.13 Load-displacement tensile response of #15 (2 layers) FN-FRCM dog-bone specimens.

64
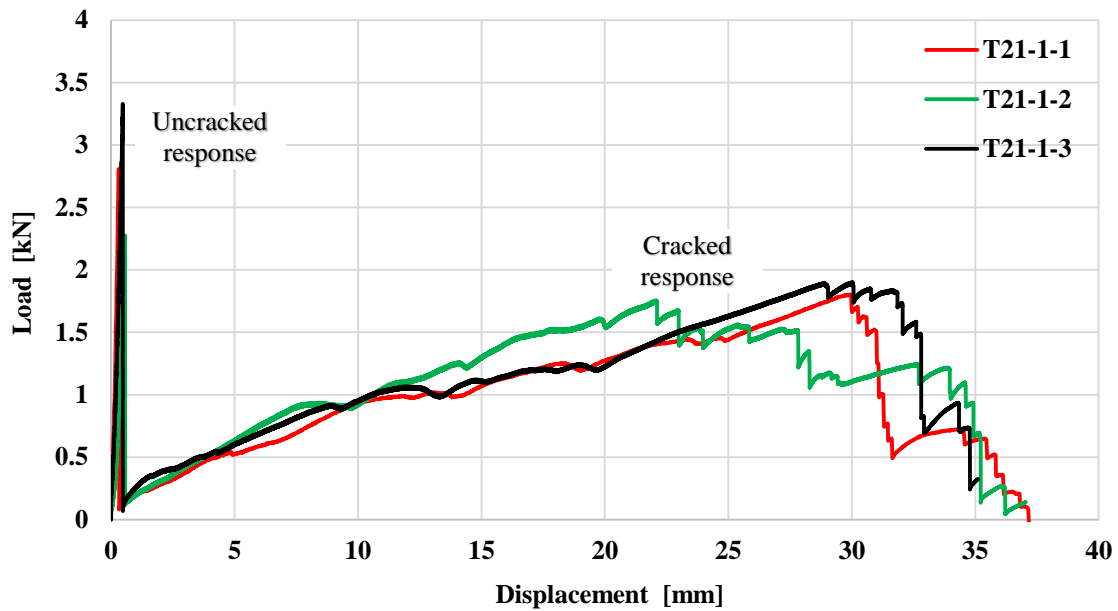
Figure 4.14 Load-displacement tensile response of #21 (1 layer) FN-FRCM dog-bone specimens.
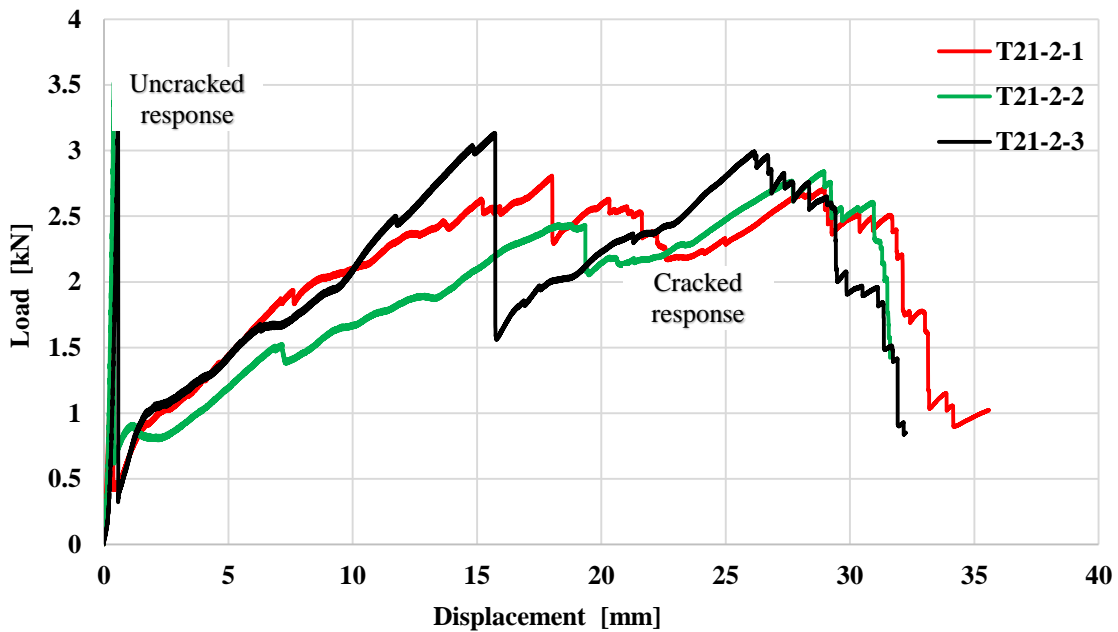
Figure 4.15 Load-displacement tensile response of #21 (2 layers) FN-FRCM dog-bone specimens.

65
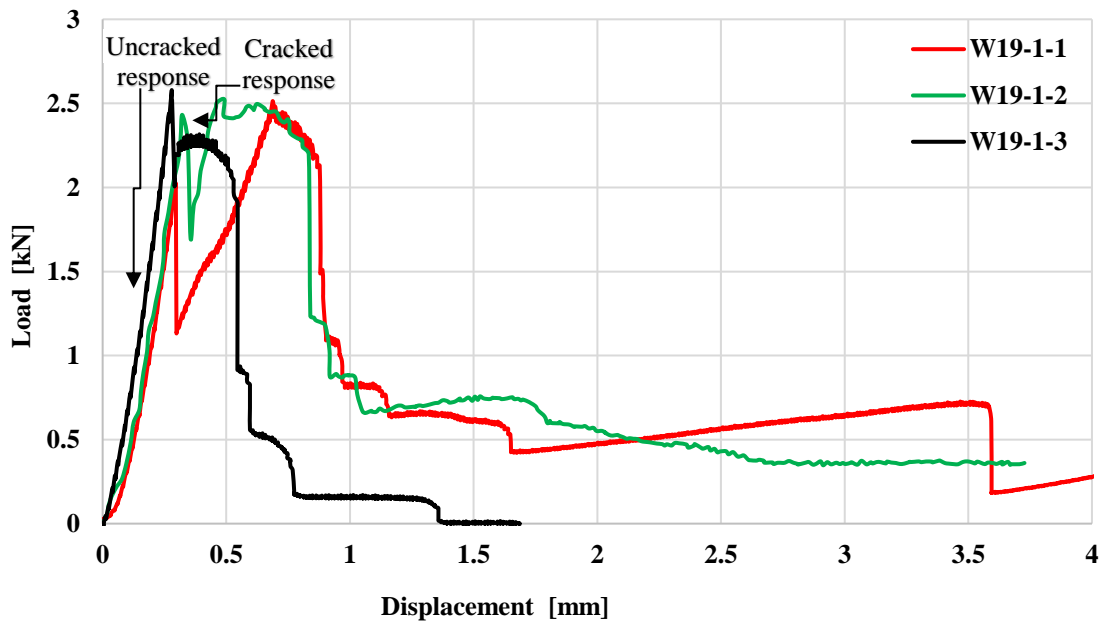
Figure 4.16 Load-displacement tensile response of 19-gage (1 layer) WWSM reinforced mortar dog-bone specimens.
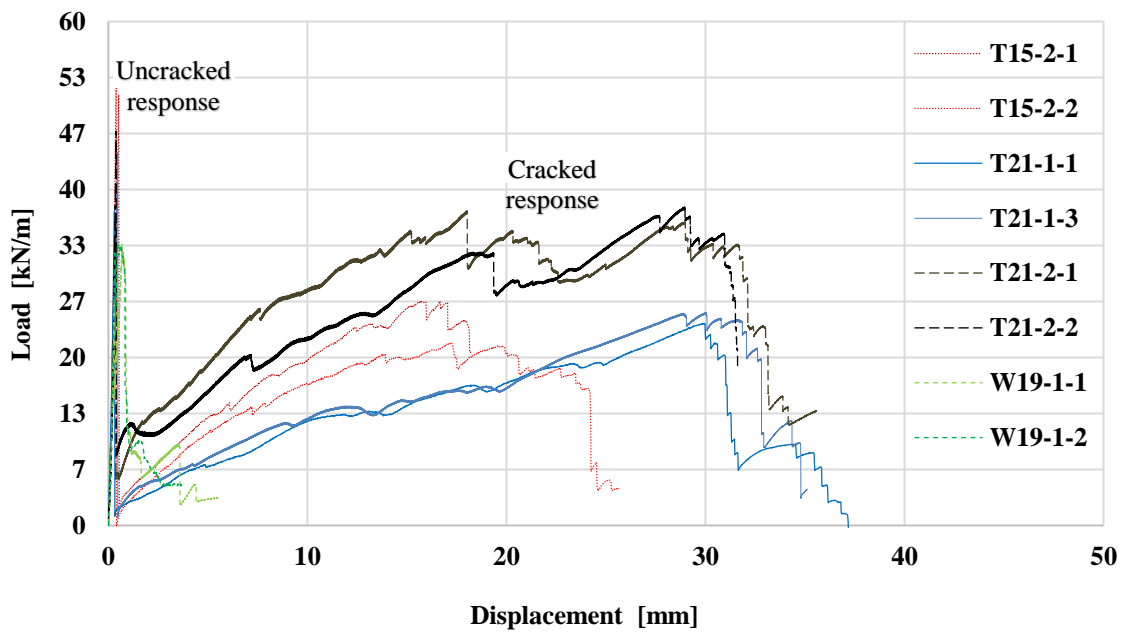
Figure 4.17 Load-displacement tensile response of representative FN and WWSM reinforced composite specimens.
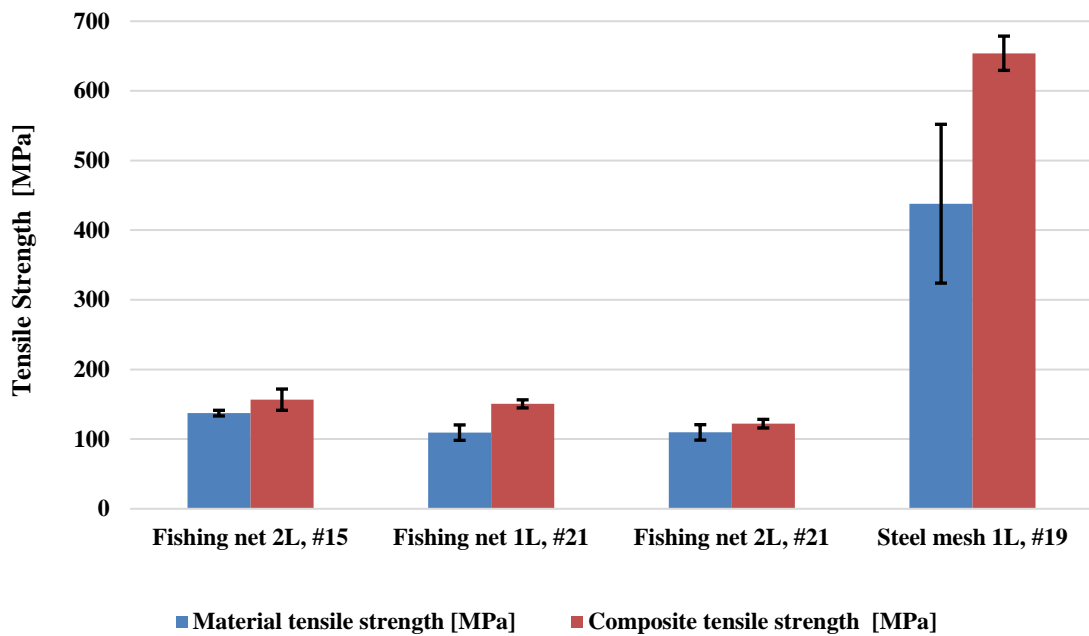
Figure 4.18 FN and WWSM material and composite tensile strength.
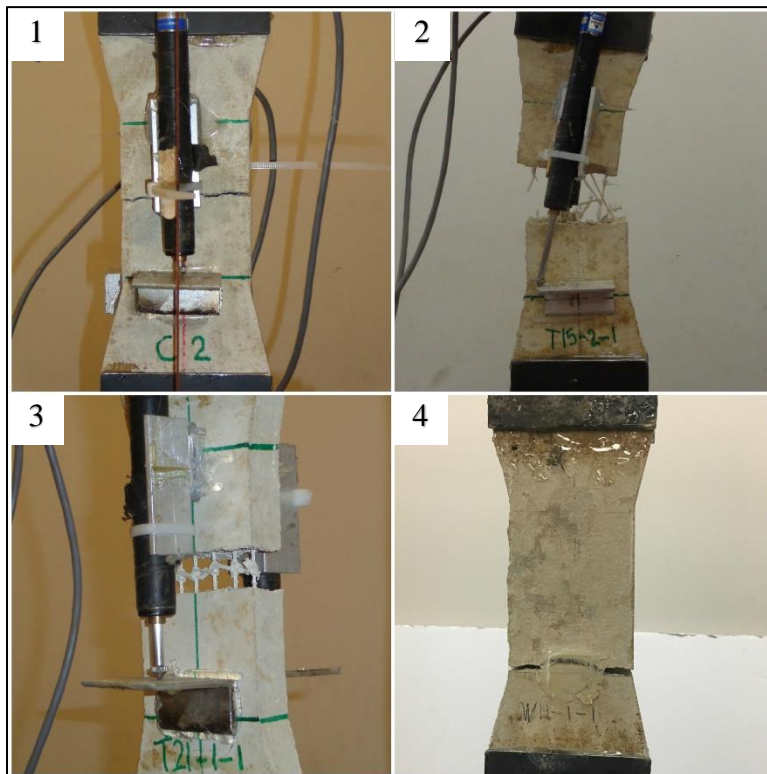
Figure 4.19 Dog-bone cracking behavior (1) control, (2) #15 FN, (3) #21 FN, and (4) WWSM.
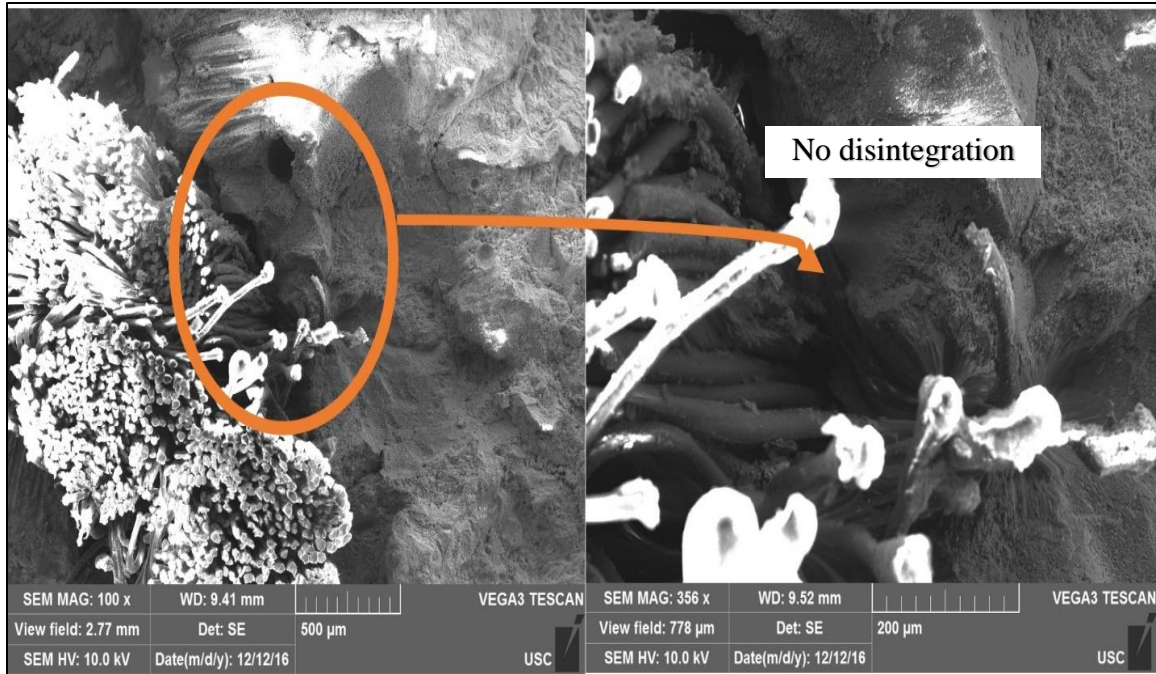
Figure 4.20 SEM micrograph showing FN thread embedment by mortar: (left) top view of cracked section, (right) close-up of thread-mortar interface.

Figure 4.21 FN thread slippage from knot at cracked section.

SEM MAG: 122 x | WD: 9.37 mm | 500 μm | VEGA3 TESCAN
View field: 2.27 mm | Det: SE | |
SEM HV: 10.0 kV | Date(m/d/y): 12/09/16 | | USC
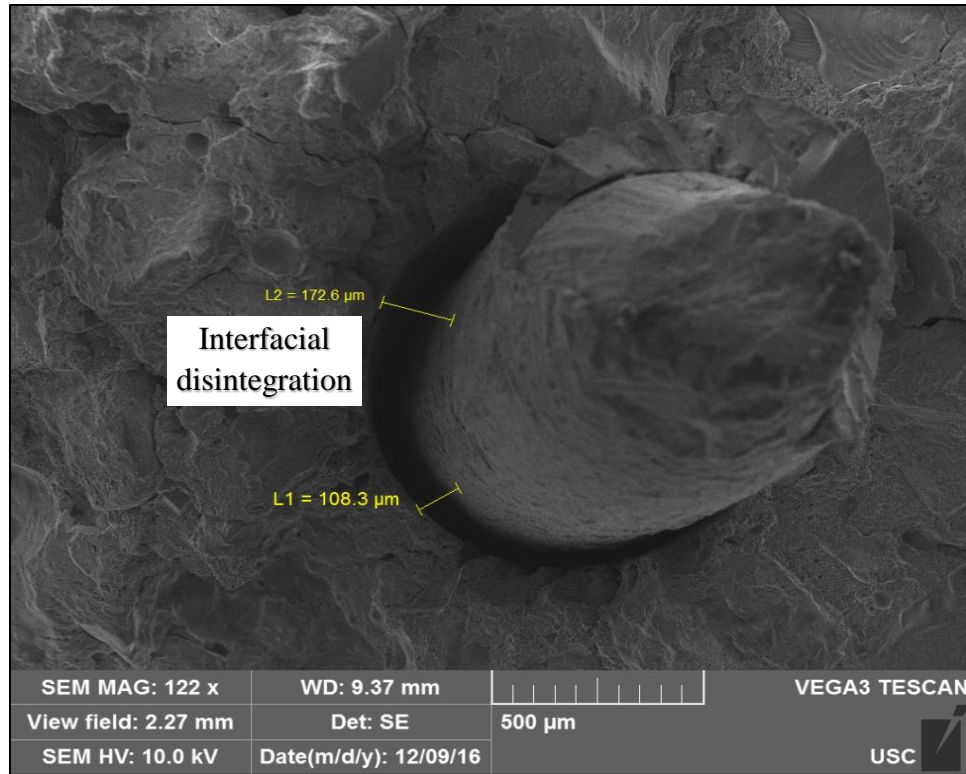
Figure 4.22 WWSM disengagement before upon wire failure.

SEM MAG: 192 x | WD: 9.97 mm | 200 μm | VEGA3 TESCAN
View field: 1.44 mm | Det: SE | |
SEM HV: 10.0 kV | Date(m/d/y): 12/09/16 | | USC
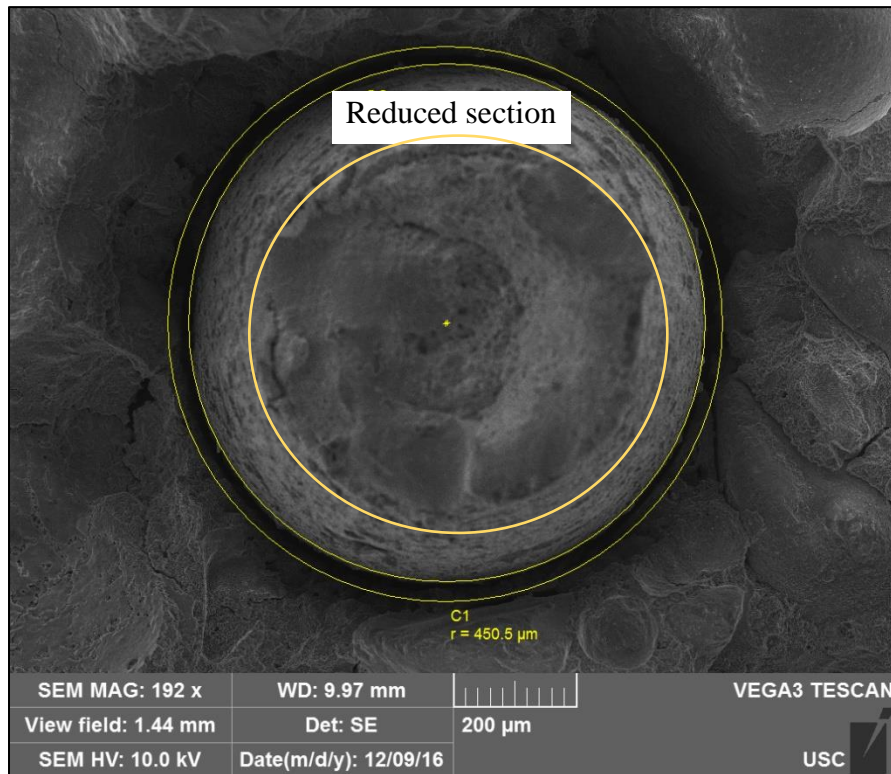
Figure 4.23 WWSM yielding upon wire failure.

69
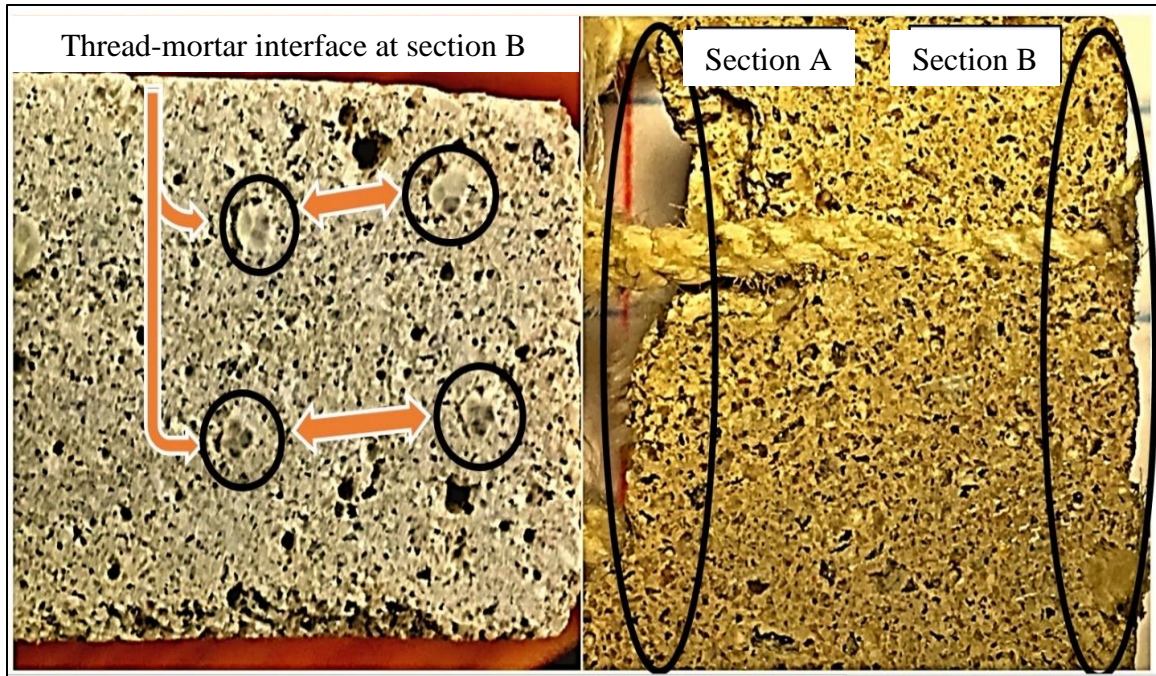
Figure 4.24 Longitudinal and cross sections of FN-mortar interface.
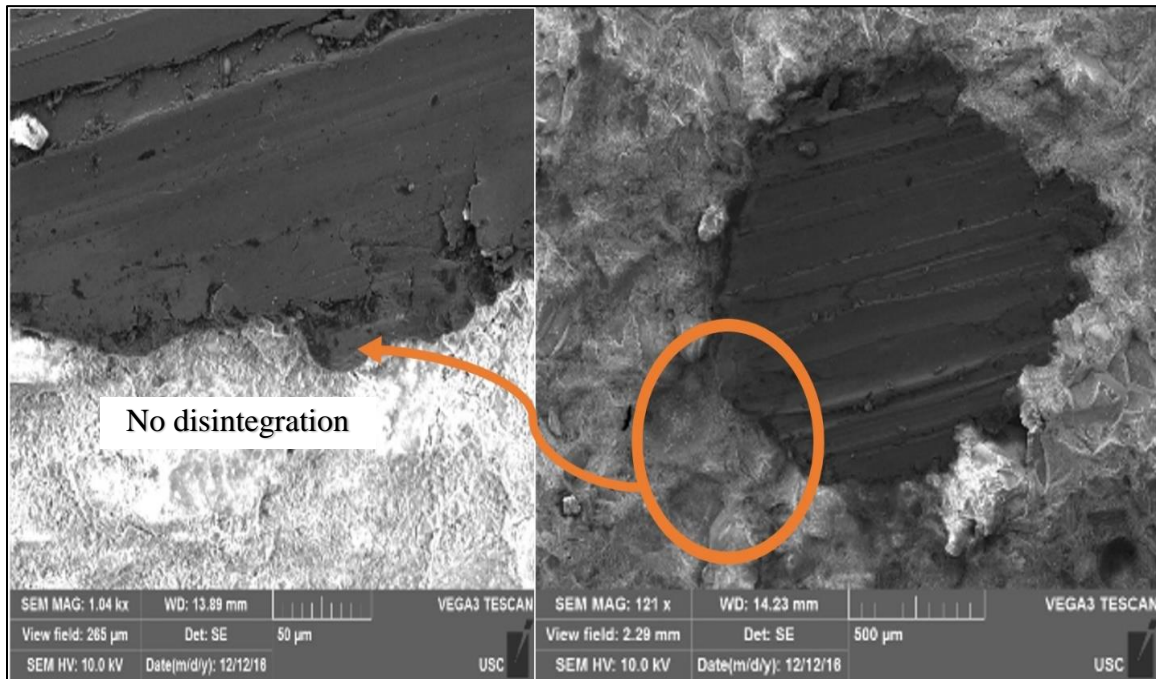
Figure 4.25 A cross section of steel wire-mortar interface away from mid-section of specimen (section B).

70
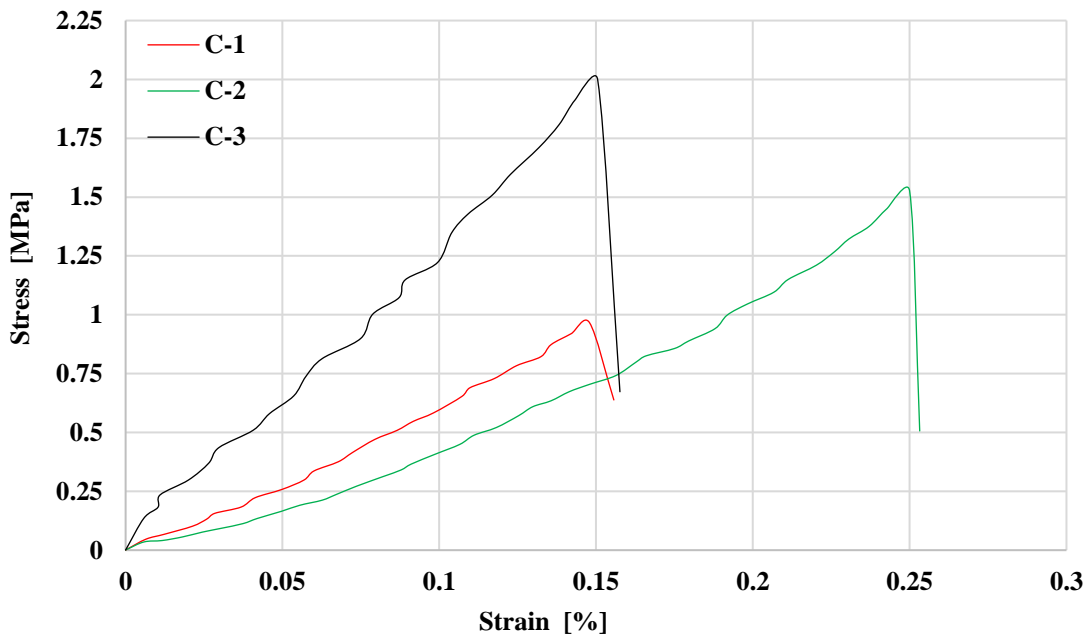
Figure 4.26 Tensile stress-strain response of control specimens.
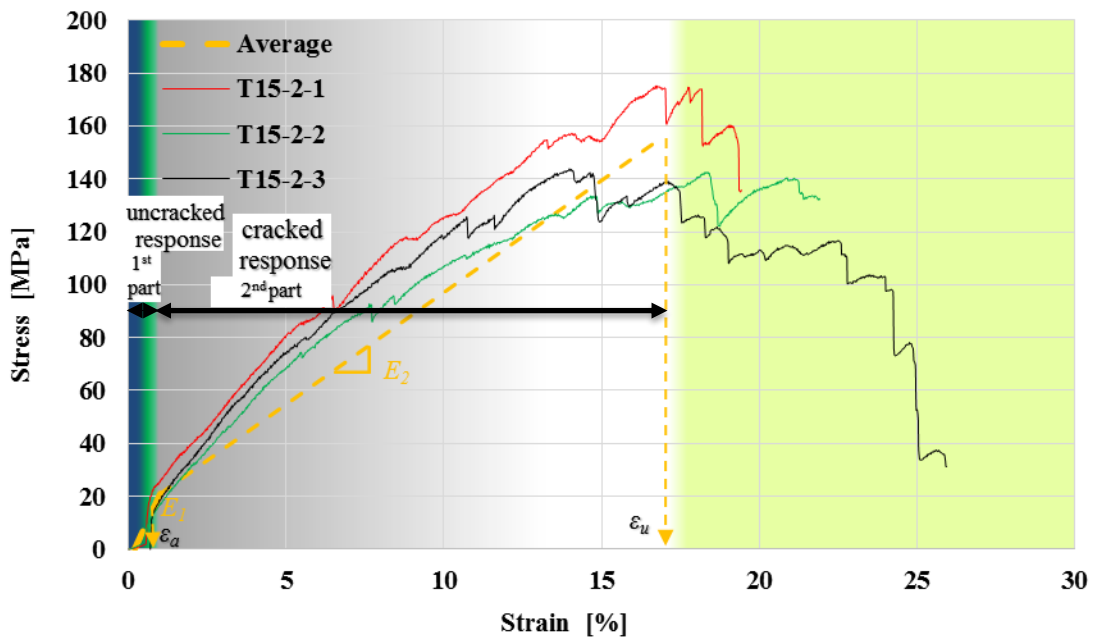
Figure 4.27 Tensile stress-strain response of #15 (2 layers) FN-FRCM dog-bone composite specimens.

71
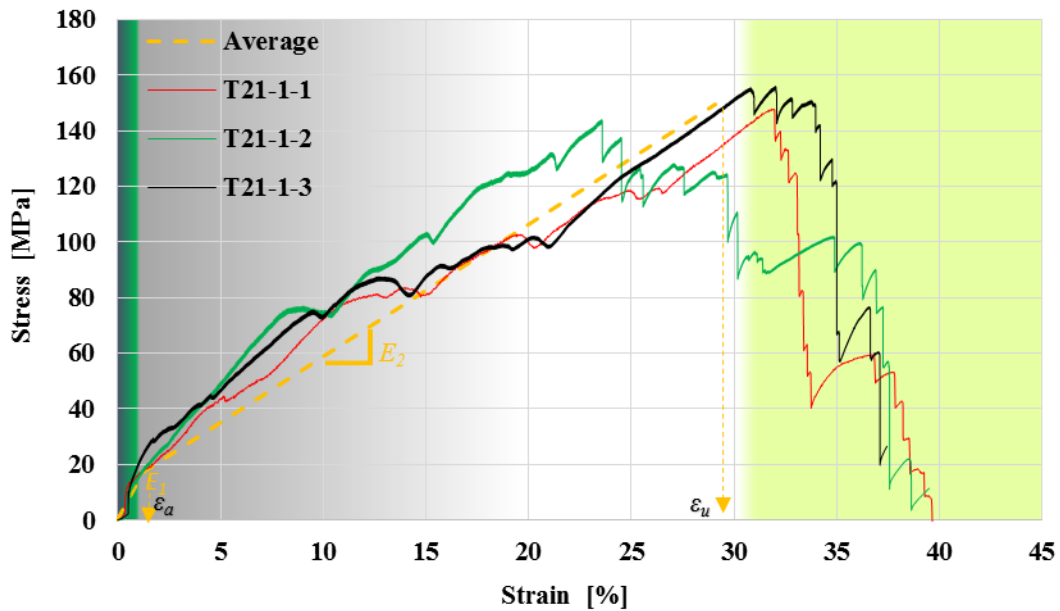
Figure 4.28 Tensile stress-strain response of #21 (1 layer) FN-FRCM dog-bone composite specimens.
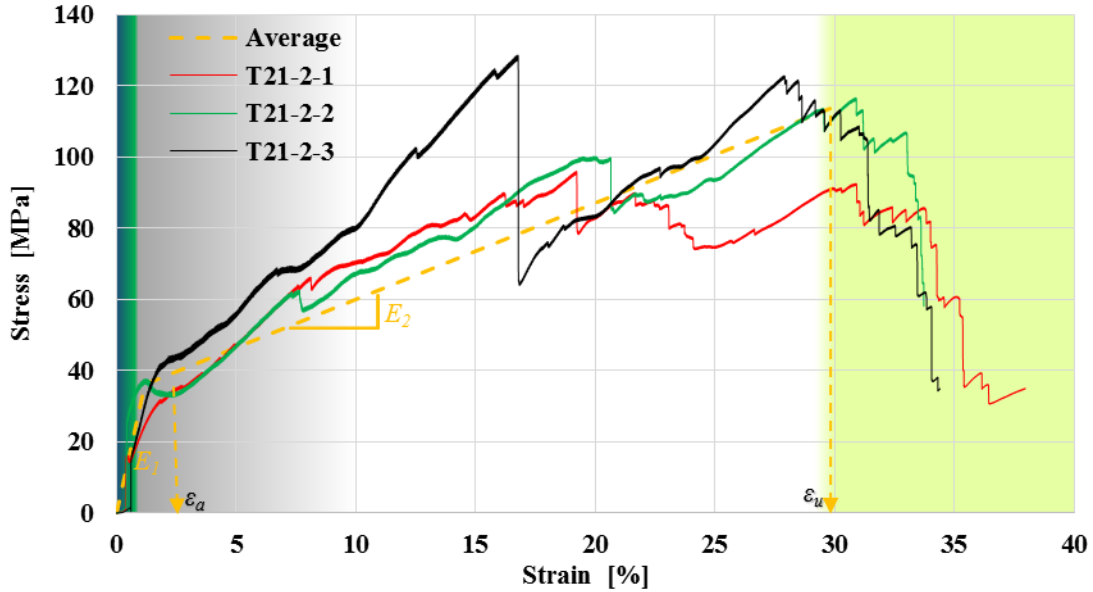
Figure 4.29 Tensile stress-strain response of #21 (2 layers) FN-FRCM dog-bone composite specimens.
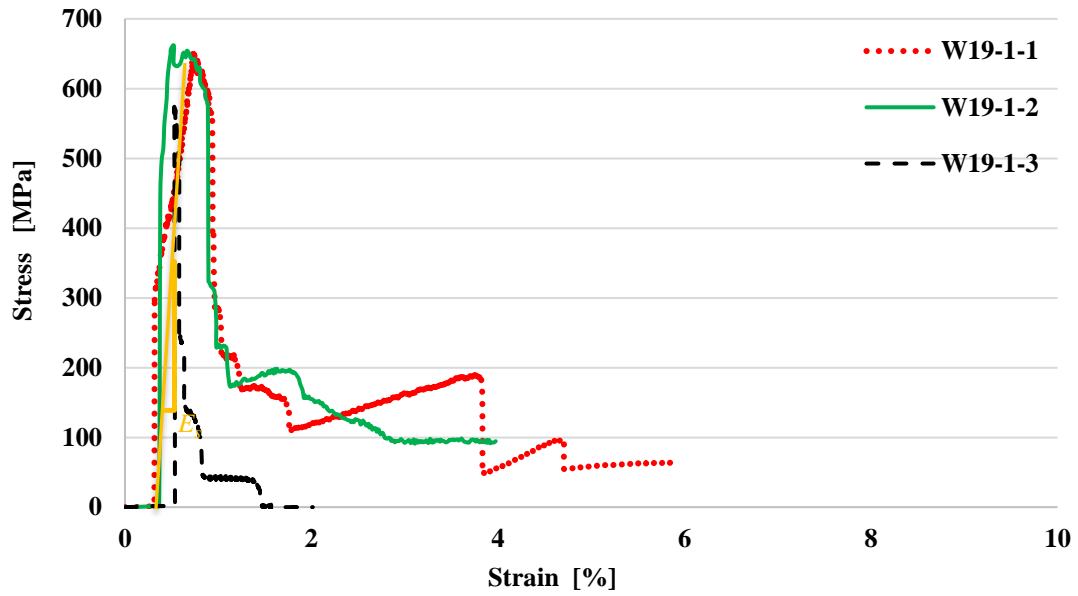
Figure 4.30 Tensile stress-strain response of gage 19 WWSM (1 layer) dog-bone composite specimens.

CHAPTER 5
THEORETICAL CONSIDERATIONS

This chapter describes a simple analytical model to predict the ultimate load carrying capacity of the strengthened walls under out-of-plane bending. The model is analogous to the procedure followed in the "Guide to Design and Construction of Externally Bonded Fabric-Reinforced Cementitious Matrix (FRCM) Systems for Repair and Strengthening Concrete and Masonry Structures" (ACI 2013). Basically, the failure mode of the strengthened walls can be considered as either tensile rupture of reinforcement or masonry crushing or both (balanced failure).

5.1 Ultimate load capacities of FRCM strengthened masonry prisms

5.1.1 Objectives

1. To predict the flexural strength and the failure mode of the masonry prisms made of substandard CMU blocks.

2. To estimate the wind velocities related to the applied loads (pressures) on the prism based on "Minimum Design Loads for Buildings and Other Structures ASCE 07-10", Chapters 26-30 (ASCE 2013).

3. Performing a parametric study for the compressive strength of the masonry to maximize the reinforcement efficiency to resist high wind loads.

5.1.2 Assumptions

The masonry prisms are composed of seven stacked CMU hollow blocks that have a low (substandard) compressive strength. Each CMU block has dimensions of (0.2 x 0.4 x 0.2) m, (Height x Width x Thickness) respectively. The dimensions of the prisms are (1.4 x 0.4 x 0.2) m, (Height x Width x Thickness) respectively. Each prism is reinforced with one or two layers of FN-FRCM composite overlay with FNs having #21 thread thickness. The prisms carry the load in four-point bending. The two load sections are located at one third of the 1.2 m clear span length.

The following prisms will be analyzed.

1. Unreinforced Masonry Prism (UM).

2. Reinforced masonry prism with one layer (RM1) of #21 thread thickness of FN-FRCM composite overlay.

3. Reinforced masonry prism with two layers (RM2) of #21 thread thickness of FN-FRCM composite overlay.

The following assumptions are made:

1. Plane sections remains plane.

2. The axial strain varies linearly throughout the cross section.

3. The FRCM composite has bilinear stress-strain behavior as shown in Figure 5.1 and Figure 5.2 for one- and two-layer options.

4. Perfect bond is assumed between the overlay and the concrete masonry substrate.

5.1.3 Material properties

1. Blocks: The compressive strength of the blocks is equal 6.2 MPa based on the lab test of the available blocks per ASTM C140.

2. <u>Mortar</u>: A ready-mix type N masonry mortar is used to build the prism. The compressive strength of the mortar is 6.8 MPa tested per ASTM C109.

3. <u>Fishing nets</u>: A twine size #21 (Denier Size 210/60), diameter approximately equal to 1.75 mm. The net area per unit width $A_f = 0.16$ mm^2/mm.

4. <u>Masonry</u>: The concrete masonry compressive strength f'_m is equal to 5.5 MPa. The ultimate compression strain of the masonry is relatively high due to the low compressive strength, and ranges between 0.0035 and 0.005 as shown in Figure 5.3. The modulus of rupture of the masonry is conservatively assumed equal to 0.18 MPa as reported by Ghorbani (2014) based on test results for a similar masonry.

5.1.4 Geometrical properties of masonry prism

1. Height, $H = 1400$ mm.

2. Length of clear span, $L = 1200$ mm.

3. Thickness, $t_w = 200$ mm.

4. Width, $b = 400$ mm.

5. Width of mortar overlay, $w_f = 400$ mm.

6. Cross-sectional area of block, $A_b = 41650$ mm^2.

7. Static moment of area of block, $S_b = 1.92 *10^6$ mm^3.

8. Static moment of area of prism per unit width, $S_w = 4.71*10^6$ mm^3/m.

9. Flexural strength of unreinforced masonry prism, M_{uu} (kN-m).

10. Flexural strength of masonry prism with one-layer reinforcement, M_{1fu} (kN-m).

11. Flexural strength of the masonry prism with two-layer reinforcement, M_{2fu} (kN-m).

5.1.5 Mechanical properties of FN-FRCM composite overlay

1. #21 FN thread nominal area per unit length, $A_f = 0.16$ mm^2/mm.

76

2. Composite strain at transition point, $\varepsilon_a = 0.005$ mm/mm (for 1 layer), 0.011 mm/mm (for 2 layers), from Figure 5.1 and Figure 5.2.

3. Ultimate strain of composite, $\varepsilon_u = 0.234$ mm/mm (for 1 layer), 0.167 mm/mm (for 2 layers), from Figure 5.1 and Figure 5.2.

4. First elastic modulus of composite, $E_1 = 1.90$ GPa (for 1 layer), 3.45 GPa (for 2 layers), from Figure 5.1 and Figure 5.2.

5. Second (post-cracking) elastic modulus of composite, $E_2 = 0.66$ GPa (for 1 layer), 0.60 GPa (for 2 layers), from Figure 5.1 and Figure 5.2.

6. Tensile stress at transition point, $f_a = 9.5$ MPa (1 layer), 37 MPa (2 layers).

7. Effective tensile stress at failure, $f_e = E_1 * \varepsilon_e$ (if $f_e < f_a$), and $f_e = f_a + E_2 * (\varepsilon_e - \varepsilon_a)$ (if $f_e > f_a$).

8. Ultimate tensile strength, $f_u = f_a + E_2 * (\varepsilon_u - \varepsilon_a) = 155$ MPa (for 1 layer), 120 MPa (for 2 layers).

9. The tensile stress-strain model is illustrated in Figure 5.1 and Figure 5.2 for one- and two-layer FN-FRCM, respectively.

5.1.6 Computing flexural strength of unreinforced prism

1. The ultimate flexural strength of the unreinforced prism UM,

$$M_{uu} = M_{cr} = f_r * S_w \quad ....(1)$$

2. The modulus of rupture, $f_r = 180$ kPa.

3. The ultimate flexural strength of the unreinforced masonry prism, from Equation (1),

$M_{uu} = 180 * 4.71 * 10^{-3} = 0.85$ kN-m/m $= 0.34$ kN-m.

77

5.1.7 Computing the flexural strength of the reinforced masonry prism RM

1. Number of reinforcement layers, $n_f = 1$ layer.

2. Width of overlay, $b = w_f = 0.4$ m.

3. When FRCM failure is the governing failure mode, the following stress block factors are assumed: $\gamma = 0.7$, $\beta_1 = 0.7$ (ACI 2013).

4. The initial assumption is that the failure mode is controlled by tensile rupture of the reinforcement. However, this assumption should be verified by determining the compressive strain in the masonry which should not exceed ε_{mu}. Similarly, if the failure mode is assumed to be governed by masonry crushing, the tensile strain of the reinforcement should then have been verified not to exceed its ultimate value.

5. Ultimate state: The neutral axis depth (kd) at the balance state is calculated from the equilibrium of the forces ($T_t = C_c$) in the section shown in Figure 5.4, where it is assumed a tensile failure ($f_e = f_u$), and masonry crushing ($f_m = f'_m$) is occurring simultaneously, then the strains in masonry and the reinforcement are checked to verify the assumption.

$$T_t = n_f * A_f * w_f * f_u \quad \text{... (2)}$$

$$C_c = \gamma * f'_m * \beta_1 * b * kd \quad \text{..(3)}$$

Equalizing the compression to tension force in the section gives,

$$n_f * A_f * w_f * f_u = \gamma * f'_m * \beta_1 * b * kd \quad \text{..(4)}$$

From Equation (4), $kd = \dfrac{n_f * A_f * w_f * f_u}{\gamma * f'_m * \beta_1 * b} = 9.2$ mm.

6. Checking the strains, by inserting the ultimate strain value of one of the components and checking the other. For example, the ultimate strain value of the composite reinforcement with one layer is 0.234 from Figure 5.1.

$$\varepsilon_{mu} = \varepsilon_u * \frac{kd}{t_w - kd} \quad\text{.. (5)}$$

From Equation (5), $0.234 *(\frac{9.2}{200 - 9.2}) = 0.011 > (0.0035)$ (not okay).

This indicates that the strain in masonry is reaching to the ultimate state first. Therefore, the effective tensile stress in the reinforcement will be adjusted by assuming a tensile stress $(f_e < f_u)$ for the reinforcement. Then, the strain in the masonry is checked until it equalizes its ultimate value by repeating the steps in Equations (3) and (4) by trial and error which is illustrated in Figure 5.5. The effective tensile strain, neutral axis depth, and the effective tensile strength values at the equilibrium state will be, $\varepsilon_e = 0.184$, $kd = 3.71$ mm, and $f_e = 127.5$ MPa $< f_u$ respectively.

7. The ultimate strength of the masonry prism reinforced with one layer and assuming $\varepsilon_{mu} = 0.0035$ is:

$$M_{1fu} = f'_m * b * kd *(\frac{t_w}{2} - \frac{kd}{2}) + n_f * w_f * A_f * f_e * \frac{t_w}{2} = 1.62 \text{ kN-m.}$$

8. For a strain value of masonry, $\varepsilon_{mu} = 0.005$ (upper boundary), repeating the procedure of step 6 provides the effective tensile strain, neutral axis depth, and the effective tensile strength values at the equilibrium state to be, $\varepsilon_u = 0.22$, $kd = 4.42$ mm, and $f_e = 151.9$ MPa respectively. It is noticed that the strain and the stress values of reinforcement are close to their ultimate where $\varepsilon_u = 0.234$, and $f_u = 155$ MPa. Therefore a tensile rupture is possible

79

to occur. This can also be checked by determining the reinforcement ratio (ρ) and comparing it with the balanced reinforcement ratio (ρ_b). Where;

$$\rho = \frac{w_f * A_f}{b * d} \quad \text{...} (6)$$

$$\rho_b = \frac{f'_m}{f_u} * \frac{\varepsilon_{mu}}{\varepsilon_{mu} + \varepsilon_u} \quad \text{...} (7)$$

Then: $\frac{\rho}{\rho_b} = 1.5$ @ $\varepsilon_{mu} = 0.0035$, and $\frac{\rho}{\rho_b} = 1.02 \approx 1.0$ @ $\varepsilon_{mu} = 0.005$.

The reinforcement ratio is close to the balance ratio which confirms that tensile rupture is possible.

9. The ultimate strength of the masonry prism reinforced with one layer and assuming the upper bound $\varepsilon_{mu} = 0.005$ is:

$M_{1fu} = 1.92$ kN-m.

10. The flexural strength for the masonry prism strengthened with a two-layer FN-FRCM overlay was calculated using the same procedure. The summary of the results is provided in Table 5.1.

5.2 Wind velocity corresponding to applied load

This method is a simple form of the velocity pressure equation in ASCE 7, Chapter 30 (ASCE 2010). Although the simplified equation does not account for the exposure effects, wind direction, and topographic conditions, it provides a meaningful estimate to understand the potential implications of deploying the proposed FN-FRCM system on substandard CM walls. For example, the selected wall for this section is a

80

simply supported external wall of a house with a height equal to 3.0 m and a clear span of 2.4 m without openings.

The estimated wind velocities applied on the composite reinforced masonry walls are extrapolated from the analytical results of the reinforced masonry prisms. The equivalent distributed load that a reinforced masonry wall can withstand is assumed equal to the wind pressure.

$$q = \frac{1}{2}\rho\ v^2 \dotfill (8)$$

Where;

q = wind pressure (Pa)

ρ = Air density equal to 1.2 (kg/m^3)

v = wind velocity (m/s).

The calculated wind pressures and the associated wind velocities as well as their hurricane category per the Saffir-Simpson scale are listed in Table 5.2.

5.3 Parametric study

A parametric study is performed to determine the influence of the masonry compressive strength, which is a measure of how substandard the masonry is, on the flexural resistance of a strengthened wall. The compressive strength values are 3.3, 5.5, 7.5, and 10 MPa. Figure 5.6 shows the flexural strength of the masonry wall for different masonry compressive strength values. Lower- and upper-bound nominal flexural strength values were calculated based on a masonry ultimate strain of 0.0035 and 0.005, respectively. The correlated wind velocities resisted by the masonry wall are provided in

81

Figure 5.7. The wind velocities are categorized based on ASCE 7 (ASCE 2010). It is noticed that the flexural capacity of the wall increases with the increase of the compressive strength of the masonry. However, the flexural capacity is limited by the strength of the reinforcement when the compressive strength of the masonry is more than 7.5 MPa, which is still a substandard value. This is because the failure mode is controlled by the tensile rupture of the reinforcement.

5.4 Summary

The masonry compressive strength and strain used to predict the out-of-plane resistance of the masonry prisms are 5.5 MPa (average) and 0.0035-0.005 (range), respectively. The flexural strength of strengthened masonry members was analytically estimated based on the test data from uniaxial load tests on dog-bone overlay specimens.

The out-of-plane capacity of the strengthened substandard concrete masonry prisms with one- and two-layer FN-FRCM overlays increased by about four and seven times, respectively, compared to the unreinforced masonry, as expected. Moreover, the resistance to high winds as a result of strengthening theoretically ranges from 98 mph to 288 mph. This result eloquently highlights the potential of the proposed system to enhance strength and safety using a locally appropriate and sustainable technique.

The parametric study showed that the flexural capacity of the wall increases with the increase of the compressive strength of the masonry. However, the flexural capacity is limited by the strength of the reinforcement when the compressive strength of the masonry is more than 7.5 MPa. This is because the failure mode is controlled by the tensile rupture of the reinforcement.

Tables:

Table 5.1 Ultimate load capacity analytical predictions.

Prism type		Ultimate flexural strength, kN-m	Failure type	Effective tensile stress, MPa	ρ/ρ_b	Ultimate flexural strength per unit length, kN-m/m	Percentage increase in flexural strength, %
UM		0.34	Tensile failure	0.18	-	0.85	0.0
RM1	@ $\varepsilon_{mu} = 0.0035$	1.62	Masonry crushing	127.5	1.50	4.05	376
	@ $\varepsilon_{mu} = 0.005$	1.92	FN rupture or masonry crushing or both	151.9	1.02	4.80	465
RM2	@ $\varepsilon_{mu} = 0.0035$	2.53	Masonry crushing	100.3	1.70	6.33	644
	@ $\varepsilon_{mu} = 0.005$	2.92	Masonry crushing	116.0	1.20	7.30	759

Table 5.2 Correlated wind pressures and velocities.

Wall type	Velocity pressure, kPa	Wind velocity, mph	Hurricane category
UM	1.18	98	1
RM1	5.63 - 6.67	214 - 233	5
RM2	8.79 - 10.14	268 - 288	5

Figures:
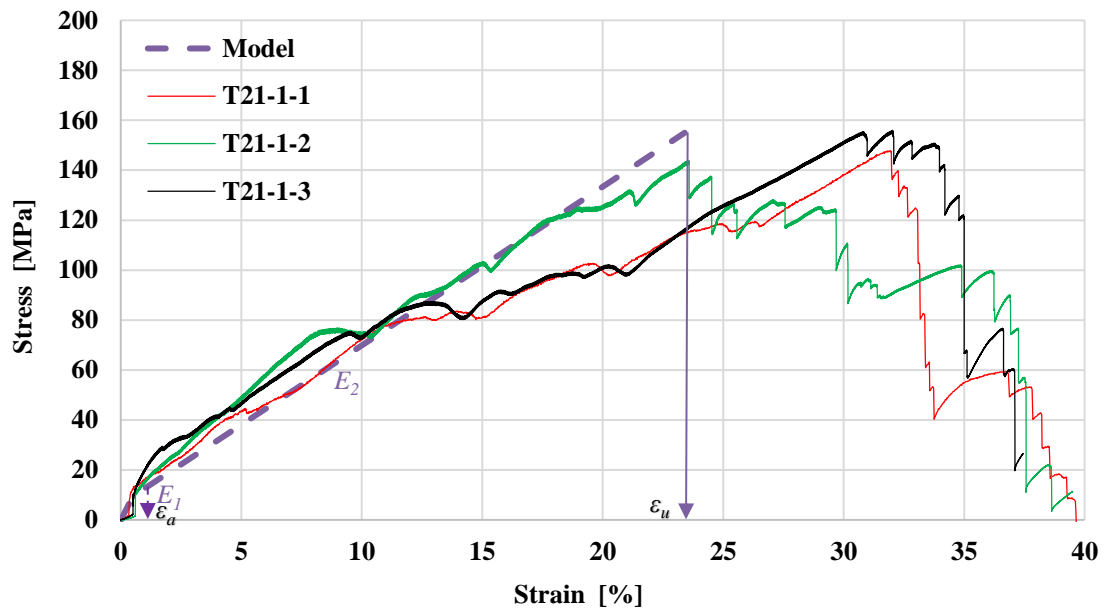
Figure 5.1 Uniaxial tensile stress-strain model of one-layer FN-FRCM overlay.
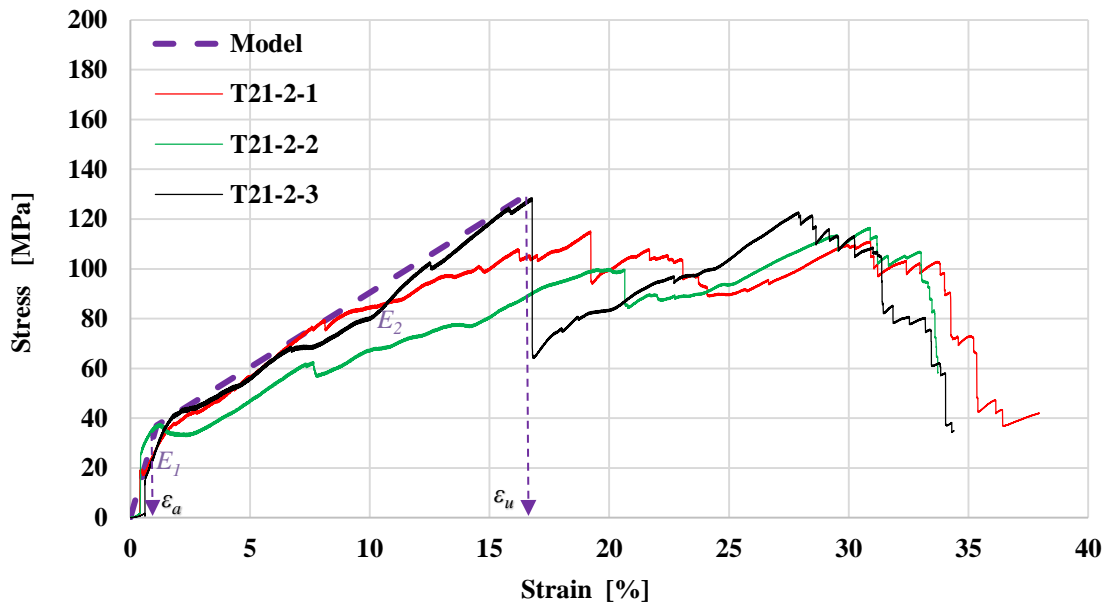
Figure 5.2 Uniaxial tensile stress-strain model of two-layer FN-FRCM overlay.

84
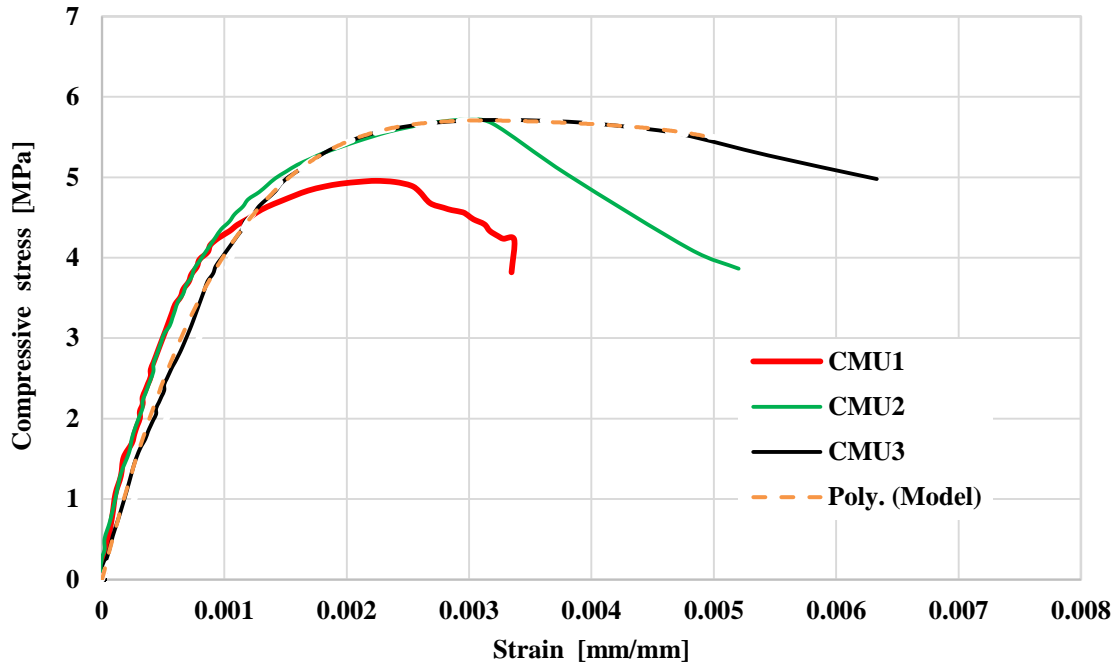
Figure 5.3 Compressive stress-strain model for substandard concrete masonry.
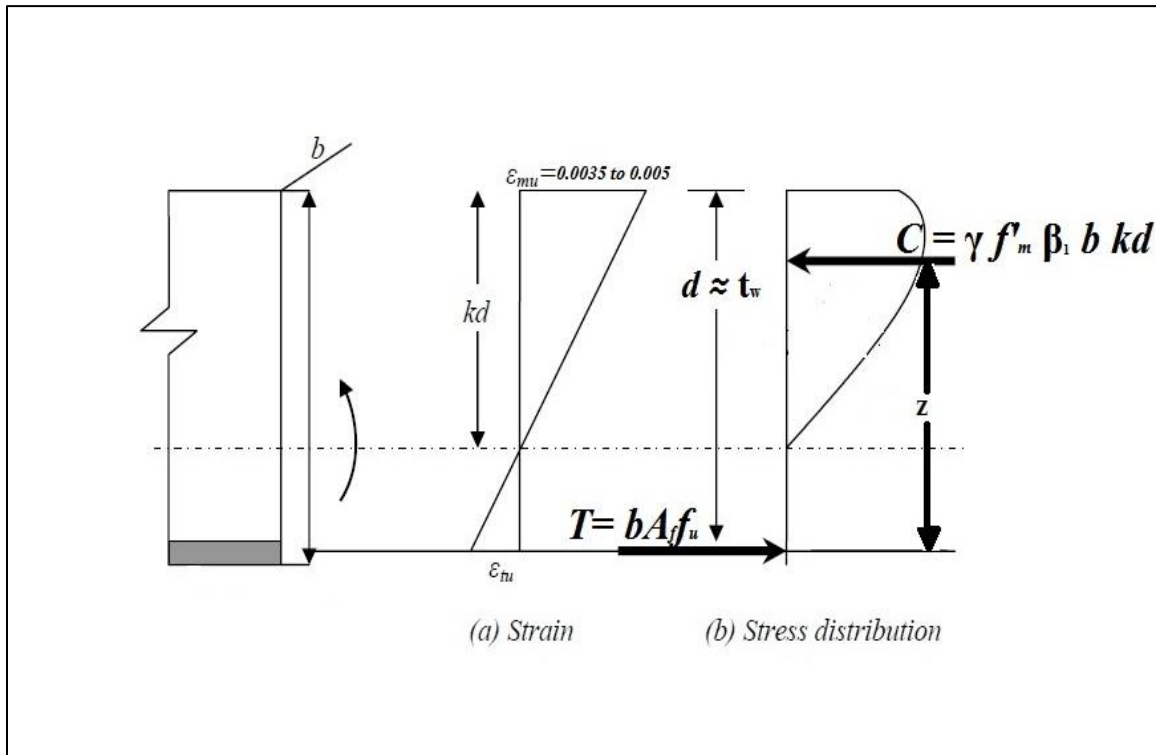
Figure 5.4 Strain and stress distributions across strengthened masonry section (balanced failure).

2.
Determine the neutral axis depth (kd), $kd = \dfrac{n_f * A_f * w_f * (f_u \text{ or } f_u)}{f'_m * b}$,

1.
Assume the failure mode (tensile or compressive). Based on that, use (f_u) if tensile rupture is assumed, otherwise, $(f_e < f_u)$.

5.
Claculate the moment,
$M_{1fu} = C_c * arm + T_t * arm$
$= f'_m * b * kd * (t_w/2 - kd/2) + n_f * A_f * w_f * t_w/2$

3.
Check the strain in masonry. Is
$\varepsilon_{mu} = \varepsilon_e * \dfrac{kd}{tw - kd}$?
if yes go to 5, otherwise continue.

4.
Plug a new f_e value, then repeat the steps 1, 2, and 3.
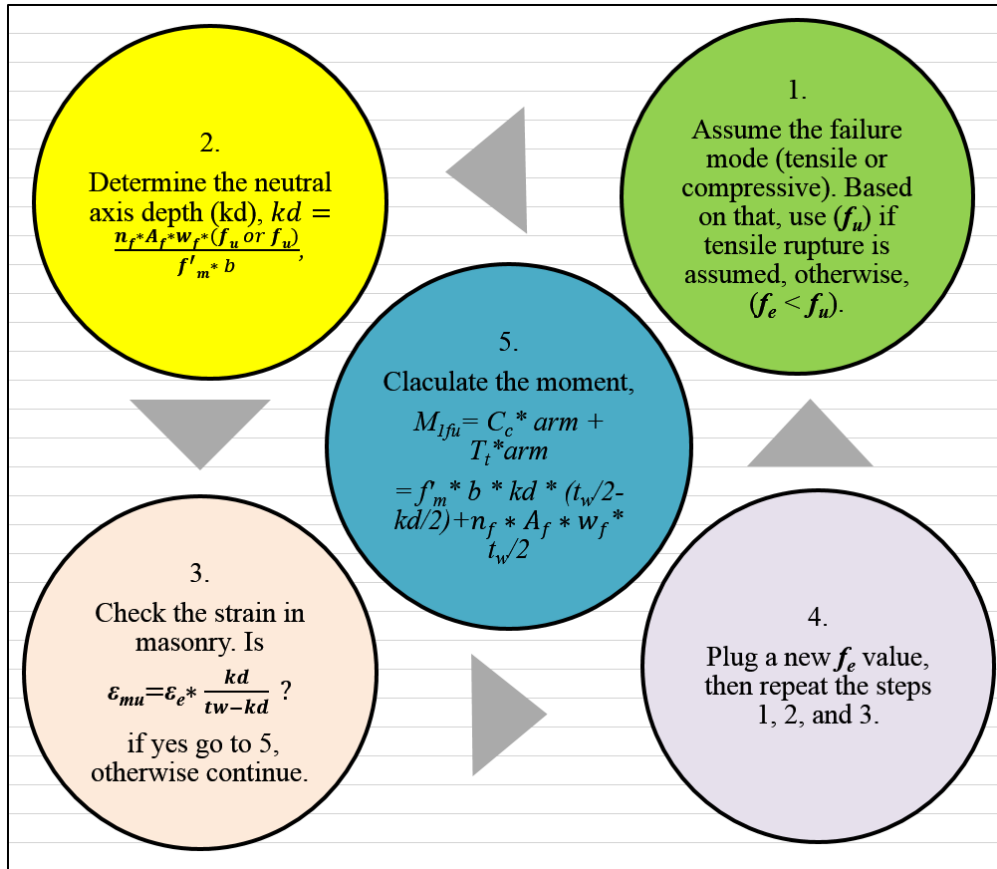
Figure 5.5 Flexural strength calculation procedure.
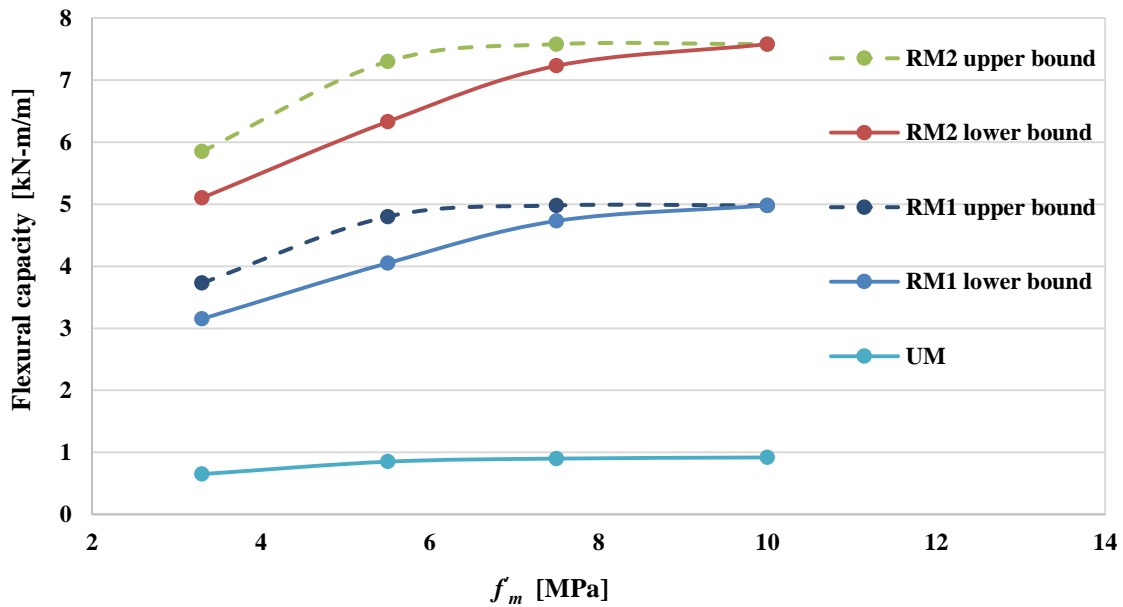
Figure 5.6 Concrete masonry wall flexural capacity as function of substandard masonry compressive strength.
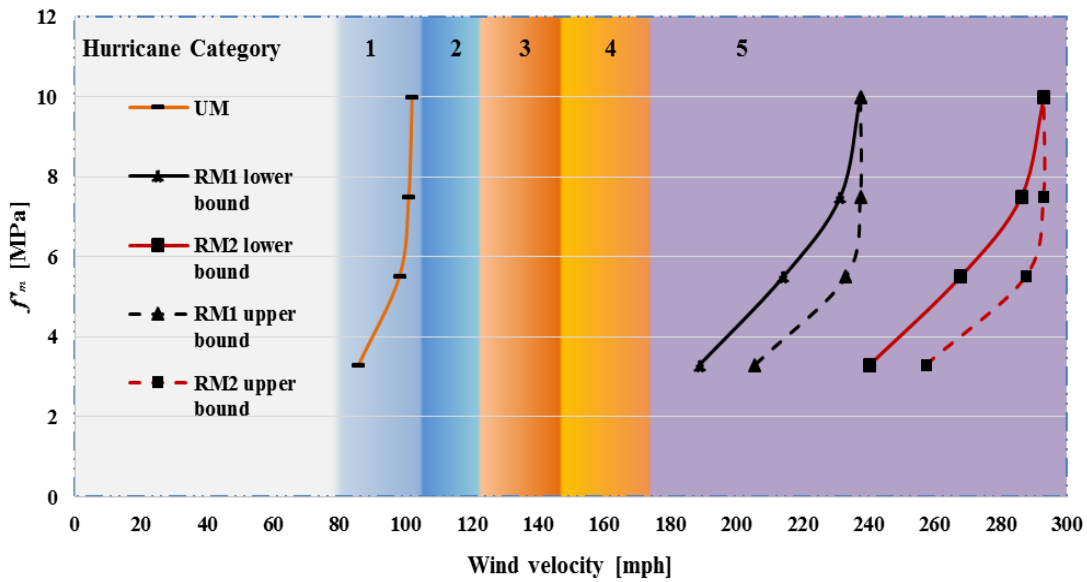
Figure 5.7 Correlated wind velocities, and Saffir/Simpson hurricane category for different substandard masonry compressive strength values.

CHAPTER 6
PRELIMINARY TESTS

In this chapter, the capability of the proposed system to enhance the out-of-plane capacity of the unreinforced concrete masonry walls is preliminarily investigated through proof-of-concept physical experiments. The experimental program includes out-of-plane flexural testing for unreinforced and reinforced masonry prisms as a proof of concept to verify the effectiveness of the proposed FN-FRCM overlay system. Also, experimental results and analytical predictions are compared.

6.1 Experimental program

6.1.1 Test matrix

Four concrete masonry prisms were fabricated; the test matrix is presented in Table 6.1. Three of the prisms were intended to be strengthened and a fourth prism was used as a control (unstrengthened) specimen. Two prisms were strengthened with one- and two-layer FN-FRCM overlay, respectively. One prism was strengthened with a WWSM-reinforced mortar overlay. The FN-FRCM strengthened prisms are designated by F-x where x refers to the number of reinforcing layers. The WWSM-reinforced mortar overlay strengthened prism are designated by S, and control specimen is designated by C.

6.1.2 Fabrication of concrete masonry prisms

Figure 6.1 shows the mortar mixing, the constructed prisms, and the curing method. The prisms were built by stacking seven substandard CMU blocks having an average compressive strength of 6.2 MPa and dimensions of 400 x 200 x 200 mm. A Type N mortar bed joint with a 10 mm thickness was used. The mixing of the mortar was done by hand, and the prisms were cured for 28 days. To this end, a wet burlap was wrapped around the prisms to retain moisture as a practical curing technique.

The overlaying process for the WWSM reinforcement is illustrated step by step in Figure 6.2. Type N mortar was used for the overlays. This mortar is similar to the one used for the dog-bone composite specimens. The WWSM is secured onto the masonry surface using hot-glue silicon at a constant distance from the face of the prism. Then, the masonry surface is sprayed with water, and the mortar is overlaid manually. The overlay thickness is approximately 19 mm.

The step by step overlaying process for the FN reinforcement is illustrated in Figure 6.3. Strengthening the prisms with FN-FRCM overlays is accomplished as follows. First, one side of the mesh is secured to the bottom of the prism. Then, the masonry surface is sprayed with water to prevent water absorption from the mortar, and the first (base) mortar layer is overlaid and the fishing net is stretched and secured to the other side (upper side) of the prism. The fishing net is impregnated into the first mortar layer by troweling (step 6 in Figure 6.3), and the second (cover) mortar layer is overlaid. The procedure for the second reinforcing layer is similar. The overlay thickness is

89

approximately 19 mm and 25 mm for the one-layer and two-layer FN-FRCM overlay, respectively. Wet burlap is then used to cure the overlay for 7 days.

6.1.3 Test setup and instrumentation

The prisms are subjected to four-point bending as illustrated in Figure 6.4. The load is slowly applied using a manually-operated hydraulic jack. The load is measured using a 22 kN load cell. The out-of-plane displacement is measured by using two LVDT mounted on each side of the prism at midspan. The test instrumentation is connected to a data acquisition system to acquire data at a rate of 100 Hz. A representative instrumented specimen is shown in Figure 6.5.

6.1.3 Test results and discussion

The out-of-plane load-midspan displacement response under four-point bending for all specimens is presented in Figure 6.6 for the tested specimens. The maximum load, flexural strength, out-of-plane displacement at maximum load, and the failure mode are summarized in Table 6.2. The out-of-plane flexural response of all specimens is detailed using photographs in Figure 6.7 through Figure 6.10.

From Table 6.2, it is noted that the flexural strength of the unreinforced prisms has increased by 4.0, 6.3 and 4.7 times after strengthening using one-layer FN-FRCM, two-layer FN-FRCM, and one-layer WWSM-reinforced mortar overlay, respectively. It is also noted that the FN-FRCM overlay provides a comparable strength to that of the WWSM system. Negligible mortar debonding is observed either between the mortar and the substrate or between the mortar and the reinforcement.

90

The out-of-plane displacement of the reinforced prisms has significantly increased in the case of the FN-FRCM overlay due to the high deformation capacity of the FN reinforcement. Further, the strengthened prisms with FN-FRCM overlay developed multiple cracks compared to the unreinforced and WWSM reinforced prisms which have only a single crack upon failure. The flexural stiffness of the prisms decreases as more cracks in the specimen develop.

Finally, the failure mode has changed from tensile failure in a bed joint for the unreinforced prism, to masonry crushing for the FN-FRCM strengthened prisms. However, the prism strengthened with a one-layer FN-FRCM overlay also developed a tensile rupture due to the reinforcement ratio being close to the balance, as shown in Chapter 5, Table 5.1. The failure mode of the WWSM reinforced prism is tensile rupture of the steel reinforcement as the reinforcement ratio is much less than the balanced reinforcement ratio.

6.2 Comparison between the experimental and the analytical results

This section compares between the predicted and the experimental flexural strength of the masonry prisms. Table 6.3 provides the flexural strength and failure mode of both analytical predictions and the experimental results. Table 6.3 shows the predicted failure mode of the tested prisms is consistent with the experimental test for all the prisms. However, the flexural strength predictions are underestimated compared to the experimental results.

Two principle reasons are causing the analytical model to underestimate the flexural strength. The first reason is due to underestimating the FN strength when tested

under uniaxial tensile load as dog-bone composites. Significant stress variations occur across the section due to the boundary conditions of the uniaxial tensile test, with pinned supports that allow rotation as illustrated in Figure 6.11. The threads in the specimens fail non-simultaneously which leads to an underestimation of the actual maximum stress in the reinforcement as it is calculated by dividing the maximum load by the total number of threads. The FN-FRCM overlay has smaller stress variations as the mortar is bounded by the masonry surface, facilitating a more uniform distribution of tensile stresses in the FN threads.

The second reason is that the strain of the reinforcement is overestimated in the case of the tensile tests on the dog-bone specimens because its value is calculated only at the LVDT location. However, some threads can have less or more strain value due to rotation as illustrated in Figure 6.11. Therefore, for prediction purposes, the tensile stress-strain behavior of the reinforcement is modified to have a more realistic representation based on single-thread tensile behavior.

6.3 Modified composite tensile stress-strain model

The model is based on the single thread tensile stress-strain response. It is assumed that each thread of the FN reinforcement can be simulated by a single thread behavior. The stress developed in the single thread has a more realistic value than the stress in the FN because the FN can have high stress variations, as discussed above. The modified tensile stress-strain behavior of the thread compared to the FN-FRCM composite is illustrated in Figure 6.12.

The analytical predictions of the out-of-plane flexural strength based on the composite and the modified thread models are shown together with the experimental results in Figure 6.13 and Table 6.4. The modified tensile behavior of the composite provides a more accurate prediction of the range of the flexural strength. The correlation between the first model (based on the tensile stress-strain response of the dog-bone FN-FRCM specimens) and the modified model is compared based on a modification factor φ. This factor ranges between 1.05 and 1.10 depending on the number of layers and regardless of the ultimate strain of the masonry, as shown in Table 6.4.

6.4 Summary

This chapter includes an experimental program to implement the building, plastering, and testing of the CM masonry prisms under out-of-plane flexural load. The flexural strength of the overlaid masonry prisms is increased by 4-6 times when plastered with 1, 2 layers of FN-mortar, or 1 layer of WWSM mortar composite. Also, the analytical predictions were compared with the experimental results. The analytical predictions provide a conservative flexural strength range. Therefore, a modified model based on the tensile thread behavior is proposed to provide a more accurate prediction of the range of the flexural strength.

Tables:

Table 6.1 Test matrix for masonry prisms.

Wall type	Designation	Reinforcing material	Number of layers	Number of specimens
Unreinforced	C	-	0	1
Reinforced	F-1	#21 FN	1	1
Reinforced	F-2	#21 FN	2	1
Reinforced	S	WWSM	1	1

Table 6.2 Masonry prisms flexural test results.

Specimen type	Maximum load, kN	Flexural strength, kN-m	Flexural strength per unit length, kN-m/m	Displacement @ maximum load, mm	Failure mode
C	2.55	0.50	1.27	0.06	Tensile failure
F-1	10.1	2.02	5.05	59.0	Masonry crushing followed by tensile rupture
F-2	16.1	3.23	8.07	75.0	Masonry crushing
S	11.9	2.38	5.95	1.25	Tensile rupture

94

Table 6.3 Analytical predictions and experimental results.

| Specimen type | Analytical predictions | | Experimental results | | Ratio of experimental to analytical strength |
	Flexural strength, kN-m	Failure mode	Flexural strength, kN-m	Failure mode	
C	0.34	Tensile failure	0.50	Tensile failure	1.47
F-1 $\varepsilon_{mu} = 0.0035$	1.62	Masonry crushing	2.02	Masonry crushing followed by tensile rupture	1.24
F-1 $\varepsilon_{mu} = 0.005$	1.92	Tensile rupture or masonry crushing or both.			1.05
F-2 $\varepsilon_{mu} = 0.0035$	2.53	Masonry crushing	3.23	Masonry crushing	1.27
F-2 $\varepsilon_{mu} = 0.005$	2.92	Masonry crushing			1.11
S	2.46	Tensile rupture	2.38	Tensile rupture	0.97

Table 6.4 Modified analytical predictions and experimental results.

Specimen type		Analytical predictions			Experimental results	Ratio of experimental to modified analytical model strength
		Flexural strength, kN-m	Modified flexural strength, kN-m	Mod analy. / Analy. (φ)	Flexural strength, kN-m	
F-1	$\varepsilon_{mu} = 0.0035$	1.62	1.78	1.10	2.02	1.13
	$\varepsilon_{mu} = 0.005$	1.92	2.09	1.09		0.97
F-2	$\varepsilon_{mu} = 0.0035$	2.53	2.66	1.05	3.23	1.21
	$\varepsilon_{mu} = 0.005$	2.92	3.08	1.05		1.04

96
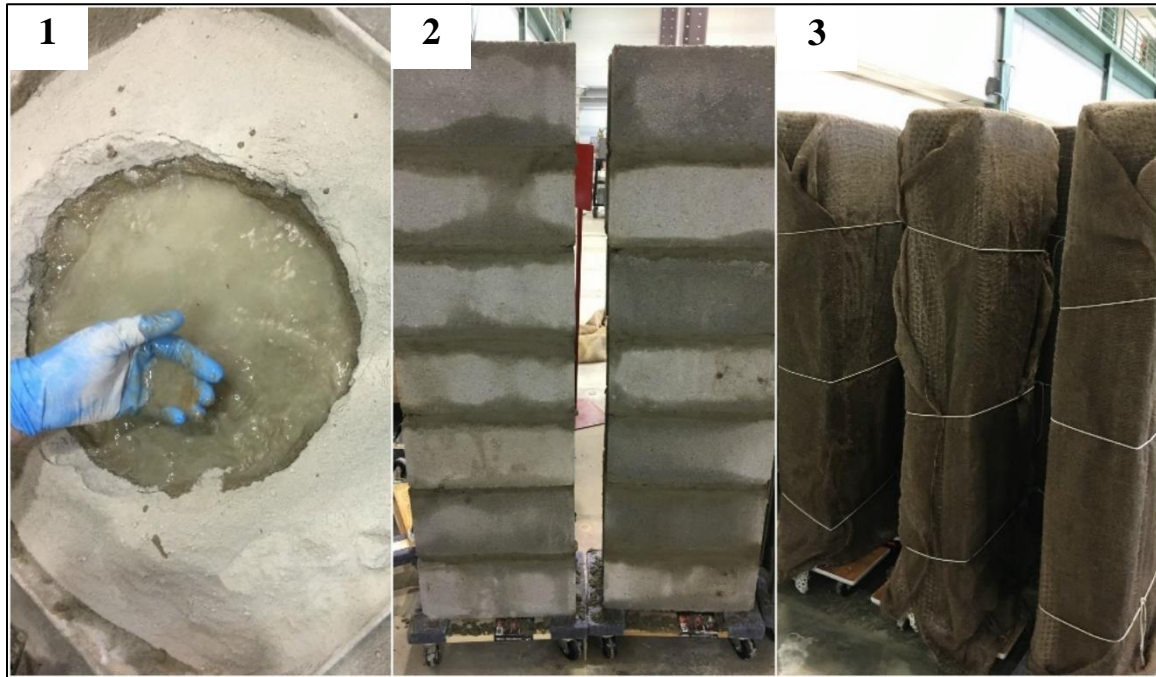
Figures:

Figure 6.1 Manufacturing of concrete masonry prism specimens, (1) mortar mixing (manually), (2) CM prisms, and (3) curing with wet burlap.

Figure 6.2 WWSM plastering process, (1) securing WWSM using hot-glue silicon at selected spots, (2) checking spacing between mesh and substrate, (3) masonry spraying with water, (4-6) applying mortar overlay, (7) checking overlay thickness, (8) overlay surface troweling, and (9) curing with wet burlap.
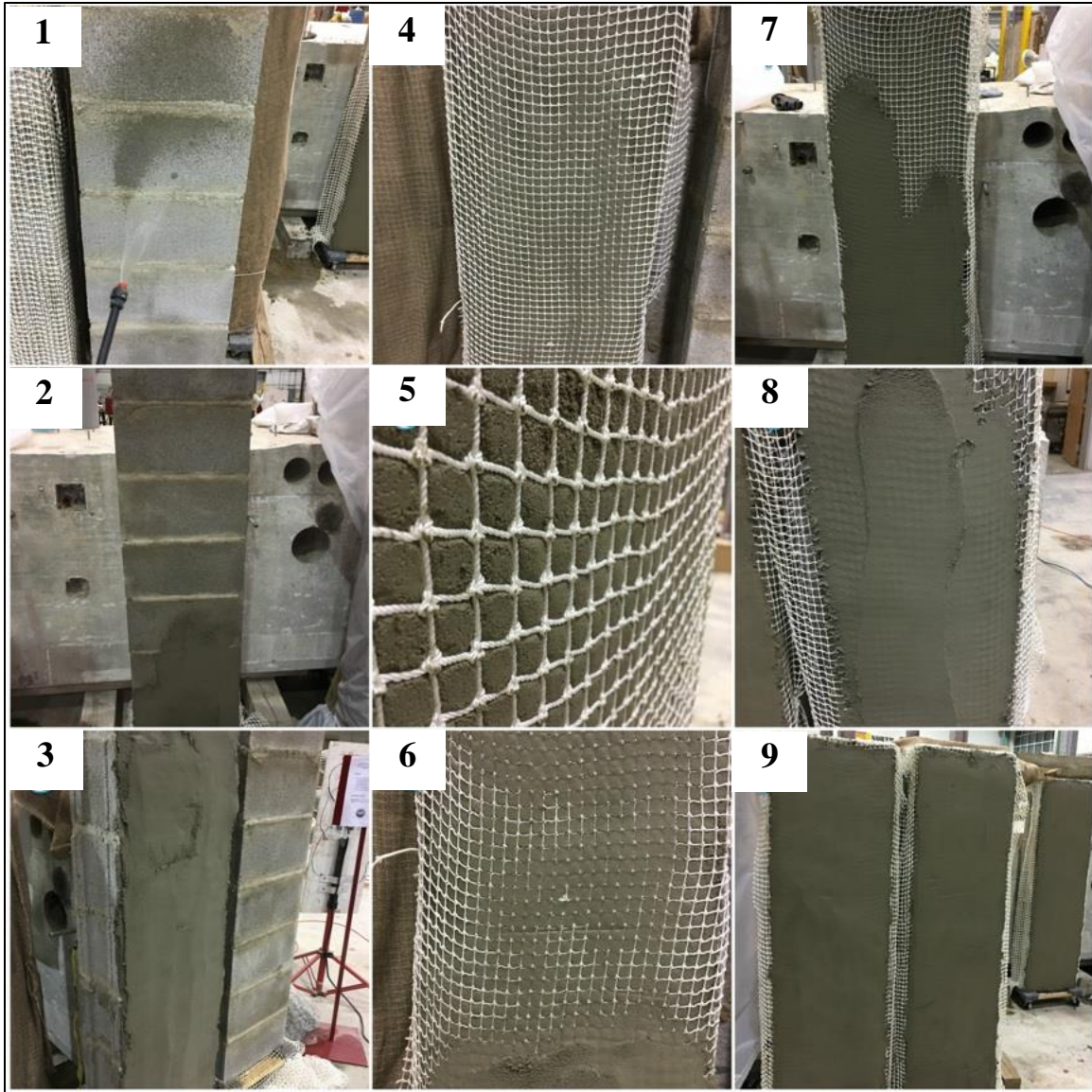
Figure 6.3 FN plastering process, (1) spraying masonry surface with water, (2-3) applying first mortar layer, (4) applying FN reinforcement, (5, 6) placing FN reinforcement on mortar, (7, 8) applying second mortar layer, and (9) surface troweling.
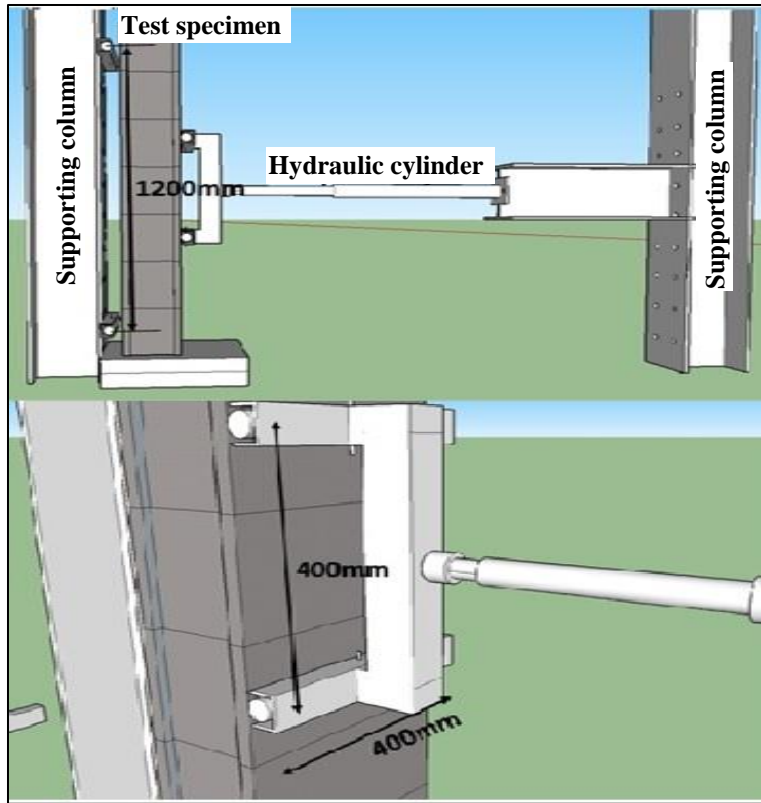
Figure 6.4 Masonry prism flexural test setup.

Figure 6.5 Flexural test instrumentation.

100
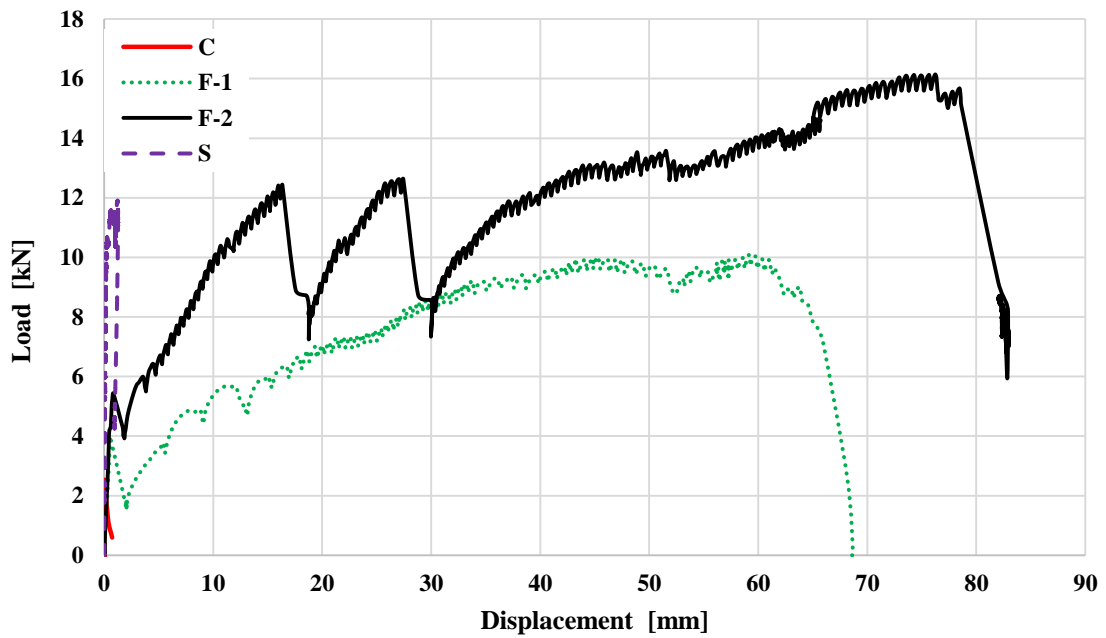
Figure 6.6 Out-of-plane load-displacement response of masonry prisms.
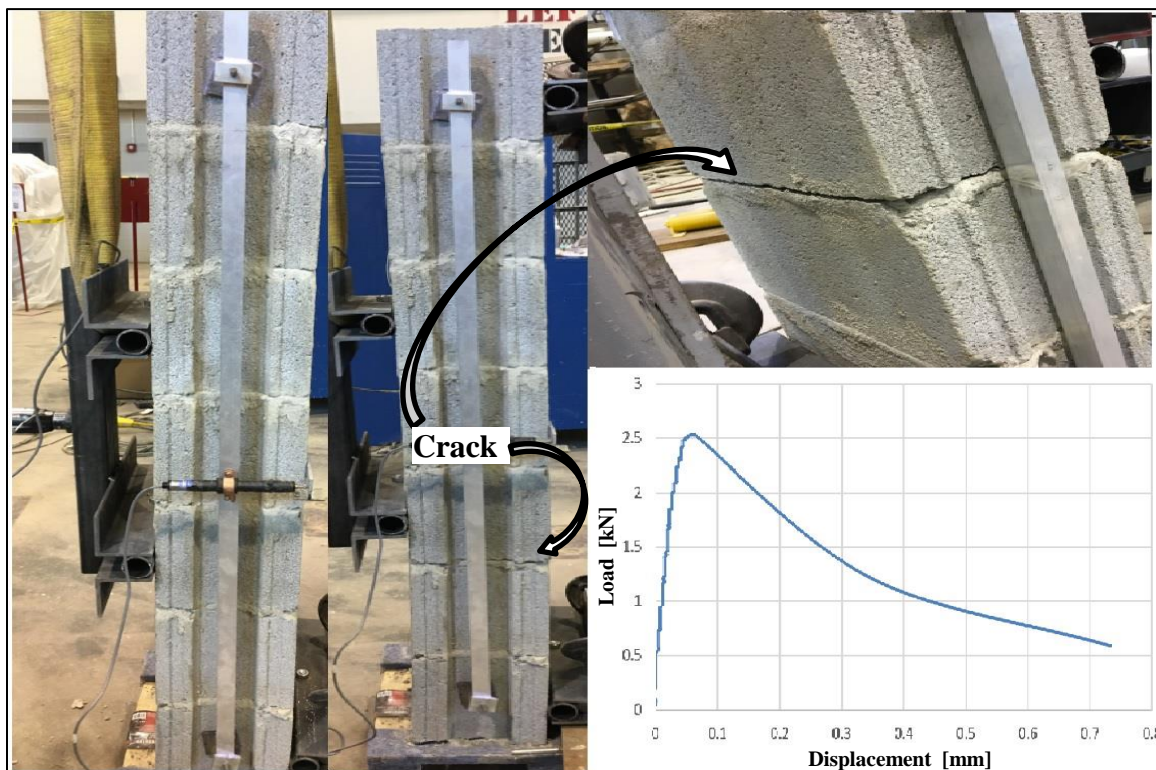
Figure 6.7 Out-of-plane load-displacement response of unreinforced masonry prism.

101
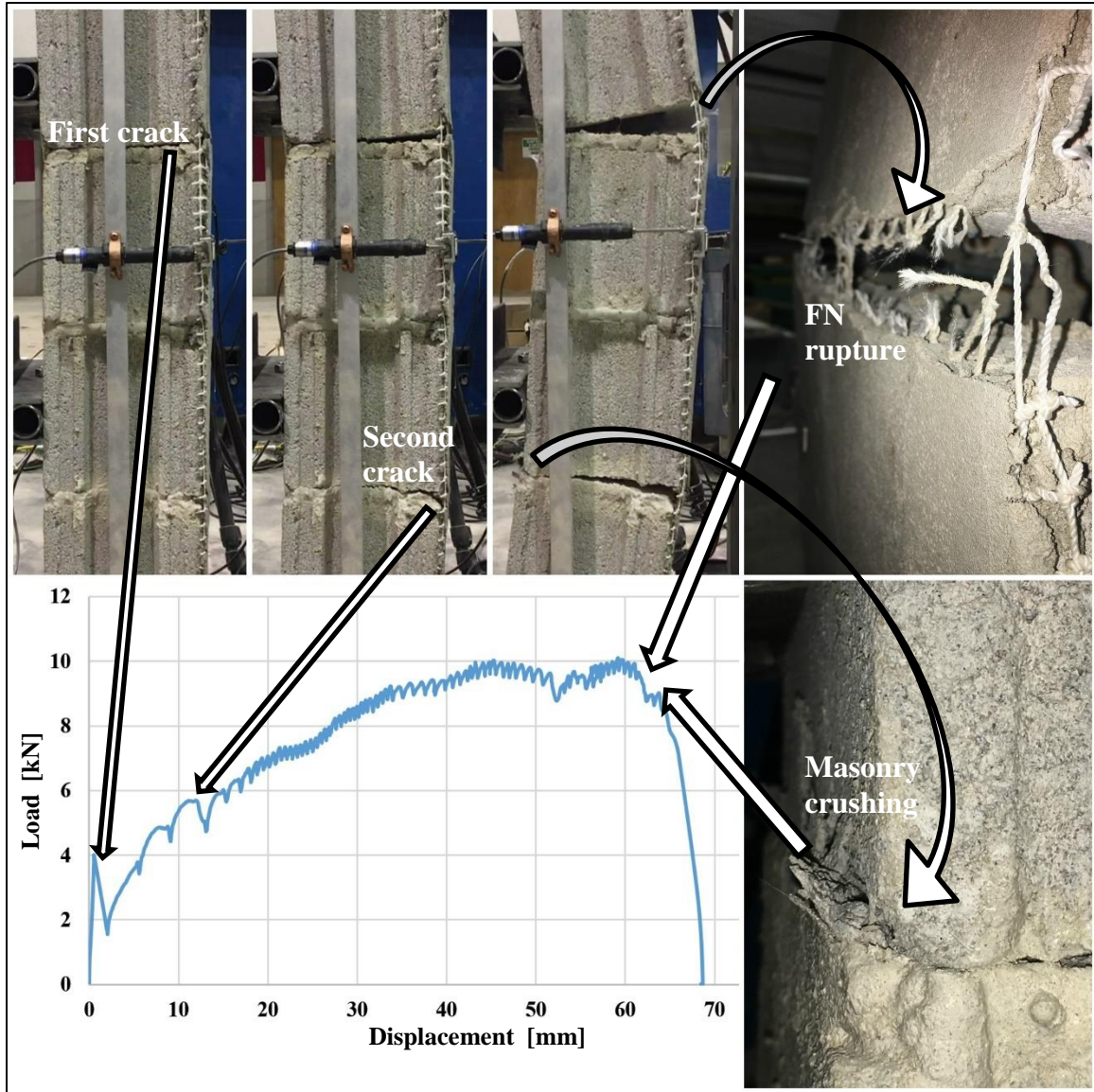
Figure 6.8 Out-of-plane load-displacement response of one-layer FN-FRCM strengthened masonry prism.
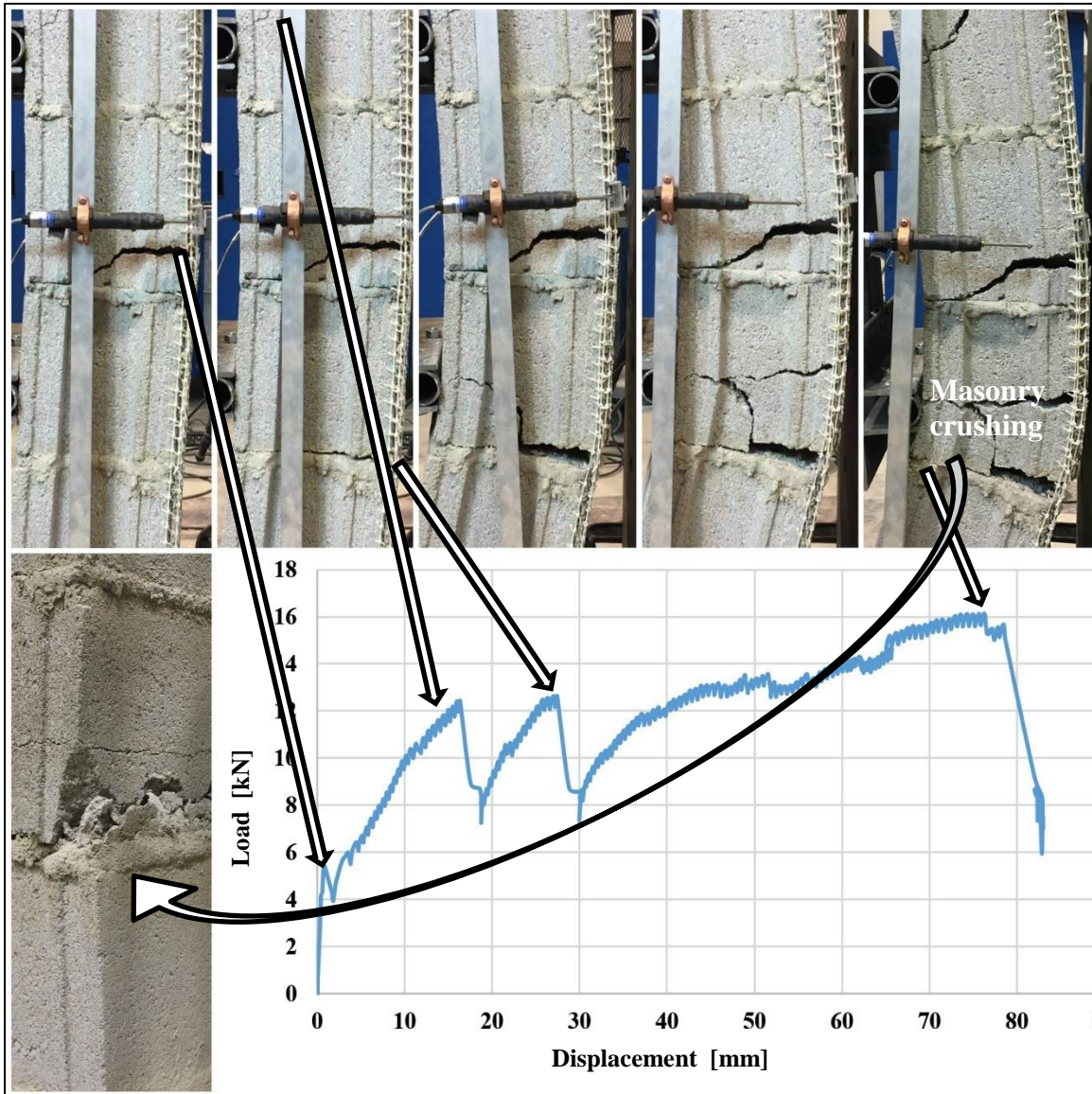
Figure 6.9 Out-of-plane load-displacement response of two-layer FN-FRCM
strengthened masonry prism.
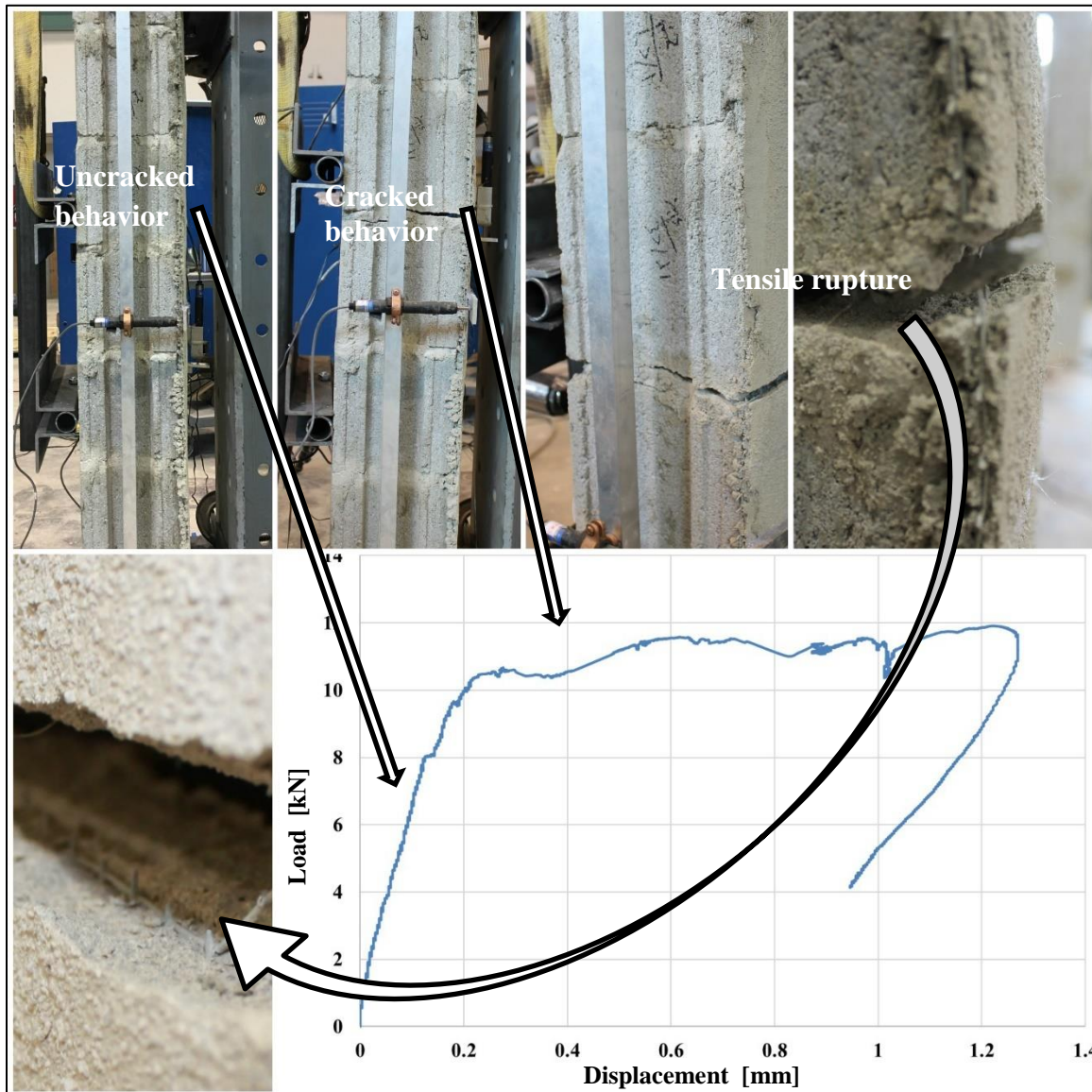
Figure 6.10 Out-of-plane load-displacement response of WWSM-reinforced mortar strengthened masonry prism.
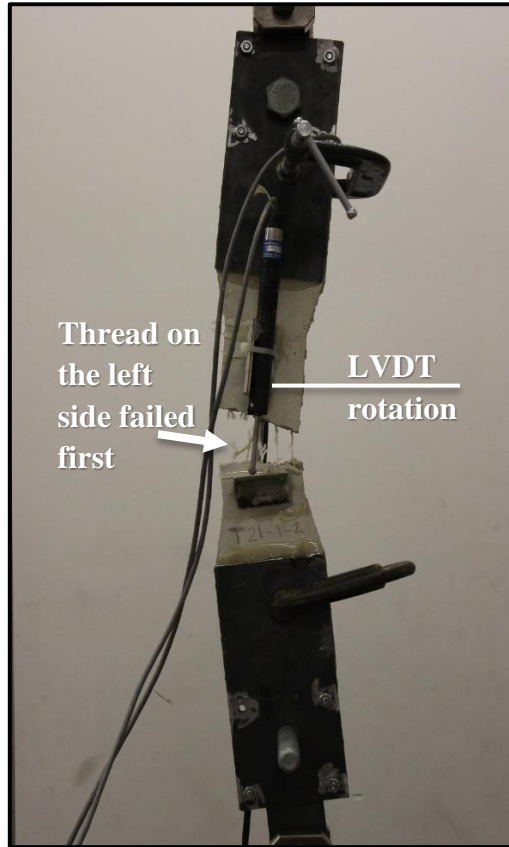
Figure 6.11 Influence of specimen rotation on stress variation (associated with different forces resisted by threads) and position of LVTD sensors.
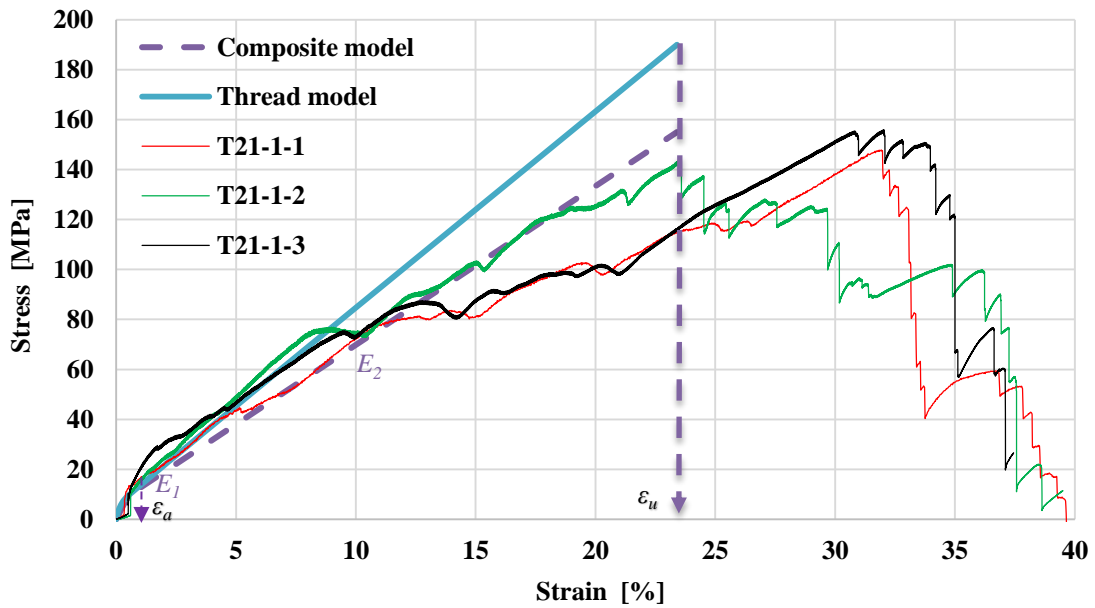
Figure 6.12 Modified thread and composite tensile stress-strain models.

105
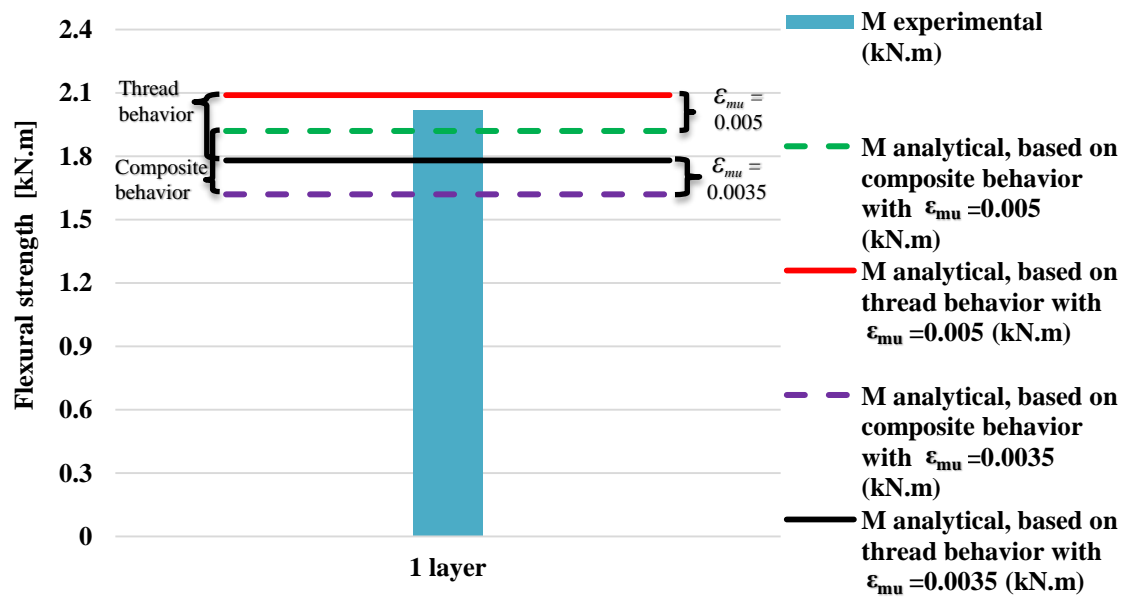
Figure 6.13 Flexural strength analytical predictions and experimental results for one-layer FN-FRCM strengthened masonry prism.

CHAPTER 7
REVIEW AND CONCLUSIONS

7.1 Review of research

The aim of this project is to investigate a novel and affordable option to externally strengthen substandard concrete masonry (CM) walls for out-of-plane loads (e.g., high winds and flying debris). Two types of strengthening materials for fiber-reinforced cement mortar (FRCM) overlays are investigated; namely, fishing net (FN) and welded wire steel mesh (WWSM) reinforcements.

Salient mechanical properties of representative materials including substandard concrete masonry unit (CMU) blocks, mortar, nylon FN and WWSM reinforcements, and FRCM composite, were experimentally characterized. A simple bilinear model is proposed to describe the tensile behavior of the FRCM composite. An analytical model was then used to estimate the flexural capacity and failure mode of strengthened CM walls as a function of the amount of FN reinforcement. The wind velocity that a strengthened CM wall can withstand was evaluated based on a standard velocity pressure equation, and a parametric study was performed to determine the influence of the CM compressive strength (as a measure of substandard properties) on the out-of-plane flexural capacity.

Finally, an experimental program was implemented to provide proof of concept. A four-point bending test was performed on four concrete masonry

107

specimens, including: one plain masonry (control) specimen; two specimens strengthened with one and two layers of FN-reinforced mortar overlay, respectively; and, one specimen strengthened with a WWSM-reinforced mortar overlay, which served as benchmark specimen for the newly-conceived FN system.

It is shown that the out-of-plane flexural capacity of substandard CM walls can be made suitable to resist high wind pressures by means of FN- as well as WWSM-FRCM overlays. In fact, the out-of-plane capacity contributed by the FN-FRCM system is comparable to that contributed by the WWSM-FRCM counterpart. However, the FN-FRCM overlay outperforms the WWSM system in term of deformability and thus energy-absorption capacity. The evidence produced through this research attests to the potential of the novel FN-FRCM system presented herein to retrofit substandard CM walls against high-wind pressures, and possibly the impact of flying debris during hurricanes and tornadoes.

7.2 Conclusions

1. The nylon multifilament fishing nets have higher deformation capacity (around 15 times) compared to the steel welded wire mesh WWSM. The high deformation capacity of the fishing nets results from the lower stiffness of the nylon material compared to steel, and the presence of knots. The knots contribute to thread deformation due to knot tightening or thread slippage through the knot.

2. The presence of the knot decreases the thread strength and increases the thread deformation because the failure is initiated by knot unraveling or thread slippage through the knot.

3. The tensile strength of fishing net reinforcement specimens decreases as the number of threads increases. This effect is due to the uneven stress distribution among the threads.

4. The ultimate strain of fishing net reinforcement specimens increases as the number of threads increases. This effect is due to the geometry configuration of the mesh specimen, which results in higher maximum deformations for wider specimens having an inevitably uneven stress distribution.

5. The uniaxial tensile response of FN-FRCM is either bilinear or trilinear because of the boundary conditions of the test and the properties of the constituent materials.

6. The FRCM composite overlays reinforced with FNs shows comparable strength, between 72 – 120 %, to that of counterparts having WWSM reinforcement.

7. SEM images suggest effective interfacial bond between the mortar and the FN and WWSM reinforcement.

8. The boundary conditions influence the tensile strength of FN reinforcement and FN-FRCM composite specimens. Higher tensile strength values are attained by the composite due to the mortar role in better distributing the load to the reinforcing threads.

9. The tensile stress-strain response of dog-bone FN-FRCM composite specimens represents a conservative behavior because of the difference of the boundary conditions with respect to actual bonded overlays. In the latter case, the presence of

an adhesive bond onto the masonry surface facilitates a more uniform distribution of tensile stresses (and thus damage) to the FN reinforcing threads.

10. The masonry flexural strength analytical predictions based on dog-bone specimen test data are conservative in comparison with the experimental results. Also, the relatively high ultimate strain of the substandard concrete masonry contributes to increase the overlay strengthening efficiency as it allows the FN reinforcement to reach higher effective tensile strain and stress.

11. The failure modes of the masonry prisms predicted by the analytical model are similar to the failure modes observed in physical experiments.

12. The experimental out-of-plane flexural strength of substandard masonry prisms strengthened with FN-FRCM overlays is comparable to that of counterparts strengthened with WWSM-reinforced mortar overlays. This evidence supports the hypothesis that substandard confined masonry walls can be strengthened using FN-FRCM overlays to safely resist hurricane wind pressures.

13. The out-of-plane flexural capacity of strengthened masonry prisms increases by 60% when using two-layer instead of one-layer FN-FRCM overlays.

14. The parametric study showed that the out-of-plane flexural capacity of CM walls increases with the increase of the compressive strength of the masonry. However, the wall flexural capacity is limited by the tensile strength of the FN reinforcement when the compressive strength of the masonry is more than 7.5 MPa.

110

REFERENCES

ACI (2013). *Guide to Design and Construction of Externally Bonded Fabric- Reinforced Cementitious Matrix (FRCM) Systems for Repair and Strengthening Concrete and Masonry Structures*.

Al-Salloum, Y. A., Almusallam, T. H., Elsanadedy, H. M., & Iqbal, R. A. (2016). Effect of elevated temperature environments on the residual axial capacity of RC columns strengthened with different techniques. *Construction and Building Materials*, *115*, 345–361.

Alabdulhady M., Sneed, L.H., Carloni, C. (2017). Torsional Behavior of RC Beams Strengthened with PBO-FRCM Composite − An Experimental Study. *Engineering Structures*, *136*, 393–405.

Alecci, V., Focacci, F., Rovero, L., Stipo, G., & de Stefano, M. (2016). Extrados strengthening of brick masonry arches with PBO-FRCM composites: Experimental and analytical investigations. *Composite Structures*, *149*, 184–196.

Alhozaimy, a. M., Soroushian, P., & Mirza, F. (1996). Mechanical properties of polypropylene fiber reinforced concrete and the effects of pozzolanic materials. *Cement and Concrete Composites*, *18*(2), 85–92.

American Society of Civil Engineers. (2010). *Minimum Design Loads for Buildings and Other Structures*.

Andrew Smith & Thomas Redman. (2009). A critical review of retrofitting methods for unreinforced masonry structures. In *EWB-UK Research Conference*.

Arboleda, D. (2014). *Fabric Reinforced Cementitious Matrix (FRCM) Composites for Infrastructure Strengthening and Rehabilitation : Characterization Methods*.

Arboleda, D., Carozzi, F., Nanni, A., & Poggi, C. (2016). Testing Procedures for the Uniaxial Tensile Characterization of Fabric-Reinforced Cementitious Matrix Composites. *Journal of Composites for Construction*, *20*(3).

Arif, M., Pankaj, & Kaushik, S. K. (1999). Mechanical behaviour of ferrocement composites: An experimental investigation. *Cement and Concrete Composites*, *21*(4), 301–312.

Ascione, L., De Felice, G., & De Santis, S. (2015). A qualification method for externally bonded Fibre Reinforced Cementitious Matrix (FRCM) strengthening systems. *Composites Part B: Engineering*, *78*, 497–506.

ASTM. (2003a). *Standard Test Method for Compressive Strength of Masonry Prisms, C1413*. *American Society for Testing and Materials*.

ASTM. (2003b). *Standard Test Method for Tensile Strength and Young's Modulus of Fibers, C1557*. *American Society for Testing and Materials*.

ASTM. (2005a). *Standard Test Method for Compressive Strength of Hydraulic Cement Mortars (Using 2-in. or [50-mm] Cube Specimens), C109*. *American Society for Testing and Materials*. West Conshohocken, PA.

ASTM. (2005b). *Standard Test Methods for Sampling and Testing Concrete Masonry Units and Related Units, C140*. *American Society for Testing and Materials*. West Conshohocken, PA.

ASTM. (2006). *Standard Specification for Mortar for Unit Masonry, C270*. *American Society for Testing and Materials*. West Conshohocken, PA.

ASTM. (2014). *Standard test method for flexural strength of hydraulic-cement mortars, C348. American Society for Testing and Materials*.

Audefroy, J. F. (2011). Haiti: post-earthquake lessons learned from traditional construction. *Environment and Urbanization*, *23*(2), 447–462.

Awani, O. (2015). *Shear Strengthening of Reinforced Concrete Beams Using Textile-Reinforced Mortar*.

Awani, O., Refai, A. El, & El-Maaddawy, T. (2015). Bond characteristics of carbon fabric-reinforced cementitious matrix in double shear tests. *Construction and Building Materials*, *101*, 39–49.

Babaeidarabad, S., Arboleda, D., Loreto, G., & Nanni, A. (2014). Shear strengthening of un-reinforced concrete masonry walls with fabric-reinforced-cementitious-matrix. *Construction and Building Materials*, *65*, 243–253.

Babaeidarabad, S., De Caso, F., & Nanni, A. (2014). Out-of-Plane Behavior of URM Walls Strengthened with Fabric-Reinforced Cementitious Matrix Composite. *ASCE*, *549*(2013), 1–11.

Babaeidarabad, S., Loreto, G., & Nanni, A. (2014). Flexural strengthening of RC beams with an externally bonded fabric-reinforced cementitious matrix. *Journal of Composites for Construction*, *18*(5), 1–12.

Badanoiu, A., & Holmgren, J. (2003). Cementitious composites reinforced with continuous carbon fibres for strengthening of concrete structures. *Cement Concr Compos, 25*, 387–394.

Balaguru, P., & Slattum, K. (1995). Test Methods for Durability of Polymeric Fibers in Concrete and UV Light Exposure. *ACI Special Publication*, *155*, 115–136.

113

Banthia, N., & Nandakumar, N. (2003). Crack growth resistance of hybrid fiber reinforced cement composites, *25*, 3–9.

BBC News - Haiti devastation exposes shoddy construction. (2010). Retrieved February 27, 2017, from http://news.bbc.co.uk/2/hi/8460042.stm

Bernat-Maso, E., Escrig, C., Aranha, C. a., & Gil, L. (2014). Experimental assessment of Textile Reinforced Sprayed Mortar strengthening system for brickwork wallettes. *Construction and Building Materials*, *50*, 226–236.

Bertelsen, I., & Schmidt, J. W. (2016). Recycled fishing nets as reinforcement of existing concrete structures.

Bertolesi, E., Carozzi, F. G., Milani, G., & Poggi, C. (2014). Numerical modeling of Fabric Reinforce Cementitious Matrix composites (FRCM) in tension. *Construction and Building Materials*, *70*, 531–548.

Bisby, L., Stratford, T. ; Joanna Smith, J. and; Halpin, S. (2011). FRP versus Fiber Reinforced Cementitious Mortar Systems at Elevated Temperature. *Special Publication*, *275*, 1–20.

Briccoli Bati, S., Rovero, L., & Tonietti, U. (2007). Strengthening Masonry Arches with Composite Materials. *Journal of Composites for Construction*, *11*(1), 33–41.

Cai, Y., Shi, B., Ng, C. W. W., & Tang, C. S. (2006). Effect of polypropylene fibre and lime admixture on engineering properties of clayey soil. *Engineering Geology*, *87*(3–4), 230–240.

Carney, P., & Myers, J. J. (2005). Out-of-Plane Static and Blast Resistance of Unreinforced Masonry Wall Connections Strengthened with FRP. *ACI Special Publications*, *1*(2005, NUMB 230), 229–248.

Chithambaram, S. J., & Kumar, S. (2017). Flexural behaviour of bamboo based ferrocement slab panels with flyash. *Construction and Building Materials*, *134*, 641−648.

Colajanni, P., De Domenico, F., Recupero, A., & Spinella, N. (2014). Concrete columns confined with fibre reinforced cementitious mortars: Experimentation and modelling. *Construction and Building Materials*, *52*, 375−384.

Colombo, M.Colombo, A.Magri, G. Zani, M. di P. (2011). Tensile behaviour of Textile: influence of multilayer reinforcement.

Contamine, R., Si Larbi, A., & Hamelin, P. (2011). Contribution to direct tensile testing of textile reinforced concrete (TRC) composites. *Materials Science and Engineering A*, *528*(29−30), 8589−8598.

Corradi, M., Borri, A., & Vignoli, A. (2008). Experimental evaluation of in-plane shear behaviour of masonry walls retrofitted using conventional and innovative methods. *Masonry International*, *21*(1), 29.

Cuny, F. C. (1982). *Improvement of Rural Housing in Haiti to withstand Hurricanes*.

D'Ambrisi, A., Feo, L., & Focacci, F. (2012). Bond-slip relations for PBO-FRCM materials externally bonded to concrete. *Composites Part B: Engineering*, *43*(8), 2938–2949.

D'Ambrisi, A., Feo, L., & Focacci, F. (2013a). Experimental analysis on bond between PBO-FRCM strengthening materials and concrete. *Composites Part B: Engineering*, *44*(1), 524–532.

D'Ambrisi, A., Feo, L., & Focacci, F. (2013b). Experimental and analytical investigation on bond between Carbon-FRCM materials and masonry. *Composites Part B:*

Engineering, *46*, 15–20.

D'Ambrisi, A., & Focacci, F. (2011). Flexural Strengthening of RC Beams with Cement-Based Composites. *Journal of Composites for Construction*, *15*(5), 707–720.

D'Antino, T., Carloni, C., Sneed, L. H., & Pellegrino, C. (2014). Matrix-fiber bond behavior in PBO FRCM composites: A fracture mechanics approach. *Engineering Fracture Mechanics*, *117*(February), 94–111.

D'Antino, T., Carloni, C., Sneed, L. H., & Pellegrino, C. (2015). Fatigue and post-fatigue behavior of PBO FRCM-concrete joints. *International Journal of Fatigue*, *81*, 91–104.

Daniel, I. M., & Ishai, O. (1994). *Engineering mechanics of composite materials*. *Mechanics of Composite Materials*.

Daniel, I. M., & Ishai, O. (1994). Engineering mechanics of composite materials. *Mechanics of Composite Materials*.

de Felice, G., De Santis, S., Garmendia, L., Ghiassi, B., Larrinaga, P., Lourenco, P. B., … Papanicolaou, C. G. (2014). Mortar-based systems for externally bonded strengthening of masonry. *Materials and Structures*, *47*(12), 2021–2037.

de Felice, G., De Santis, S., Garmendia, L., Ghiassi, B., Larrinaga, P., Lourenço, P. B., … Papanicolaou, C. G. (2014). Mortar-based systems for externally bonded strengthening of masonry. *Materials and Structures*.

De Santis, S., & De Felice, G. (2015). Tensile behaviour of mortar-based composites for externally bonded reinforcement systems. *Composites Part B: Engineering*, *68*, 401–413.

Donnini, J., Corinaldesi, V., & Nanni, A. (2016). Mechanical properties of FRCM using

carbon fabrics with different coating treatments. *Composites Part B: Engineering*, *88*(December 2015), 220–228.

Donnini, J., y Basalo, F. D. C., Corinaldesi, V., Lancioni, G., & Nanni, A. (2017). Fabric-reinforced cementitious matrix behavior at high-temperature: Experimental and numerical results. *Composites Part B: Engineering*, *108*, 108–121.

Ebead, U., Shrestha, K. C., Afzal, M. S., Refai, A. El, & Nanni, A. (2015). Effectiveness of Fabric-Reinforced Cementitious Matrix in Strengthening Reinforced Concrete Beams. *Journal of Composites for Construction*, *1*(August), 1–14.

Efendy, M. G. A., & Pickering, K. L. (2014). Composites : Part A Comparison of harakeke with hemp fibre as a potential reinforcement in composites, *67*, 259–267.

El-Maaddawy, T., & El Refai, A. (2015). Innovative repair of severely corroded t-beams using fabric-reinforced cementitious matrix. *Journal of Composites for Construction*, *20*(3), 4015073.

El Debs, M. K., & Naaman, A. E. (1995). Bending behavior of mortar reinforced with steel meshes and polymeric fibers. *Cement and Concrete Composites*, *17*(4), 327–338.

Elsanadedy, H. M., Almusallam, T. H., Alsayed, S. H., & Al-Salloum, Y. A. (2013). Flexural strengthening of RC beams using textile reinforced mortar - Experimental and numerical study. *Composite Structures*, *97*, 40–55.

Escrig, C., Gil, L., & Bernat-Maso, E. (2017). Experimental comparison of reinforced concrete beams strengthened against bending with different types of cementitious-matrix composite materials. *Construction and Building Materials*, *137*, 317–329.

Fonteyne, R., & Galbraith, R. D. (2004). Mesh size measurement revisited. *ICES*

Cooperative Research Report, 266(266).

Foraboschi, P. (2004). Strengthening of Masonry Arches with Fiber-Reinforced Polymer Strips. *Journal of Composites for Construction*, *8*(3), 191–202.

Fothergill, A., DeRouen Darlington, J., Maestas, E. G. M., & Darlington, J. D. (1999). Race, ethnicity and disasters in the United States: A review of the literature. *Disasters*, *23*(2), 156–173.

Ghorbani, R. (2014). Context-Sensitive Seismic Strengthening and Repair of Substandard Confined Masonry.

Ghorbani, R., Garbin, E., & Matta, F. (2013). Rapid and Affordable Seismic Retrofit of Substandard Confined Masonry. *Structures Congress 2013*, (May), 1193–1204.

Hannant, D. J. (1989). Ten Year Flexural Durability Tests on Cement Sheets Reinforced with Fibrillated Polypropylene Networks. Fibre Reinforced Cements and Concrete: Recent Developments. *Proceedings of an International Conference Held At the University of Wales, College of Cardiff, School of Engineering, United Kingdom.*

Hashemi, S., & Al-Mahaidi, R. (2011). Investigation of bond strength and flexural behaviour of FRP-strengthened reinforced concrete beams using cement-based adhesives.(technical paper). *Australian Journal of Structural Engineering*, *11*(2), 129(11).

Hinrichsen, D. (1998). The Coastal Population Explosion. *The Next 25 Years: Global Issues*, 27–29.

ICC-ES (2013). *Acceptance criteria for masonry and concrete strengthening using fabric-reinforced cementitious matrix (FRCM) composite systems.* Whittier, CA.

Ida Maria Gieysztor Bertelsen, L. M. O. (2016). Engineering Properties of Fibres from Waste Fishing Nets (pp. 1–10).

ISO 1806. (2002). *Fishing nets — Determination of mesh breaking force of netting*.

Johnston, C. (2010). *Fiber-reinforced cements and concretes*. CRC Press.

Jung, K., Hong, K., Han, S., Park, J., & Kim, J. (2015). Prediction of Flexural Capacity of RC Beams Strengthened in Flexure with FRP Fabric and Cementitious Matrix. *International Journal of Polymer Science*.

Kadam, S. B., Singh, Y., & Li, B. (2014). Strengthening of unreinforced masonry using welded wire mesh and micro-concrete - Behaviour under in-plane action. *Construction and Building Materials*, *54*, 247–257.

Kadam, S. B., Singh, Y., & Li, B. (2015). Out-of-plane behaviour of unreinforced masonry strengthened using ferrocement overlay. *Materials and Structures*, *48*(10), 3187–3203.

Khajuria A., Bohra K., and B. P. (1991). Long-Term Durability of Synthetic Fibers in Concrete. *ACI Special Publication*, *126*, 851–868.

Kijewski-Correa, T., & Taflanidis, A. A. (2012). The haitian housing dilemma: Can sustainability and hazard-resilience be achieved? *Bulletin of Earthquake Engineering*, *10*(3), 765–771.

Klust, G. (1982). *Netting Materials for Fishing Gear. FAO Fishing Manuals*.

Kolsch, H. (1998). Carbon Fiber Cement Matrix (CFCM) Overlay System for Masonry Strengthening. *Journal of Composites for Construction*, *2*(2), 105–109.

Koutas, L., Bousias, S. N., & Triantafillou, T. C. (2015). Seismic Strengthening of Masonry-Infilled RC Frames with TRM: Experimental Study. *Journal of*

119

Composites for Construction, *19*(2).

Krimgold, F. (2011). Disaster risk reduction and the evolution of physical development regulation. *Environmental Hazards*, *10*(January 2015), 53–58.

Larrinaga, P., Chastre, C., Biscaia, H. C., & San-José, J. T. (2013). Experimental and Numerical Modelling of Basalt Textile Reinforced Mortar Behavior Under Uniaxial Tensile Stress. *Materials & Design*, *55*, 66–74.

M Lafuente, E Castill, and C. G. (1998). Experimental and analytical evaluation of the seismic resistant behaviour of masonry walls. *Masonry International*.

Mamlouk, M. S., & Zaniewski, J. P. (2011). *Materials for Civil and Construction Engineers*.

Marshall, J. D., Lang, A. F., Baldridge, S. M., & Popp, D. R. (2011). Recipe for disaster: Construction methods, materials, and building performance in the January 2010 haiti earthquake. *Earthquake Spectra*, *27*(SUPPL. 1).

Marshall, O. S., Sweeney, S. C., & Trovillion, J. C. (2000). *Performance Testing of Fiber-Reinforced Polymer Composite Overlays for Seismic Rehabilitation of Unreinforced Masonry*.

Mayorca, P., & Meguro, K. (2004). Proposal of an efficient technique for retrofitting unreinforced masonry dwellings. *13th World Conference on Earthquake Engineering Conference Proceedings, Vancouver, British Columbia, Canada, August 1-6, 2004*.

McMaster-Carr. (n.d.-a). Retrieved February 26, 2017, from https://www.mcmaster.com/#welded-wire-cloth-screens/=16cslo6

McWilliams, H., & Griffin, C. T. (2013). A critical assessment of concrete and masonry

120

structures for reconstruction after seismic events in developing countries. *Structures and Architecture*, 857–864.

Meli, R., & Alcocer, S. M. (2004). Implementation of Structural Earthquake-Disaster Mitigation Programs in Developing Countries. *Natural Hazards Review*, *5*(1), 29–39.

Mesaglio, G. (2014). *Tensile behavior of Fabric Reinforced Cementitious Matrix (FRCM) composites*.

Minimum Design Loads for Buildings and Other Structures. (2013). Reston, VA: American Society of Civil Engineers.

Moroni, M. O., Astroza, M., & Acevedo, C. (2004). Performance and Seismic Vulnerability of Masonry Housing Types Used in Chile. *Journal of Performance of Constructed Facilities*, *Vol. 18,*(No. 3,), 173–179.

MSJC. (2011). Building Code Requirements and Specification for Masonry Structures. *Masonry Standards Joint Committee, The Masonry Society.*

Mu, B., Meyer, C., & Shimanovich, S. (2002a). Improving the interface bond between f iber mesh and cementitious matrix, *32*(2001), 783–787.

Mu, B., Meyer, C., & Shimanovich, S. (2002b). Improving the interface bond between fiber mesh and cementitious matrix. *Cement and Concrete Research*, *32*(5), 783–787.

Nanni, A. (2012). A New Tool for Concrete and Masonry Repair. *Concrete International*, (april), 43–49.

Netting - The Fish Net Company LLC. (n.d.). Retrieved from https://fishnetco.com/products/fishing-nets/netting

Oceans, Fisheries and Coastal Economies. (2017). Retrieved April 19, 2017, from http://www.worldbank.org/en/topic/environment/brief/oceans

Olivito, R. S., Cevallos, O. A., & Carrozzini, A. (2014). Development of durable cementitious composites using sisal and flax fabrics for reinforcement of masonry structures. *Materials and Design*, *57*, 258–268.

Olivito, R. S., Dubois, F., Venneri, A., & Zuccarello, F. (2012). Experimental And Numerical Analysis Of Masonry Macroelements Reinforced By Natural-Fibre-Composite Materials. In *6th international conference on FRP composites in civil engineering (CICE2012)* (pp. 1–8).

Ombres, L. (2011). Flexural analysis of reinforced concrete beams strengthened with a cement based high strength composite material. *Composite Structures*, *94*(1), 143–155.

Ombres, L. (2015a). Analysis of the bond between Fabric Reinforced Cementitious Mortar (FRCM) strengthening systems and concrete. *Composites Part B: Engineering*, *69*, 418–426.

Ombres, L. (2015b). Structural performances of reinforced concrete beams strengthened in shear with a cement based fiber composite material. *Composite Structures*, *122*, 316–329.

P. Paramasivam and R. Sri Ravindrarajah. (1988). Effect of arrangements of reinforcements on mechanical properties of ferrocement. *ACI Structural Journal*.

P.N.Balaguru, S. P. S. (1992). *Fiber Reinforced Cement Composite*. *Mc Graw Hill-Inc. New York*. Mc Graw Hill-Inc. New York.

Papanicolaou, C., Triantafillou, T., & Lekka, M. (2011). Externally bonded grids as

strengthening and seismic retrofitting materials of masonry panels. *Construction and Building Materials*, *25*(2), 504–514.

Prevatt, Dupigny-Giroux, & Masters. (2010). Engineering Perspectives on Reducing Hurricane Damage to Housing in CARICOM Caribbean Islands. *Natural Hazards Review*, *11*(4), 140–150.

Ramamurthy, K., & Kunhanandan Nambiar, E. K. (2004). Accelerated masonry construction review and future prospects. *Progress in Structural Engineering and Materials*, *6*(1), 1–9.

Rupika, W. K. S. (2010). *Out of plane strengthening of unreiforced masonry walls using textile reinforced mortar systems*. University of Moratuwa, Sri Lanka.

Santis, S. De, Roscini, F., & Felice, G. De. (2016). Experimental characterization of mortar-based reinforcements with carbon fabrics (pp. 381–386).

Sathiparan, N., & Meguro, K. (2013). Seismic Retrofitting of Non-Engineering Masonry Houses using Polypropylene Band Meshes. *2nd International Symposium on Advances in Civil and Environmental Engineering Practices for Sustainable Development*, (July 2016).

Sawpan, M. (2010). *Mechanical performance of industrial hemp fibre reinforced polylactide and unsaturated polyester composites*.

Schladitz, F., Frenzel, M., Ehlig, D., & Curbach, M. (2012). Bending load capacity of reinforced concrete slabs strengthened with textile reinforced concrete. *Engineering Structures*, *40*, 317–326.

Shackelford, J. F. (2005). *Introduction to Materials Science for Engineers*.

Shop Blue Hawk Rolled Wire Galvanized Steel Hardware Cloth (Common: 10-ft x 2-ft;

Actual: 10-ft x 2-ft) at Lowes.com. (n.d.). Retrieved from http://www.lowes.com/pd/Blue-Hawk-Rolled-Wire-Galvanized-Steel-Hardware-Cloth-Common-10-ft-x-2-ft-Actual-10-ft-x-2-ft/4780947

Shrestha, H., Pradhan, S., & Guragain, R. (2012). Experiences on Retrofitting of Low Strength Masonry Buildings by Different Retrofitting Techniques in Nepal. *15th World Conference on Earthquake Engineering, Lisbon Portugal*, (January 2006).

Sneed, L. H., D'Antino, T., & Carloni, C. (2014). Investigation of bond behavior of polyparaphenylene benzobisoxazole fiber-reinforced cementitious matrix composite-concrete interface. *ACI Materials Journal*, *111*(5), 569–580.

Sneed, L. H., D'Antino, T., Carloni, C., & Pellegrino, C. (2015). A comparison of the bond behavior of PBO-FRCM composites determined by double-lap and single-lap shear tests. *Cement and Concrete Composites*, *64*(December), 37–48.

Song, P. S., Hwang, S., & Sheu, B. C. (2005). Strength properties of nylon- and polypropylene-fiber-reinforced concretes. *Cement and Concrete Research*, *35*(8), 1546–1550.

Spadea, S., Farina, I., Carrafiello, A., & Fraternali, F. (2015). Recycled nylon fibers as cement mortar reinforcement. *Construction and Building Materials*, *80*, 200–209.

Stewart, S. R. (2017). Hurricane MATTHEW. *National Hurricane Center*.

Suaris, B. W., & Khan, M. S. (1995). Residential construction failures caused by hurricane andrew, *9*(6944), 24–33.

Tang, C.-S., Shi, B., & Zhao, L.-Z. (2010). Interfacial shear strength of fiber reinforced soil. *Geotextiles and Geomembranes*, *28*(1), 54–62.

Tang, C., Shi, B., Gao, W., Chen, F., & Cai, Y. (2007). Strength and mechanical behavior

of short polypropylene fiber reinforced and cement stabilized clayey soil. *Geotextiles and Geomembranes*, *25*(3), 194–202.

Tena-Colunga, A., Juárez-Ángeles, A., & Salinas-Vallejo, V. H. (2009). Cyclic behavior of combined and confined masonry walls. *Engineering Structures*, *31*(1), 240–259.

Tetta, Z. C., Koutas, L. N., & Bournas, D. A. (2015). Textile-reinforced mortar (TRM) versus fiber-reinforced polymers (FRP) in shear strengthening of concrete beams. *Composites Part B: Engineering*, *77*, 338–348.

Trapko, T. (2013). Fibre reinforced cementitious matrix confined concrete elements. *Materials and Design*, *44*, 382–391.

Triantafillou, T. C., Karlos, K., Kefalou, K., & Argyropoulou, E. (2017). An innovative structural and energy retrofitting system for URM walls using textile reinforced mortars combined with thermal insulation : Mechanical and fire behavior, *133*, 1–13.

Triantafillou, T. C., Papanicolaou, C. G., Zissimopoulos, P., & Laourdekis, T. (2006). Concrete confinement with textile-reinforced mortar jackets. *ACI Structural Journal*, *103*(1), 28–37.

UN. (2008). *Percentage of Total Population Living in Coastal Areas*. *United Nations*. Retrieved from http://www.un.org/esa/sustdev/natlinfo/indicators/methodology_sheets/oceans_seas_coasts/pop_coastal_areas.pdf%0Ahttp://sedac.ciesin.columbia.edu/es/papers/Coastal_Zone_Pop_Method.pdf%5Cnhttp://www.un.org/esa/sustdev/natlinfo/indicators/methodology_sheets/

Understanding Wire Gauges Used In Welded; Woven Wire Mesh; and Fence. (n.d.). Retrieved March 11, 2017, from

http://www.louispage.com/blog/bid/7075/Understanding-Wire-Gauges-Used-In-Welded-Woven-Wire-Mesh-Fence

Vasconcelos, G., Abreu, S., Fangueiro, R., & Cunha, F. (2012). Retrofitting masonry infill walls with textile reinforced mortar. *15th World Conference on Earthquake Engineering, Lisbon Portugal*.

Yetimoglu, T., Inanir, M., & Inanir, O. E. (2005). A study on bearing capacity of randomly distributed fiber-reinforced sand fills overlying soft clay. *Geotextiles and Geomembranes*, *23*(2), 174–183.

Yetimoglu, T., & Salbas, O. (2003). A study on shear strength of sands reinforced with randomly distributed discrete fibers. *Geotextiles and Geomembranes*, *21*(2), 103–110.

Zhang, P., & Li, Q. F. (2013). Effect of polypropylene fiber on durability of concrete composite containing fly ash and silica fume. *Composites Part B: Engineering*, *45*(1), 1587–1594.

APPENDIX A – TESTS RESULTS

This appendix presents the fishing nets uniaxial tensile test results for different combinations of the tested specimens, knotted, knotless thread, 2 threads, 4 threads, and 6 threads FN of #15 and #21 threads. Salient tensile test data are presented in Table A.1 through A.10. The load-displacement response for these specimens is shown in Figure A.1 through A.10.

The compressive strength of the overlay cement mortar is presented in Table A.11. Also, the compressive strength of the cement mortar used for masonry building is presented in Table A.12.

Tables:

Table A.1 Tensile test results for #15 knotted thread

Specimen #	Peak load, N	Displacement at peak load, mm	Maximum stress, MPa	Ultimate strain, %
1	159.5	89.8	141.1	98.0
2	148.5	90.1	131.4	102.8
3	157.8	101.5	139.6	101.5
4	141.6	84.5	125.3	96.2
5	162.9	88.4	144.1	106.0
Average	154.1	90.9	136.3	100.9
(SD)	(±7.85)	(±5.68)	(±6.94)	(±3.47)

127

Table A.2 Tensile characteristics for #15 knotless thread.

Specimen #	Total load, N	Displacement at peak load, mm	Maximum stress, MPa	Ultimate strain, %
1	189.7	25.3	167.8	34.2
2	216.0	22.4	191.1	39.0
3	168.8	15.9	149.3	29.2
4	197.5	20.7	174.8	35.0
Average	193.0	21.1	170.7	34.4
(SD)	($\pm$16.9)	($\pm$3.41)	($\pm$15.0)	($\pm$3.49)

Table A.3 Tensile characteristics for #21 knotted thread.

Specimen #	Total load, N	Displacement at peak load, mm	Maximum stress, MPa	Ultimate strain, %
1	274.5	79.5	128.4	92.7
2	261.0	83.3	122.1	90.9
3	314.6	82.1	147.2	110.0
4	329.0	89.2	153.9	102.3
5	276.9	101.3	119.5	112.3
Average	291.2	87.1	134.2	101.6
(SD)	($\pm$26.0)	($\pm$7.79)	($\pm$13.8)	($\pm$8.71)

128

Table A.4 Tensile characteristics for #21 knotless thread.

Specimen #	Total load, N	Displacement at peak load, mm	Maximum stress, MPa	Ultimate strain, %
1	400.1	35.2	166.4	42.0
2	458.8	56.4	190.9	66.4
3	436.6	29.0	181.6	42.1
4	432.7	39.0	180.0	30.0
5	393.5	24.0	163.7	51.5
Average	424.3	36.7	176.5	46.4
(SD)	(±24.3)	(±11.1)	(±10.1)	(±12.1)

Table A.5 Tensile characteristics for #15, 2 threads FN specimens.

Specimen #	Total load, N	Displacement at peak load, mm	Maximum stress, MPa	Ultimate strain, %
1	319.9	56.7	141.5	64.1
2	284.7	47.2	125.9	63.2
3	433.8	66.3	191.9	66.3
4	357.9	42.3	158.3	63.1
Average	349.1	53.1	154.4	64.2
(SD)	(±55.3)	(±9.20)	(±24.5)	(±1.29)

Table A.6 Tensile characteristics for #15, 4 threads FN specimens.

Specimen #	Total load, N	Displacement at peak load, mm	Maximum stress, MPa	Ultimate strain, %
1	481.0	86.9	106.4	104.5
2	455.2	64.7	100.7	121.1
3	531.8	75.1	117.6	75.9
4	516.7	68.1	114.3	74.7
5	459.6	88.7	101.6	88.7
Average (SD)	488.9 (±30.6)	76.7 (±9.68)	108.1 (±6.76)	93.0 (±17.71)

Table A.7 Tensile characteristics for #15, 6 threads FN specimens.

Specimen #	Total load, N	Displacement at peak load, mm	Maximum stress, MPa	Ultimate strain, %
1	793.0	54.4	116.9	88.5
2	786.7	72.5	116.0	83.5
3	741.0	69.3	109.3	102.9
4	937.4	78.8	138.2	94.6
5	661.7	86.4	97.6	93.0
Average (SD)	784.0 (±89.9)	72.3 (±10.7)	115.6 (±13.3)	92.5 (±6.48)

130

Table A.8 Tensile characteristics for #21, 2 threads FN specimens.

Specimen #	Total load, N	Displacement at peak load, mm	Maximum stress, MPa	Ultimate strain, %
1	625.4	72.1	130.1	105.1
2	730.4	90.0	151.9	120.0
3	526.2	64.5	109.4	128.7
4	649.0	76.9	135.0	106.2
5	509.4	64.4	106.0	108.4
Average	608.1	73.6	126.5	113.7
(SD)	(±81.7)	(±9.48)	(±17.0)	(±9.21)

Table A.9 Tensile characteristics for #21, 4 threads FN specimens.

Specimen #	Total load, N	Displacement at peak load, mm	Maximum stress, MPa	Ultimate strain, %
1	553.0	112.2	57.5	112.2
2	701.6	121.1	73.0	121.1
3	877.9	79.9	91.3	126.1
4	782.0	122.8	81.3	122.8
5	615.2	117.2	64.0	117.2
Average	705.9	110.6	77.4	119.9
(SD)	(±72.1)	(±15.8)	(±10.1)	(±4.79)

Table A.10 Tensile characteristics for #21, 6 threads FN specimens.

Specimen #	Total load, N	Displacement at peak load, mm	Maximum stress, MPa	Ultimate strain, %
1	1472.4	122.4	102.1	168.6
2	1398.6	110.7	97.0	157.6
3	1460.2	90.3	101.2	138.2
4	1401.7	123.7	97.2	124.2
5	1482.0	92.4	102.7	139.7
Average	1443.0	107.9	100.8	145.7
(SD)	(±35.7)	(±14.3)	(±2.25)	(±15.6)

Table A.11 Compressive strength of overlay masonry cement mortar.

Specimen #	Compressive strength, MPa
1	16.30
2	18.30
3	19.70
4	19.72
5	18.18
6	18.38
Average	18.4
(SD)	(±1.15)

Table A.12 Compressive strength of cement mortar used for masonry building.

Specimen #	Compressive strength, MPa
1	6.87
2	7.44
3	6.21
Average	6.84
(SD)	($\pm$0.5)

Figures:
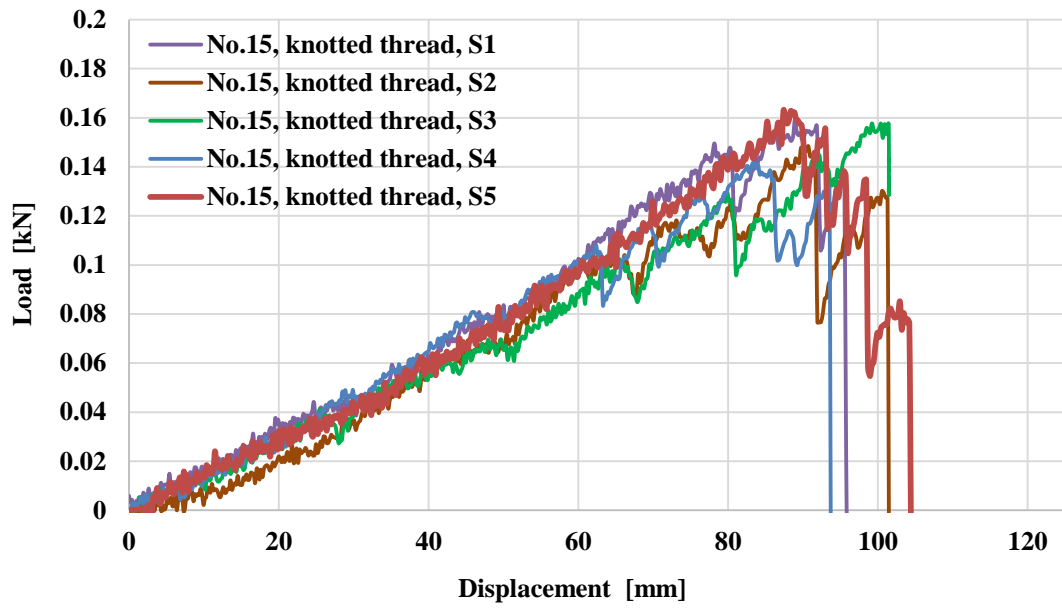
Figure A.1 Load-displacement response of No.15 knotted thread.
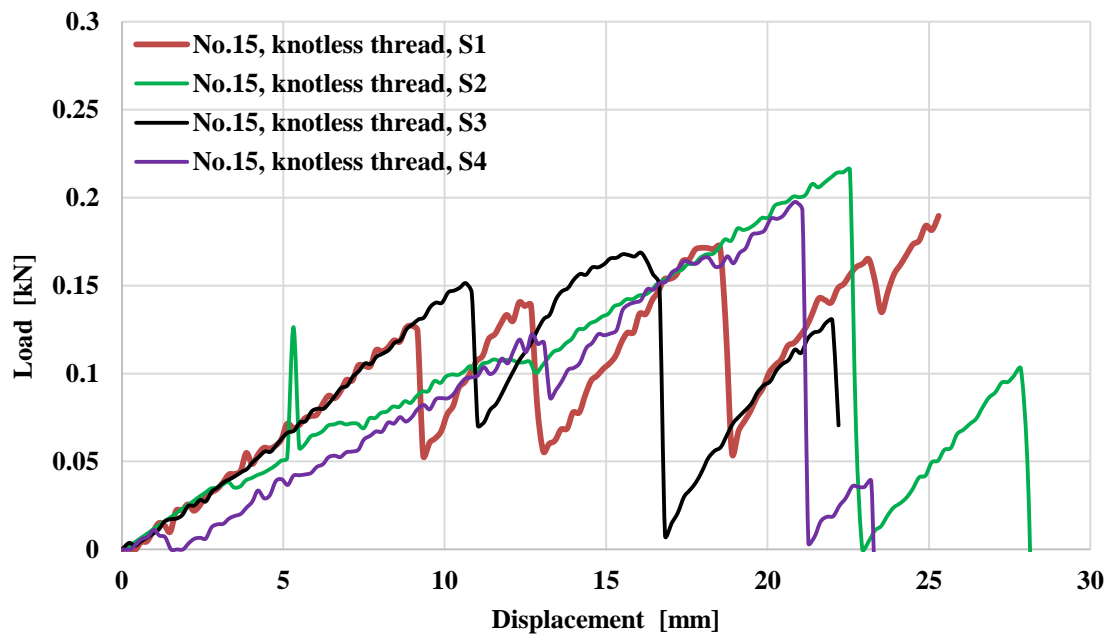
Figure A.2 Load-displacement response of No.15 knotless thread.
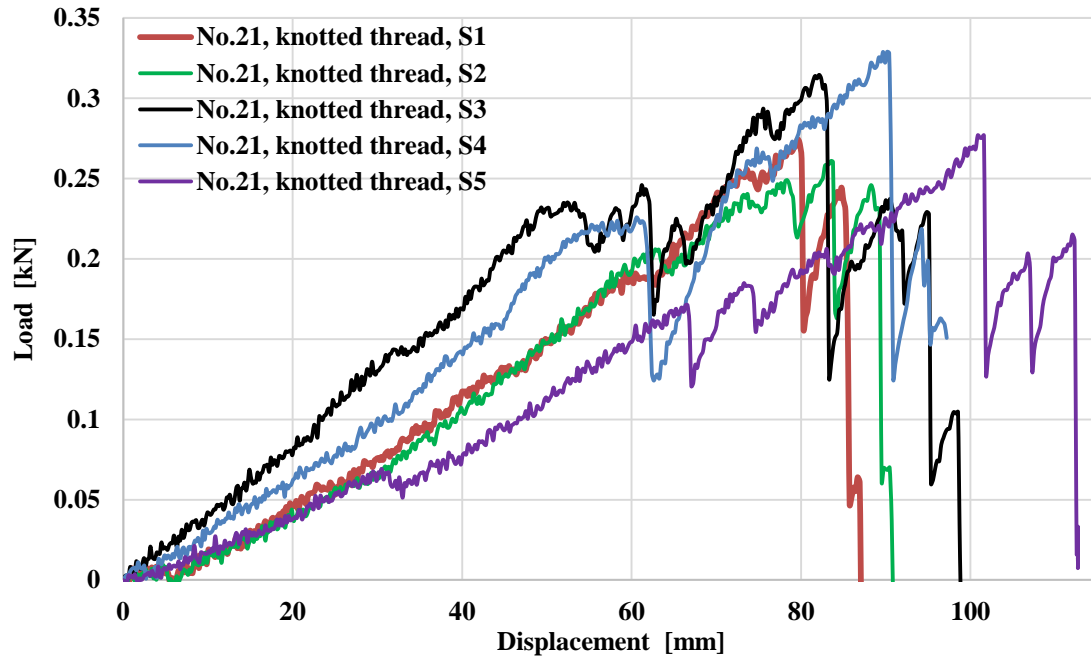
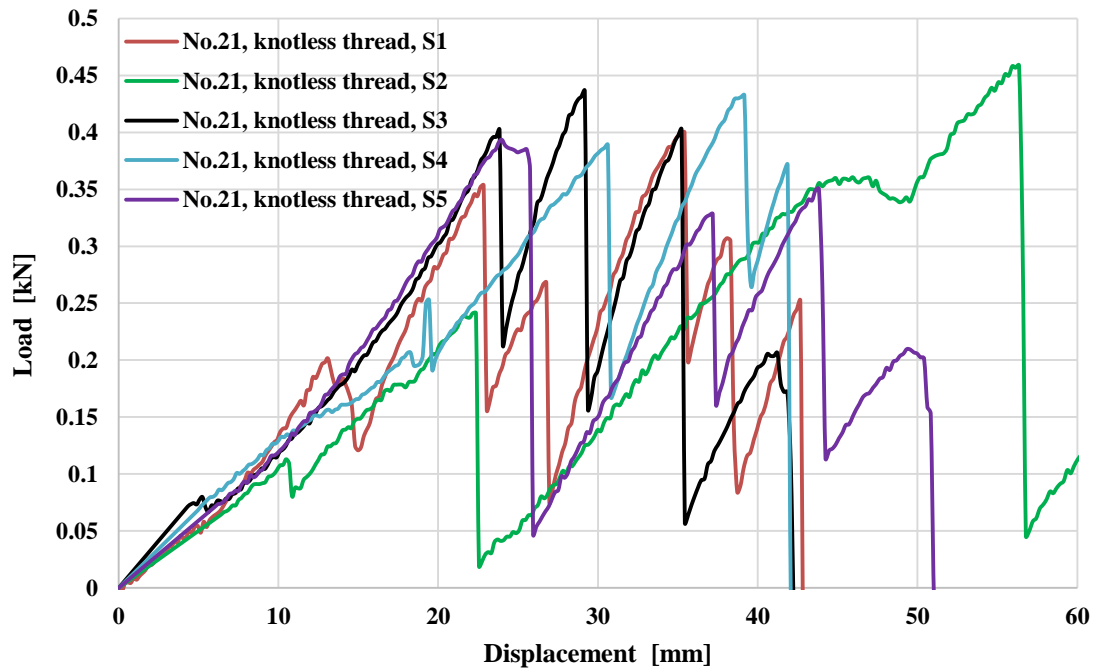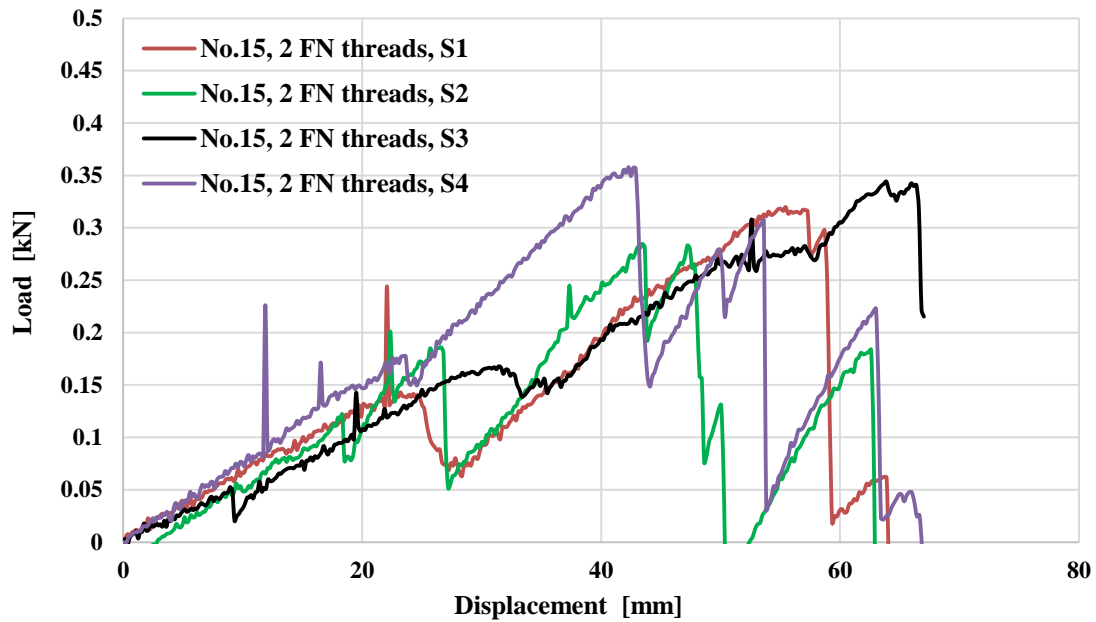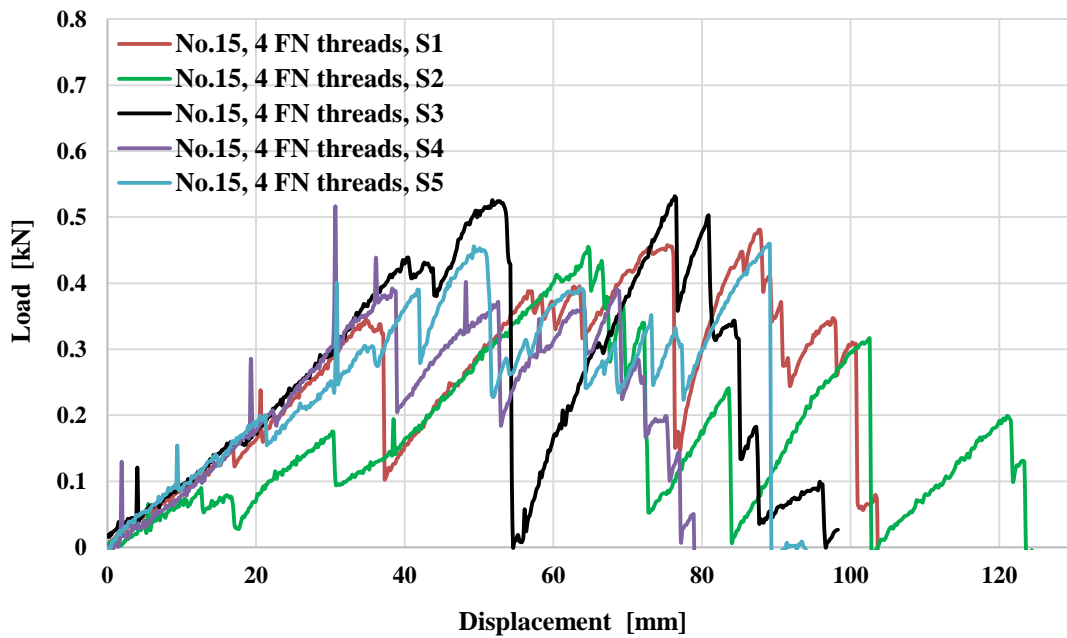Figure A.3 Load-displacement response of No.21 knotted thread.

Figure A.4 Load-displacement response of No.21 knotless thread.

135

Figure A.5 Load-displacement response of No.15, 2 FN threads.

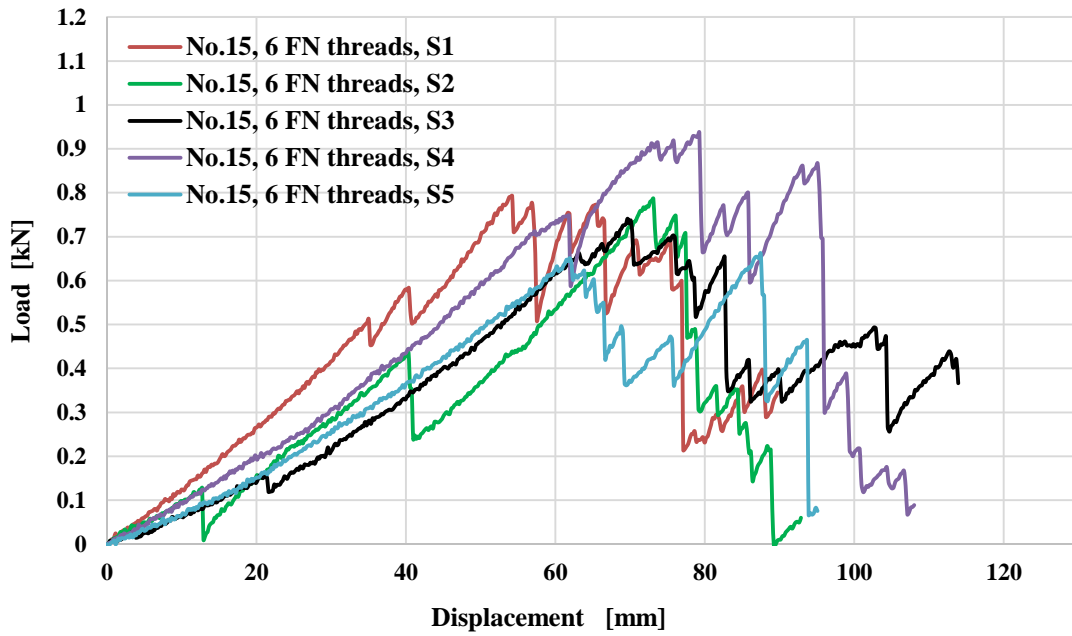

Figure A.6 Load-displacement response of No.15, 4 FN threads.

136

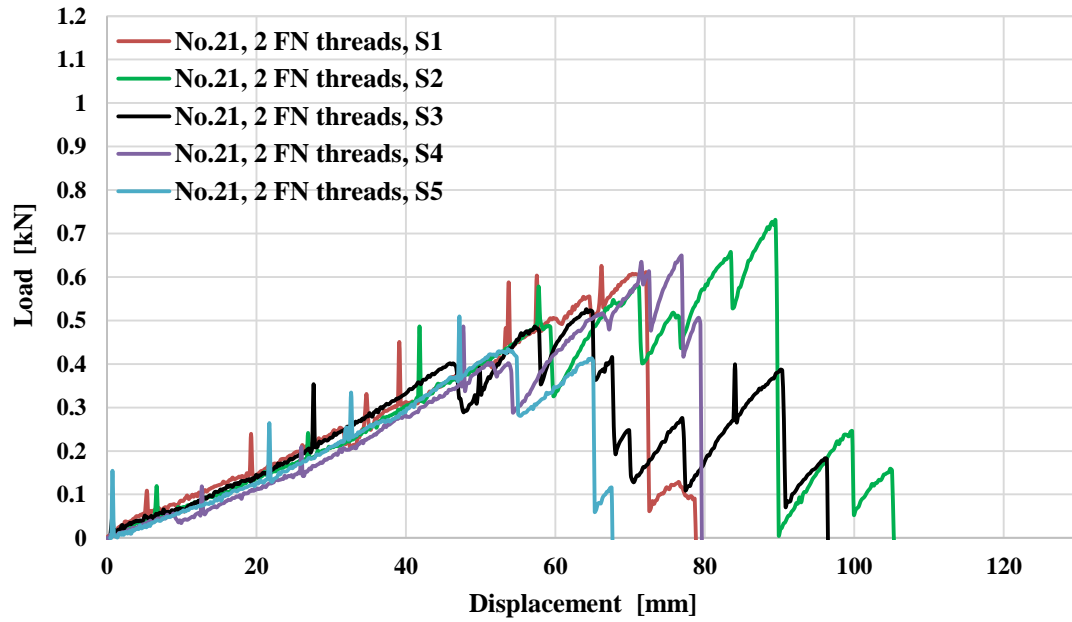Figure A.7 Load-displacement response of No.15, 6 FN threads.

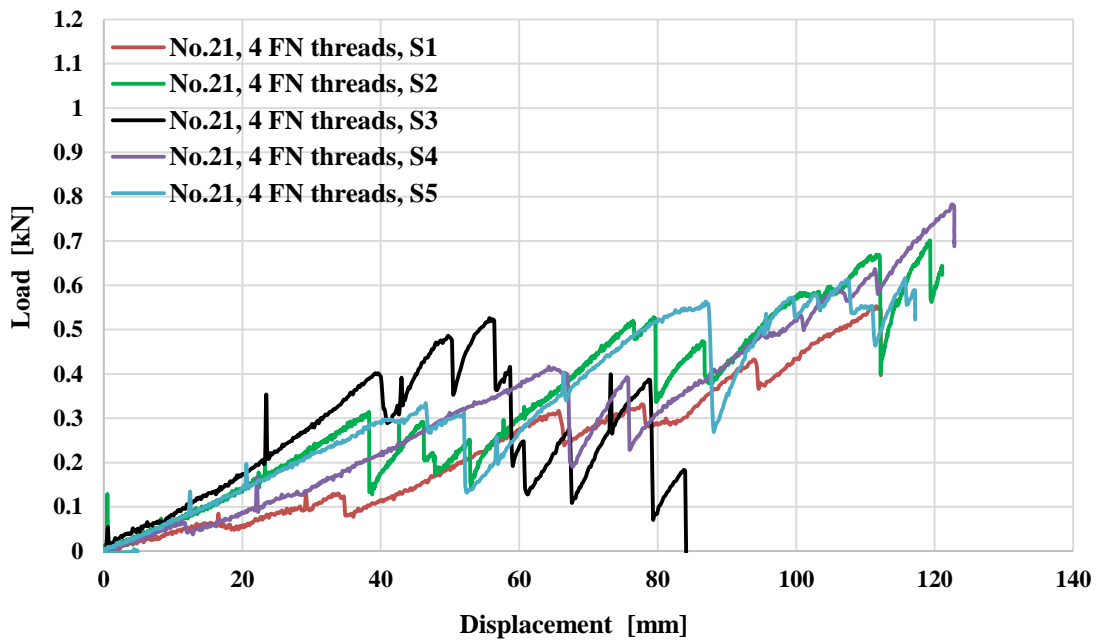Figure A.8 Load-displacement response of No.21, 2 FN threads.

137

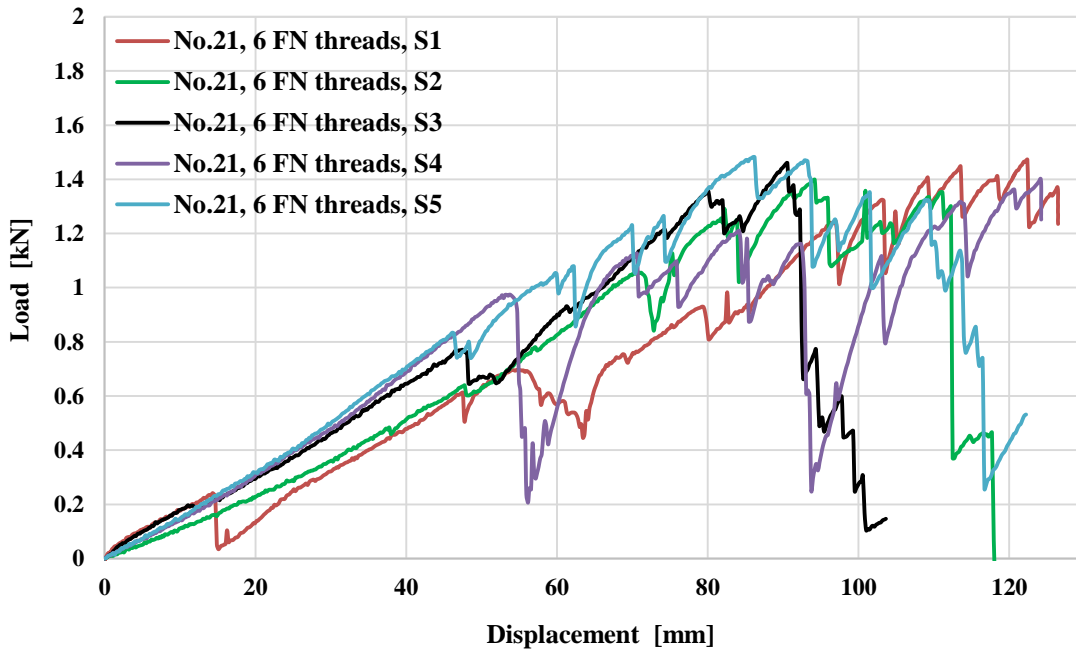Figure A.9 Load-displacement response of No.21, 4 FN threads.

Figure A.10 Load-displacement response of No.21, 6 FN threads.